National Library
of Canada

Canadian Theses Service

Ottawa, Canada
K1A 0N4

Bibliothèque nationale
du Canada

Services des thèses canadiennes

CANADIAN THESES

NOTICE

The quality of this microfiche is heavily dependent upon the quality of the original thesis submitted for microfilming. Every effort has been made to ensure the highest quality of reproduction possible.

If pages are missing, contact the university which granted the degree.

Some pages may have indistinct print especially if the original pages were typed with a poor typewriter ribbon or if the university sent us an inferior photocopy.

Previously copyrighted materials (journal articles, published tests, etc.) are not filmed.

Reproduction in full or in part of this film is governed by the Canadian Copyright Act, R.S.C. 1970, c. C-30. Please read the authorization forms which accompany this thesis.

THIS DISSERTATION
HAS BEEN MICROFILMED
EXACTLY AS RECEIVED

THÈSES CANADIENNES

AVIS

La qualité de cette microfiche dépend grandement de la qualité de la thèse soumise au microfilmage. Nous avons tout fait pour assurer une qualité supérieure de reproduction.

S'il manque des pages, veuillez communiquer avec l'université qui a conféré le grade.

La qualité d'impression de certaines pages peut laisser à désirer, surtout si les pages originales ont été dactylographiées à l'aide d'un ruban usé ou si l'université nous a fait parvenir une photocopie de qualité inférieure.

Les documents qui font déjà l'objet d'un droit d'auteur (articles de revue, examens publiés, etc.) ne sont pas microfilmés.

La reproduction, même partielle, de ce microfilm est soumise à la Loi canadienne sur le droit d'auteur, SRC 1970, c. C-30. Veuillez prendre connaissance des formules d'autorisation qui accompagnent cette thèse.

LA THÈSE A ÉTÉ
MICROFILMÉE TELLE QUE
NOUS L'AVONS REÇUE

NL 339 (r. 86/01)

Canada

National Library of Canada
Bibliothèque nationale du Canada

Canadian Theses Division
Division des thèses canadiennes

Ottawa, Canada
K1A 0N4

180

0-315-24916-1

PERMISSION TO MICROFILM — AUTORISATION DE MICROFILMER

- Please print or type — Écrire en lettres moulées ou dactylographier

Full Name of Author — Nom complet de l'auteur
BRUCE GEORGE VEIDT

Date of Birth — Date de naissance
JAN. 03, 1959

Country of Birth — Lieu de naissance
CANADA

Permanent Address — Résidence fixe
c/o GEORGE VEIDT
BOX 12
GRIMSHAW, ALBERTA
TOH IWO

Title of Thesis — Titre de la thèse
A 408 MHz SYNTHESIS RADIO TELESCOPE

University — Université
UNIVERSITY OF ALBERTA, EDMONTON, ALBERTA.

Degree for which thesis was presented — Grade pour lequel cette thèse fut présentée
MASTER OF SCIENCE, ELECTRICAL ENGINEERING

Year this degree conferred — Année d'obtention de ce grade
1984

Name of Supervisor — Nom du directeur de thèse
J.F. VANELDIK / T.L. LANDECKER

Permission is hereby granted to the NATIONAL LIBRARY OF CANADA to microfilm this thesis and to lend or sell copies of the film.

The author reserves other publication rights, and neither the thesis nor extensive extracts from it may be printed or otherwise reproduced without the author's written permission.

L'autorisation est, par la présente, accordée à la BIBLIOTHÈQUE NATIONALE DU CANADA de microfilmer cette thèse et de prêter ou de vendre des exemplaires du film.

L'auteur se réserve les autres droits de publication; ni la thèse ni de longs extraits de celle-ci ne doivent être imprimés ou autrement reproduits sans l'autorisation écrite de l'auteur.

Date
July 20, 1984

Signature
Bruce Veidt

NL-91 (4/77)

THE UNIVERSITY OF ALBERTA

A 408 MHZ SYNTHESIS RADIO TELESCOPE

by

© BRUCE VEIDT

A THESIS

SUBMITTED TO THE FACULTY OF GRADUATE STUDIES AND RESEARCH

IN PARTIAL FULFILMENT OF THE REQUIREMENTS FOR THE DEGREE

OF MASTER OF SCIENCE

DEPARTMENT OF ELECTRICAL ENGINEERING

EDMONTON, ALBERTA

FALL, 1984

THE UNIVERSITY OF ALBERTA

RELEASE FORM

NAME OF AUTHOR	Bruce George Veidt
TITLE OF THESIS	A 408 MHz SYNTHESIS RADIO TELESCOPE
DEGREE FOR WHICH THESIS WAS PRESENTED	Master of Science
YEAR THIS DEGREE GRANTED	Fall 1984

Permission is hereby granted to THE UNIVERSITY OF ALBERTA LIBRARY to reproduce single copies of this thesis and to lend or sell such copies for private, scholarly or scientific research purposes only.

The author reserves other publication rights, and neither the thesis nor extensive extracts from it may be printed or otherwise reproduced without the author's written permission.

(SIGNED) Bruce Veidt

PERMANENT ADDRESS:

Box 12
Grimshaw, Alberta
TOH 1WO

DATED June 15 1984

THE UNIVERSITY OF ALBERTA

FACULTY OF GRADUATE STUDIES AND RESEARCH

The undersigned certify that they have read, and recommend to the Faculty of Graduate Studies and Research, for acceptance, a thesis entitled "A 408 MHz SYNTHESIS RADIO TELESCOPE" submitted by Bruce George Veidt in partial fulfillment of the requirements for the degree of Master of Science.

JFVaneldik
....
Supervisor

T. Landecker
....
Supervisor

....

Art Peterson
....

D. Routledge
....

ABSTRACT

The synthesis radio telescope at the Dominion Radio Astrophysical Observatory at Penticton, British Columbia has been modified to observe simultaneously with a second continuum channel. To accomplish this, the 1420 MHz feed horns were modified and new independent receivers were added to the telescope.

The new dual-frequency feed consists of a coaxial-cavity feed horn designed for 1420 MHz operation within which 408 MHz monopoles have been placed. These probes excite the horn as a cylindrical waveguide horn. The presence of these probes has a negligible effect on the 1420 MHz performance. The edge illumination of the parabolic reflector by this feed is ~10 dB. The combination of the feed and reflector has the following performance: 5.3° half-power beamwidth; 60% aperture efficiency; 30K spillover; 52K zenith temperature excluding the galactic contribution.

A highly phase stable receiver has been developed that corrects for the signal path length uncertainties from the receiver mixers to the intermediate frequency outputs. The stability of the receiver is at least seven times better than earlier receiver systems that only stabilized the local oscillator phase. The receiver uses GaAsFET low noise amplifiers with an effective noise temperature of 50K, which results in a typical system temperature of 104K excluding the galactic contribution.

The design of this system is described in this thesis. Detailed analysis of the phase locked loop in the local oscillator is also included. System tests are described and preliminary results from the first complete survey at 408 MHz (the HB3 supernova remnant) are shown.

ACKNOWLEDGMENTS

This thesis would not have been possible without the help and encouragement of many people. I must thank my supervisors, Tom Landecker, Dave Routledge, and Fred Vaneldik for their encouragement and for sharing their knowledge of radio astronomy instrumentation with me. I must also thank John Galt and Lloyd Higgs (directors of the Dominion Radio Astrophysical Observatory) for allowing me to do my thesis work at the Observatory.

Everyone at the Observatory has helped me in one way or another. Two technicians, Ev Sheehan and Rod Stuart, assisted in the manufacture and installation of my designs. Peter Lawson and Ron Casorso also constructed pieces of electronic equipment. Harry Mielke machined components for this project. Geoff Croes and Carman Costain modified the telescope software to enable 408 MHz observations to be made. I had many useful conversations with Jim Caswell regarding the interpretation of the first observations made with the telescope. Cindy Furtado typed this thesis. Erika Rohner handled the paperwork for ordering parts. I am indebted to these people and their colleagues for making this thesis possible and for making my stay at the Observatory a very worthwhile and enjoyable experience.

My parents have always encouraged me throughout my studies and this is appreciated very much.

Financial support was received from the NRC and from NSERC grants to Drs. Routledge and Vaneldik.

The components used in the construction of this radio telescope receiver were purchased using funds donated to the Observatory by Grote Reber. I hope that he will consider the construction of this telescope to be a worthy use of his gift.

TABLE OF CONTENTS

Chapter Page

1. THEORY AND JUSTIFICATION OF 408 MHz TELESCOPE 1
   A. Introduction 1
   B. Mechanisms of Radio Emission 1
   C. Aperture Synthesis Theory 4
   D. The DRAO Supersynthesis Telescope 11
   E. Justification of 408 MHz Addition to Telescope 15
   F. What Has Been Done 17
   G. What Had To Be Done 18

2. 408 MHz ANTENNA 20
   A. Introduction 20
      1. Requirements for a "Good" Reflector Antenna Feed 20
      2. Antenna Test Range Measurements 23
   B. 1420 MHz Reception 25
   C. Modification for 408 MHz Radiating Structure 30
   D. Combining Network 44
   E. Frequency Independence Measurements 52
   F. Performance on Dish 54
      1. Dish Radiation Patterns 55
      2. Aperture Efficiency 59
      3. Spillover 59
   G. Conclusion 61

3. 408 MHz RECEIVER 62
    A. The General Problem 62
    B. Receiver Front Ends 68
    C. Automatic Gain Control 75
    D. The Local Oscillator System and Phase Stability 78
        1. Need for Phase Stability 78
        2. Sources of Phase Instability 81
        3. Phase Stabilization Techniques Used With Other Telescopes 84
        4. Theory of 408 MHz Local Oscillator 86
        5. Design of 408 MHz Local Oscillator 95
            Sources of Error 95
            Voltage Controlled Oscillator 100
            Phase Detector and Loop Filter 103
            Synthesizers 109
            204 MHz Source 112
            Phase Shifter 113
            RF/DC Combining Network 117
            RF Combining Network 121
            Coaxial Line 127
            Phase Locked Loop Design 130
            Filter Specification 146
            Packaging of the System 149
        6. System Tests 151

4. ASTRONOMICAL OBSERVATIONS 167
    A. Introduction 167
    B. Repeatability 167

C. Long-term Phase Stability 169

D. Solar Interference 172

E. Man-made Interference 174

F. Cross Talk 175

G. Telescope Dynamic Range; Observations of 3C295 176

H. Telescope Sensitivity: Maps of the 5C2 Region 182

I. A Complete Survey: HB3 Supernova Remnant 187

LIST OF FIGURES

Figure Page

1.1 Typical Continuum Radio Spectra 5
1.2 Basic Interferometer 8

2.1 Dimensions of SST Feed 26
2.2 Theoretical Patterns and Aperture Distributions 27
2.3 Radiation Patterns of Feed Horn at 1420 MHz 31
2.4 408 MHz Probe Dimensions 36
2.5 Return Loss of One Probe 38
2.6 Radiation Patterns of Feed Horn at 408 MHz 42
2.7 Antenna Combining Network 46
2.8 Return Loss of Entire Feed System 53
2.9 408 MHz Primary Radiation Pattern 58

3.1 Block Diagram of a Radio Astronomy Receiver 63
3.2 GaAsFET Low Noise Amplifier 70
3.3 Automatic Gain Control 77
3.4 Elementary Phase Stabilized Local Oscillator 88
3.5 Phase/Frequency Scheme of Local Oscillator System 93
3.6 Local Oscillator for One Receiver 94
3.7 Voltage Controlled Oscillator 102
3.8 PLL Phase Detector and Loop Filter 106
3.9 PLL Lock Detector 107
3.10 15 MHz Digital Synthesizer 111
3.11 Phase Shifter Switch Driver 115

3.12 Phase Shifter PIN Diode Switch 117
3.13 RF/DC Combining Network 119
3.14 RF/DC Combining Network Return Loss vs. Frequency 119
3.15 RF Combining Network 123
3.16 Input Impedances of the Components Connected to the RF Combining Network 125
3.17 High Frequency Combining Network Characteristics 128
3.18 Phase Locked Loop Simplified for Control System Analysis 132
3.19 Root Locus Plots 141
3.20 Response of PLL to Noise on VCO Control Voltage 142
3.21 Calculated Closed Loop Response of PLL 145
3.22 Local Oscillator Spectrum 158
3.23 LO Phase Error vs. Line Length 161
3.24 Long-term Phase Stability 164

4.1 Repeatability of Visibility Measurements 168
4.2 Calibration Phase vs. Time at 408 MHz 170
4.3 Calibration Phase vs. Time at 1420 MHz 171
4.4 An Example of Solar Interference 173
4.5 Map of 3C295 Region Before CLEANing 177
4.6 Map of 3C295 Region After CLEANing 179
4.7 Map of Region 2.65° North of 3C295 181
4.8 Identified Sources in 5C2 Region 183
4.9 CLEANed 5C2 Map with Residuals Added 184
4.10 Second 5C2 Map with Residuals 185
4.11 408 MHz Map of HB3 and Environs 190
4.12 408 MHz Map of HB3 SNR 191

LIST OF PHOTOGRAPHIC PLATES

Plate Page

1.1 DRAO Synthesis Telescope 13-14

2.1 Dual Frequency Feed Horn 40-41

2.2 Focus Box 56-57

3.1 Exterior View of LO Remote Chassis 152-153

3.2 Interior View of LO Remote Chassis 154

CHAPTER 1: BACKGROUND THEORY AND JUSTIFICATION OF 408 MHZ TELESCOPE

A. Introduction

For the length of man's collective memory, the sky with its luminous bodies has been viewed with wonder. It is this curiosity that has motivated the construction of new and better telescopes. The system to be described has added a second observing frequency to an existing radio telescope and will allow astronomers to learn more about the structure, composition, and dynamics of objects within and outside the galaxy.

In this chapter the fundamental theory explaining the sources of radio emissions as well as the basic principles of aperture synthesis imaging with radio telescopes will be put forth. The Supersynthesis Telescope (SST) at the Dominion Radio Astrophysical Observatory (DRAO) will also be described and the need for an additional observing band of frequencies on this telescope will be justified. Further chapters will describe the design and testing of the dual-frequency feeds and highly stable receivers, and will also present the first observations made with the telescope.

B. Mechanisms of Radio Emission

After Hertz's verification of Maxwell's Equations, a number of experimenters attempted without success to measure the electromagnetic radiation at radio frequencies from celestial objects such as the sun.

The first detection of radio waves of extraterrestrial origin occurred when Jansky (1933) identified the galactic center as the origin of 20 MHz radio noise. Reber (1940, 1944) made the first radio maps of the sky at 160 MHz and 480 MHz. Other workers have built instruments, some of which followed up these early efforts with greater sensitivity and resolution; others explored the sky at different wavelengths, including infrared, ultraviolet, and x-ray radiation.

Radio emissions can be divided into two classes: broadband or continuum radiation and narrow band radiation from spectral lines. Radio spectral lines (both emission and absorption), like optical lines, are the result of quantum changes in energy levels of atoms or molecules and are related to frequency by Planck's constant. The best known radio spectral line is the neutral hydrogen line at 1420 MHz (λ=21cm) which is the result of a small energy change when the spin direction of the electron changes (van de Hulst 1945). Line observations are useful because the emission is highly monochromatic at a well known frequency which enables velocity measurements to be made using the Doppler effect. The neutral hydrogen in our own galaxy as well as others has been mapped using this technique (Oort, Kerr and Westerhout 1958).

Continuum radiation is the result of other mechanisms which can be deduced from the shape of the spectrum. One type of continuum is "free-free" emission (Henyey and Keenan 1940) which is a thermal process that involves the interaction of free electrons and protons in clouds of ionized hydrogen (termed HII regions). At low frequencies the spectrum rises with an intensity proportional to f^2 until a turnover frequency is reached where the intensity becomes proportional to $f^{-.1}$. At low frequencies the cloud is called "optically thick" because of its high attenuation of radio waves propagating through it. As a result, the radiation from this region is primarily due to thermal radiation from the cloud itself. The Rayleigh-Jeans approximation to blackbody radiation can be used to describe the emission, and from this relation comes the f^2 dependence. As the frequency increases, the cloud becomes largely transparent or "optically thin" and radiation is due to either background sources or the cloud itself. At these frequencies the attenuation is a function of frequency ($f^{-2.1}$) and the net effect is an almost exact cancellation of the frequency dependence causing the spectrum to flatten. This type of emission can be seen around regions of recent star formation. After the star condenses out of a cloud of cold neutral hydrogen, it ionizes the surrounding hydrogen with ultraviolet radiation. The Orion nebula, a well-known optical object, is an example of an HII region.

A second continuum radiation mechanism is synchrotron emission, which is the result of relativistic electrons (a component of cosmic rays) moving through interstellar magnetic fields (Kiepenheuer 1950). As they are decelerated, electromagnetic radiation is emitted. Objects such as supernova remnant shells, radio galaxies, and jets from radio galaxies can be observed via synchrotron emission, and have spectra with intensity proportional to $f^{-\alpha}$ where α is between 0.3 and 0.9 typically.

It should now be apparent that observations at a number of frequencies help to identify the type of object and to understand the physical processes occurring within the object. Figure 1.1 shows the two types of continuum spectra described above.

C. Aperture Synthesis Theory

Telescopes with large apertures are desirable for two reasons: the greater the collecting area, the greater the telescope's sensitivity; and apertures of larger extent have narrower reception beams and allow the fine structure of sources to be studied. Unfortunately, the size of radio telescopes is limited by the strength of the materials that they are made of. The 100m Effelsberg dish in West Germany is the largest fully steerable filled-aperture radio telescope in the world. The Arecibo antenna in Puerto Rico at 300m is larger, but it can only point near the zenith. Fortunately, the technique of aperture synthesis can be used to produce the same results that telescopes kilometres or even thousands of kilometres in diameter would obtain if they existed (Blythe 1957).

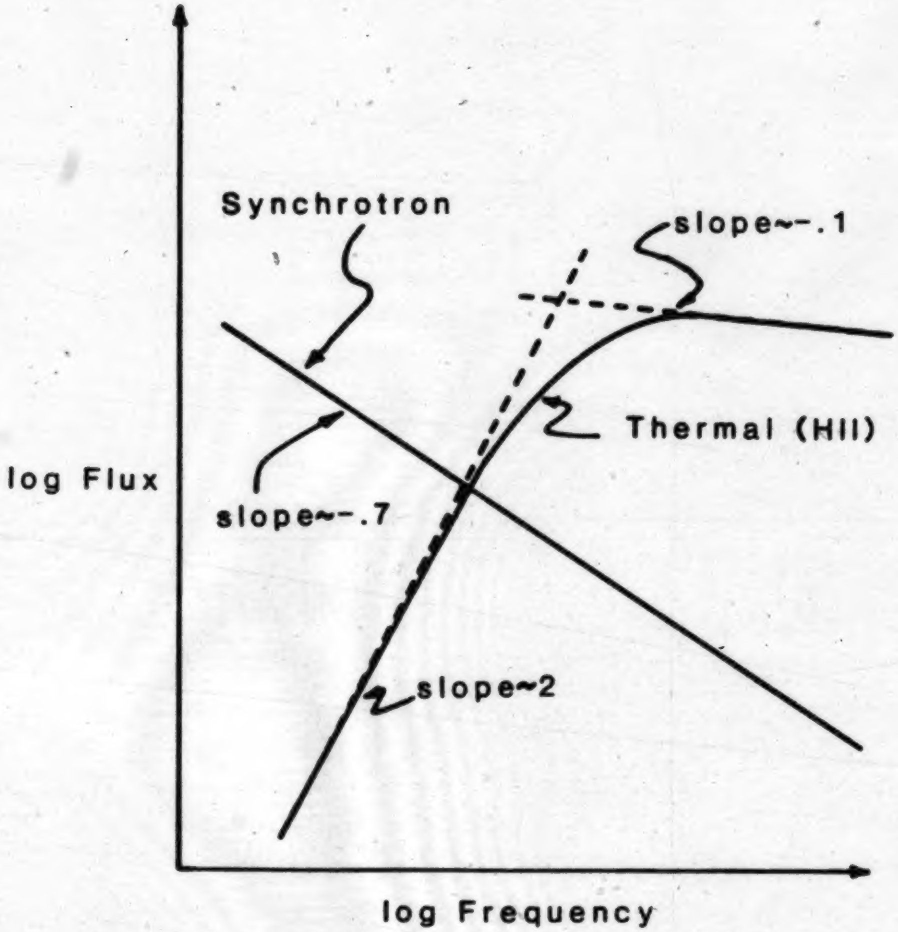

Typical Continuum Radio Spectra

Figure 1.1

An intuitive argument can be used to show that this is possible. Consider first a large reflector antenna. Waves reflecting off the surface meet at the focus and reinforce or cancel depending on the sources' locations relative to the telescope pointing. Now suppose that the sources have constant brightness so that the amplitude and phase of waves reflecting off different parts of the dish do not change with time. Because of this time invariance, only a small part of the reflecting surface need be present at any one time, as long as the amplitude and phase of the wavefront are preserved in the recording process at the focus. Over a period of time, the small piece of reflecting material is moved to all parts of the dish surface and as all the wavefronts are recorded, an image is formed at the focal plane. The phase information can be preserved if two reflecting panels are used, one of which is stationary and provides a phase reference while the other is moved. This minimum set of apparatus is known as an interferometer.

Much more rigorous explanations of aperture synthesis exist (Fomalont 1973, Fomalont and Wright 1974). The explanation to be given here is similar to that used by Dewdney (1978). This theory will help establish some of the specifications of the receiver system.

A basic interferometer (see Fig. 1.2) consists of two antennas separated by a baseline B connected to cables that carry the output of the receivers to a central point, where the signals are crosscorrelated. The correlator multiplies the two signals together and a lowpass filter extracts the difference product, which contains information on the amplitude of the signals intercepted by the antennas, and the phase difference between the two signals which arises as a result of the array-source geometry.

Now suppose the response of the interferometer is mapped by moving a monochromatic test source on the celestial sphere while noting the correlator output. (The "celestial sphere" has earth at its centre, and is arbitrarily large so that effects of the interferometer's displacement from the centre of the earth is negligible.) Of course the output will be modified by the antenna beams and by shadowing by the earth, but for the moment these two effects will be ignored. The array is rotationally symmetric about the line joining the two antennas, so if the source moves within a plane perpendicular to the line B, the correlator output does not change. However, moving the source within a plane which contains the line B changes the source-array geometry and the correlator output changes. Figure 1.2 shows that the correlator output for a source of unity intensity is:

$$C(\theta)=Ge^{j2\pi(B/\lambda)\sin\theta}$$

where G is the gain of the interferometer and λ is the observing wavelength.

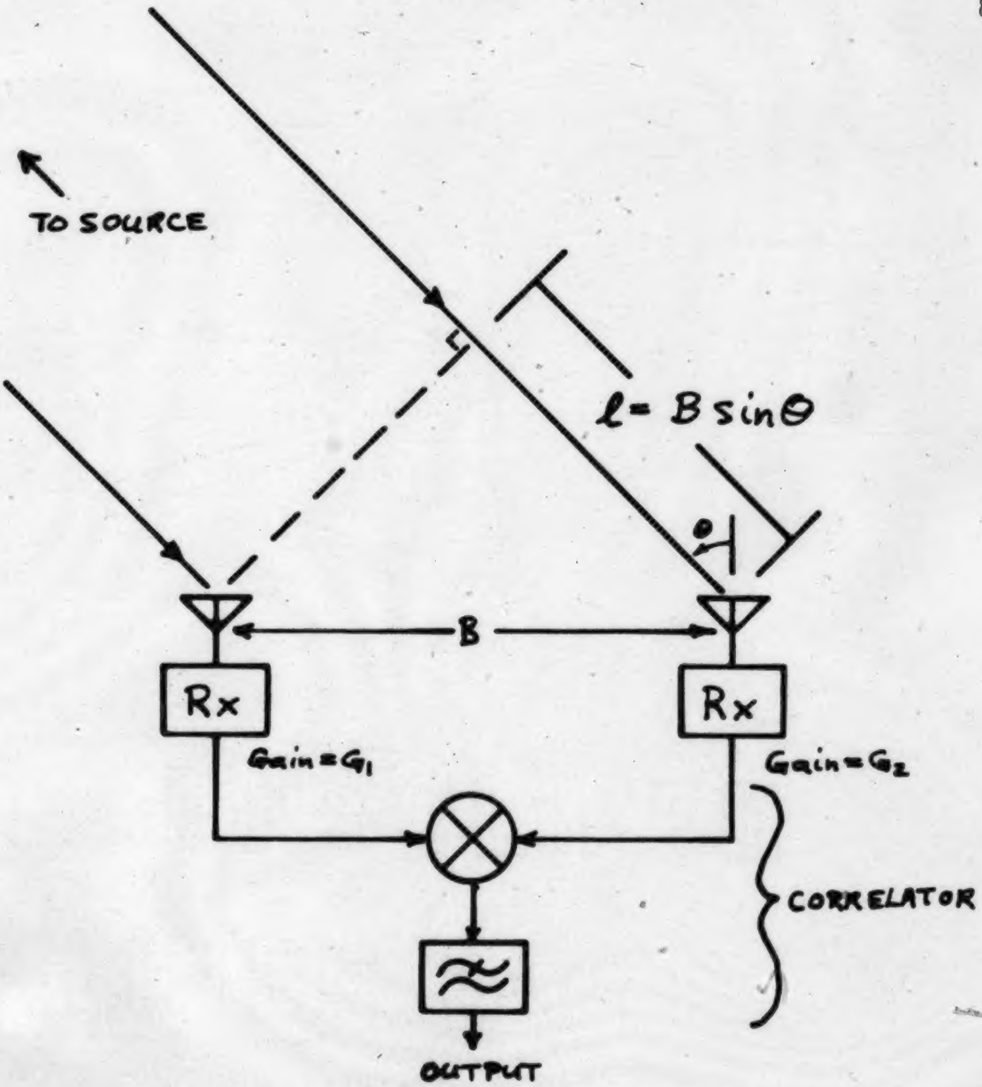

Phase = $2\pi\,\ell/\lambda = 2\pi(B/\lambda)\sin\theta$

Gain (Power) = $\sqrt{G_1}\sqrt{G_2} = G$

Interferometer Response:

$$C(\theta) = G\,e^{j2\pi(B/\lambda)\sin\theta}$$

Basic Interferometer

Figure 1.2

Now suppose that the baseline is aligned in an east-west direction. As the earth rotates, this two-dimensional interferometer pattern sweeps across the sky and the correlator real channel output has quasi-sinusoidal fluctuations, or fringes. The output of the correlator at any one time is the complex sum of the source intensities after they have been multiplied by the interferometer response. At other times the fringe pattern on the sky is aligned in different directions with respect to the sources, and the correlator outputs (called visibilities) can be different. Since the interferometer response is known, with enough independent visibility measurements (obtained by observing at different times and with different baselines), the brightness distribution in the sky can be deduced and a map drawn.

For practical reasons, the visibility measurements occur in discrete intervals of time, the baseline is adjusted in fixed step sizes, and the map of the sky is drawn with a regular grid of pixels. Thus these numbers can be placed in matrices. The measured visibilities and the gridded sky brightness can be related as follows:

$$\mathbf{V} = \mathbf{e}\mathbf{I}$$

$\mathbf{V}$ is a matrix containing the visibilities, $\mathbf{I}$ has the sky brightness distribution and $\mathbf{e}$ contains the computed interferometer responses for the source pixel locations in $\mathbf{I}$ and for the measurement position in $\mathbf{V}$. Inversion of the above equation will produce a map of the sky. If the angle θ is small, the interferometer response can be approximated by

$$Ge^{j2\pi(B/\lambda)\theta}$$

and when this is substituted into the above equation, the brightness distribution is related by the discrete Fourier transform to the visibility measurements. This is the usual case, and for this reason visibilities are often called the Fourier components of the map.

There are only two points on the celestial sphere where the angle θ is small for all rotation angles of the earth - the two celestial poles. So far the fringes on the sky have been fixed with respect to the earth, but they can be rotated at will by injecting the proper phase into the receivers. Thus, the fringes can be stopped at any point in the sky. Since the position angle of the array baseline viewed from the source rotates through 360° in 24 hours, the fringes also rotate about this point in the sky. In other words, the interferometer's "north pole" or phase centre can be moved to any point on the sky through "fringe stopping". When the field of view is restricted by the antennas' primary patterns, the fringe rate is small since observed sources are near the phase centre. The slower fringes are advantageous because this allows the use of integrators with longer time constants. The restricted field of view means that there are fewer sources in the map (than the entire sky) and hence fewer visibility measurements are needed to unambiguously define the source positions and strengths.

Another modification to the basic interferometer is necessary to allow it to measure any point on the sky: the time delay from the source through the antennas and receivers must be equalized. This is necessary because the signals from the sky are broadband noise, and decorrelation occurs if the two signals are offset in time in the correlator.

This technique is known as earth rotation aperture synthesis or supersynthesis (Ryle 1962) since the earth's rotation is used to scan the area to be mapped with the interferometer response pattern. Almost all modern radio telescope arrays utilize this method.

It is apparent that to obtain an accurate map, the matrix e must be well known. Instrumental gain and phase can be determined with calibration observations of isolated point sources for which the visibilities are easy to calculate. During regular observations between calibrations the stability of the system must be depended upon.

D. The DRAO Supersynthesis Telescope

The DRAO SST is located in a semi-arid mountain valley near Penticton, British Columbia. The primary observing frequency is nominally 1420 MHz and the instrument can map a 2°x2° region of the sky with 1 arcminute resolution. The telescope can simultaneously produce continuum radiation maps and spectral line maps of neutral hydrogen emission (absorption). Details of the instrument and performance statistics are given by Roger et al (1973) and Purton (1983). The telescope is shown in Plate 1. This thesis describes the modification of the telescope to produce continuum maps at 408 MHz simultaneously with its 1420 MHz outputs.

The antenna array consists of four 9 metre paraboloidal reflector antennas on an east-west baseline 600 metres long. Two antennas are fixed at each end of the baseline, while the other two can be moved along a precision railway track. The track is 300 metres long and runs from the centre to the west end of the array. Seventy observing locations are marked along the track, so for a complete survey with both movable dishes, thirty-five 12-hour observing periods are required.

The individual antennas are prime focus reflector antennas. The receiver front end electronics (low noise amplifier, mixer, local oscillator, and intermediate frequency amplifier) are located immediately behind the feed in a temperature controlled enclosure called the focus box. The dishes are on equatorial mounts, and the positioning is automatically controlled by the observing computer.

Coaxial cables run from the dishes to the centre of the telescope where they enter the Synthesis Telescope building. The cable is buried in the sandy ground along most of its length. Three cables are

Plate 1.

This is a view of the DRAO Synthesis Telescope as seen from the west. All four dishes along with the precision railway track are visible.

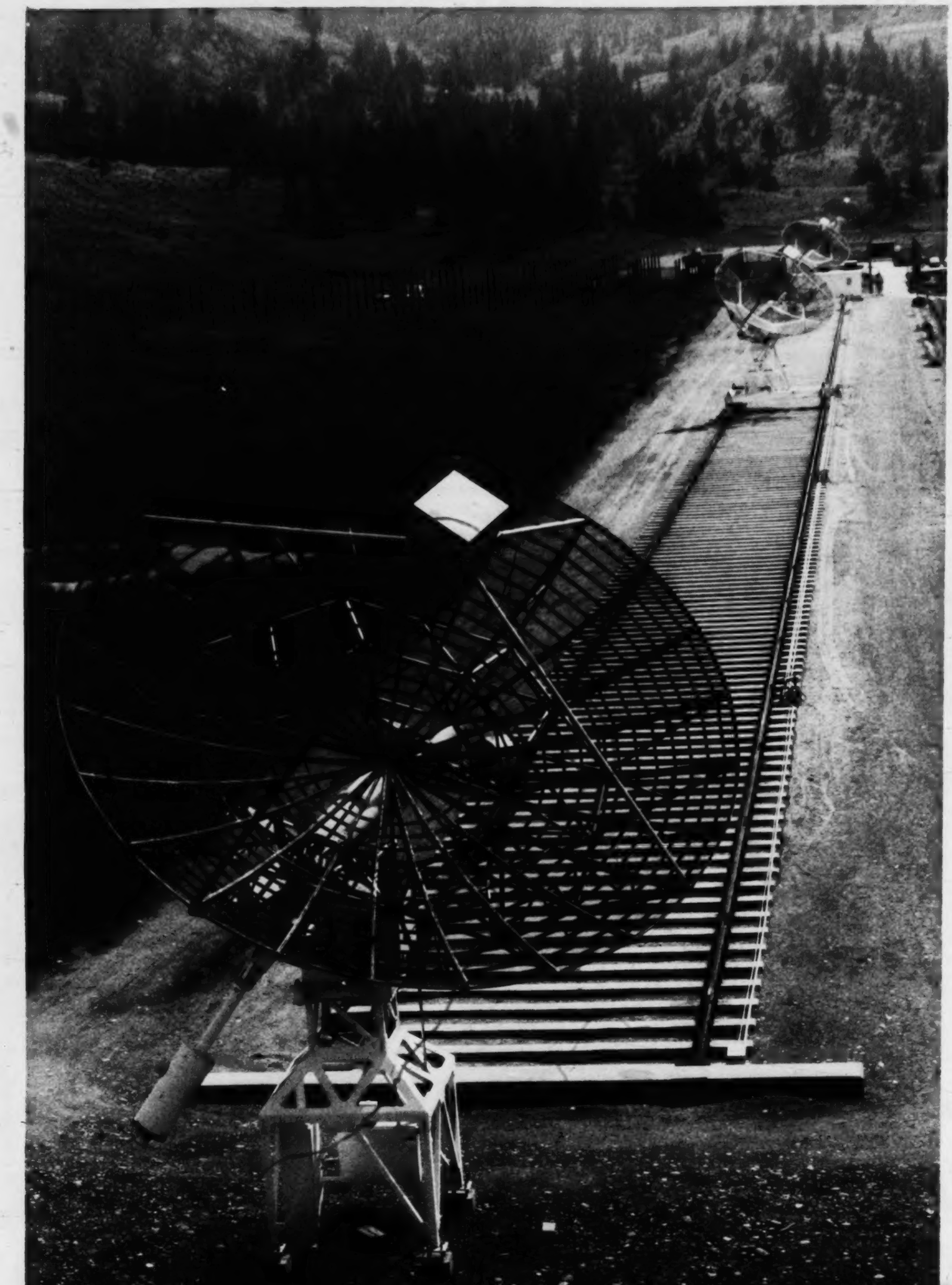

supplied to each dish: one for the 1420 MHz local oscillator; one for the 1420 MHz intermediate frequency; and a spare.

This telescope has a wide field of view and moderate resolution when compared with other instruments. This makes the instrument very well suited for mapping objects that are within our own galaxy, some of which have an angular extent larger than the field of view of other telescopes. Although astronomers are continually striving for greater resolution, the moderate resolution of this telescope does have an important advantage. As the resolution is increased, the sensitivity to extended structures (as opposed to point sources) decreases since less power is captured by the narrower beam from broad structures, but the same power is received from point sources. Thus the wide field of view coupled with the moderate resolution and good sensitivity to extended sources makes the telescope very useful in the study of supernova remnants and HII regions. Examples of such observations are given by Landecker et al (1982) and Dewdney and Roger (1982). The telescope has also been used to observe extragalactic objects such as the Andromeda Galaxy and clusters of galaxies.

E. Justification of 408 MHz Addition to Telescope

A second continuum observing frequency on the SST will be valuable for a number of reasons. The spectral indices of sources will be determined rapidly by comparing the two maps produced. Previously, observations from other observatories had to be used if they were available. With the second observing channel, these measurements will be made simultaneously and with a telescope whose instrumental parameters are very accurately known, and similar in nature to those of the primary frequency.

Another reason for adding a low frequency channel to the SST is that the intensity of synchrotron emissions increases with decreasing frequency so that the telescope will become better able to observe broad, diffuse structures. This capability is also aided by the improvement in sensitivity due to the broader synthesized beam of the second frequency system.

The frequency of 408 MHz was selected for a number of reasons. It is a protected frequency band (406.1 to 410 MHz) with radio astronomy as the primary user (ITU 1982). Other radio astronomy bands exist at 327 MHz and 610 MHz, but 408 MHz was chosen for these reasons:

- a compact 327 MHz feed would be more difficult to build than a 408 MHz feed;
- the resolution would be lower at 327 MHz
- the ionosphere is $(408/327)^2 \cong 1\frac{1}{2}$ times worse at 327 than 408 MHz;
- a full-sky radio survey at 408 MHz exists (Haslam et al. 1981, 1982) which can be used to supply the very short interferometer spacings that cannot be measured.

A low frequency observing capability is also considered to be desirable by other observatories. At the Very Large Array in the United States and at the Westerbork Synthesis Radio Telescope in the Netherlands 327 MHz feeds and receivers are being developed (Napier 1982, de Bruyn and van der Hulst 1983) and low frequency channels will be included on the Australia Telescope.

F. What Has Been Done

Prior to the commencement of this thesis project some work had been done by myself and other workers. The general specifications for the second channel were written by Landecker (1980). The new 1420 MHz feeds had been developed by myself and others, although the 408 MHz feed structure had not been developed yet. As I began my work, Lo was completing a unique digital correlator (Lo 1982).

The microprocessor-based digital correlator or Digital Signal Processor (DSP) does a number of processes in software which were previously done with hardware: the correlator imaginary channel is obtained from the real channel by a scheme of interpolation; fringe derotation phase is injected after the correlator, and not before as with most previous synthesis telescopes; and the fine delay compensation is done by interpolating between measurements at discrete delay steps. As well, coarse delay compensation is performed with digital gates so that the large analog cable delay lines as used with the 1420 MHz system are not required for the 408 MHz system.

Traditional complex correlators actually consist of two correlators: one that provides the real part of the correlation coefficient; and another correlator that is identical except for a 90° phase shift applied to one input so that the output is rotated 90° and the imaginary part of the correlation coefficient appears. This phase shift can also be applied after correlation to obtain the imaginary channel. In the microprocessor implementation, 16 correlations separated by delay steps are obtained with digital hardware, and the real channel component at zero delay is obtained through interpolation. The imaginary channel is then obtained with a different interpolation function. This complex pair of numbers is then phase shifted (to stop the fringes) to obtain the correct visibilities. These visibilities are calculated for all interferometer pairs and are transmitted to the host computer which accumulates and writes the numbers onto hard disk.

The DSP also controls the local oscillator phase in 90° steps, so that the interferometer can be calibrated, and for phase switching of the receiver in regular observations.

G. What Had To Be Done

Receivers and feeds for each of the four dishes were required with the following specifications:

- nominal centre frequency of 408 MHz;
- 4 MHz bandwidth;
- high degree of gain and phase stability;
- intermediate frequency and local oscillator to share the same cable running from the dish to the synthesis telescope building;
- local oscillator phase controllable in 90° steps;
- 408 MHz feed structure that does not degrade 1420 MHz operation;
- antennas that combine maximum efficiency with minimum spillover.

The next two chapters will explain how these general specifications were met, and the last chapter will describe observations that demonstrate the performance of the telescope.

CHAPTER 2: 408 MHZ ANTENNA

A. Introduction

The feed horns for the dishes of the SST have been replaced with new feeds that not only improve the primary observing frequency (1420 MHz) performance, but also allow the dishes to receive 408 MHz radiation simultaneously. This new design originated with a single frequency coaxial feed horn for 1420 MHz that had a higher aperture efficiency with lower spillover noise than the old rectangular horn. Adding the structures necessary for 408 MHz reception did not degrade the primary frequency feed quality. The following antenna parameters were measured at the new frequency: aperture efficiency of 60%; antenna temperature at the zenith of 73K, and half-power beamwidth of 5.3°. This section will outline the design and testing of this new feed, emphasizing the 408 MHz aspects.

1. Requirements for a "Good" Reflector Antenna Feed

An ideal antenna would receive radiation from only one direction and reject completely radiation from all other directions. This can only be approximated in practice. For a prime focus reflector antenna the closeness to ideality depends upon two components - the reflector (its diameter and surface accuracy being crucial) and the characteristics of the feed antenna. Since for this project the reflecting surfaces were in existence, the only way to modify the radiation characteristics of the antennas was to change the feed antennas.

From the transmitting point of view, the feeding antenna should illuminate the reflecting surface and nowhere else. Power radiated elsewhere is wasted power - it is not focused by the parabolic surface towards the desired direction. This is called spillover.

The reflector should be illuminated as uniformly as possible. If less than the full reflecting surface is illuminated, the width of the radiating aperture is smaller, and from the Fourier transform relation (Bracewell 1965), the width of the radiation pattern is greater than necessary. This means that the power is radiated over a larger solid angle, and the power radiated in the desired direction is reduced.

Both of these ideas can be looked at from a receiving point of view. If a reflector antenna suffers from spillover, then the feed antenna receives not only radiation off the reflecting surface from the desired direction, but also from beyond the edge of the dish. This radiation from beyond the dish edge can come from other celestial sources or it can be thermal radiation from the ground. Both of these, especially the latter, increase the noise level of the receiver, degrading its sensitivity.

The concept of aperture efficiency has been introduced from the transmitting viewpoint. If a receiving feed antenna receives power from only a small part of the reflecting surface, its efficiency is smaller than it could be because it is not receiving all the power intercepted by the reflector. In practice, only exceptional reflector antennas have an aperture efficiency greater than 50 or 60%.

A number of other characteristics are desirable:

- the radiation pattern should be circularly symmetric (ie. beamwidth in E plane and H plane should be identical);
- the level of the sidelobes should be low;
- the polarization response should be predictable.

Given a reflector that is circularly symmetric and has an accurate surface, these factors are almost entirely determined by the feed.

It is obvious that the feed parameters needed for these different antenna characteristics can be conflicting. For example, to keep the spillover low, the illumination at the dish edge should be low. This will probably result in lower antenna efficiency since to maximize the efficiency, the illumination should be high over the entire dish surface. Furthermore, with practical feeds, the amplitude response cannot drop to zero suddenly at the edge of the dish, so high edge illumination implies high spillover.

2. Antenna Test Range Measurements

The previous discussion has outlined the type of radiation pattern required for a good reflector antenna feed. The design procedure for the feed can be described as "cut and try". The radiation patterns were measured with an outdoor test range, and the antenna structure was changed to bring the antenna pattern closer to that desired.

Ideally, one would like to do pattern measurements in free space under these conditions: a source of radiation at infinity, the antenna under test capable of being positioned at will with respect to the test source, and nothing else. Of course a test range of this quality cannot be realized in practice, although an approximation was possible.

The wave from the source antenna must reach the test antenna via a direct path since reflected waves are received through a different part of the beam than that under study. To minimize reflections the test range was set up outdoors, away from structures containing metal such as buildings and fences. Reflections off the ground, test equipment and cables were minimized by covering these areas with mats made of carbon coated fibres. A simple experiment was used to test the quality of the test range: parallel dipole antennas were placed at the receiving and transmitting locations and were then rotated about the line connecting the two. Using the method of images, it can be shown that a horizontally polarized wave undergoes a 180° phase shift upon reflection, while a vertically polarized wave does not. The vector sum of the direct and reflected rays may not be the same for the two orientations. Thus by changing the plane of polarization of the pair of antennas with respect to the ground, reflections will be indicated by variation in the received amplitude.

Another approximation that was made was to move the source antenna from infinity to a location closer to the earth. The minimum antenna separation is $2D^2/\lambda$ where D is the largest antenna dimension and λ is the wavelength (Hacker and Schrank 1982). At close spacings, one is in the near field (a region of stored rather than radiated energy) and sidelobes are difficult to resolve. With D equal to 0.6m and λ equal to 0.73m at 408 MHz, the minimum separation was about 1m. At 1420 MHz (λ=0.21m), the minimum spacing was 3.4m. In practice 4 metres was used.

The antenna test range geometry was also important. The angle at which the reflected wave struck the ground was made as large as possible to minimize the reflection. With the test range used, the antennas were placed 2 metres above the ground so the angle of incidence was about 45°.

The quality of the test range was quite good at 1420 MHz. The difference between the main beam amplitudes in the two principal planes was less than 1 dB. The minor lobes were easily measured with dynamic range of about 35 dB. This could only be done if spruious reflections were at a low level. The test range was not as good at 408 MHz, but it was still adequate. The difference in main beam amplitudes was 2-3 dB and the dynamic range was ~30 dB. The ground conductivity had a more significant effect at the lower frequency, and unfortunately, the summer when most of these measurements were taken was unusually wet.

B. 1420 MHz Reception

The design for this feed originated with Scheffer (1975). It is shown in Figure 2.1. The dimensions of the feed were optimized on an outdoor antenna test range for operation at 1420 MHz, and then the feed was modified for 408 MHz operation.

To uniformly illuminate a shallow reflector antenna (such as an optical Newtonian telescope which has a large f/D ratio), the feed pattern should be constant to the edge of the dish, then drop to zero, as shown in Fig. 2.2a. The Fourier transform of the radiation pattern is the feed's aperture field distribution, and for this particular case is

$$f(x) = c\,\frac{J_1(x)}{x},$$

where J_1 is the first order Bessel function and x is the radial displacement in units of wavelengths (Goodman 1968). Since the radiation pattern is circularly symmetric (assuming a circular reflector) so is the aperture distribution. A cut through this two

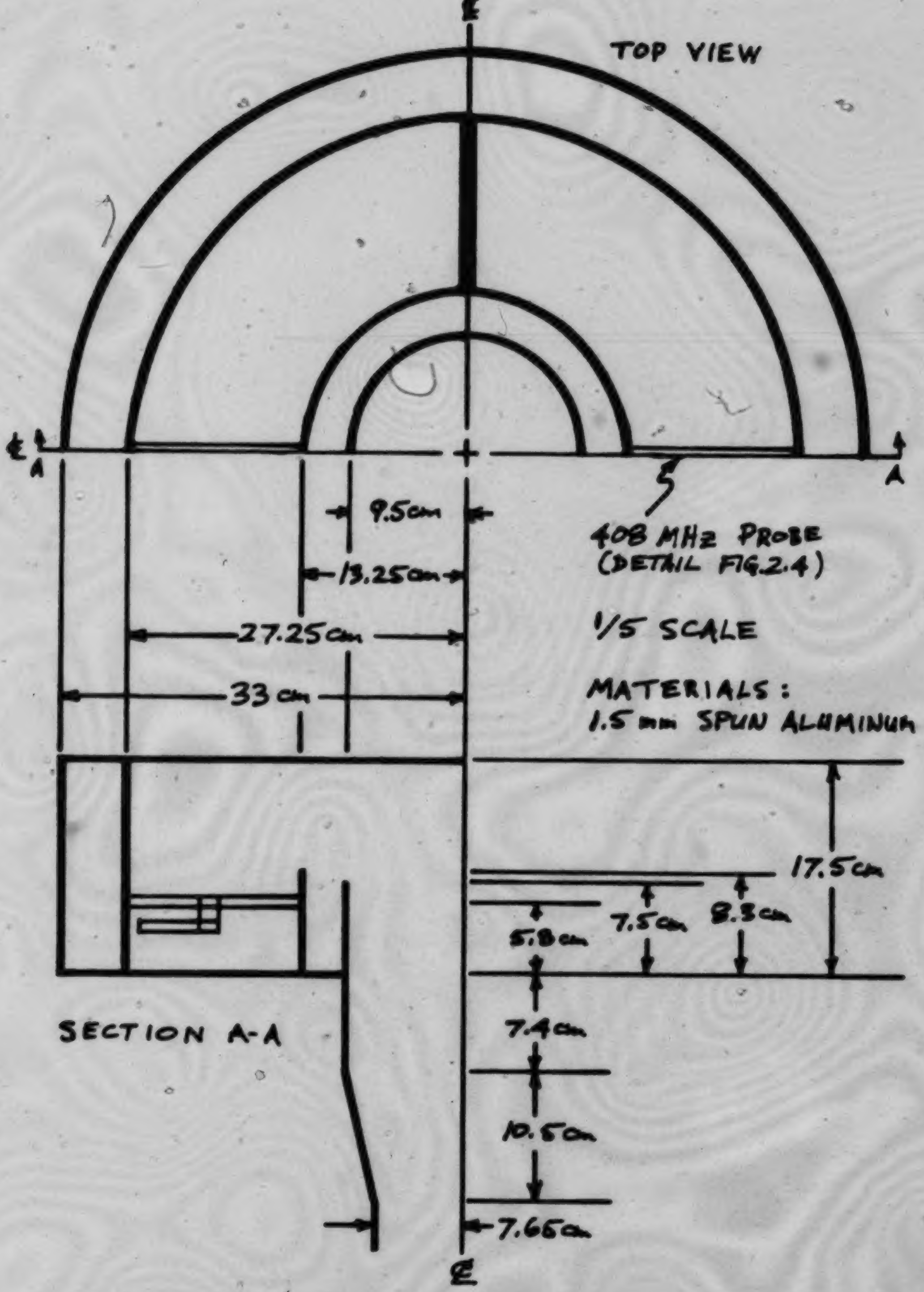

1/5 SCALE

MATERIALS:
1.5 mm SPUN ALUMINUM

FIGURE 2.1 DIMENSIONS OF SST FEED

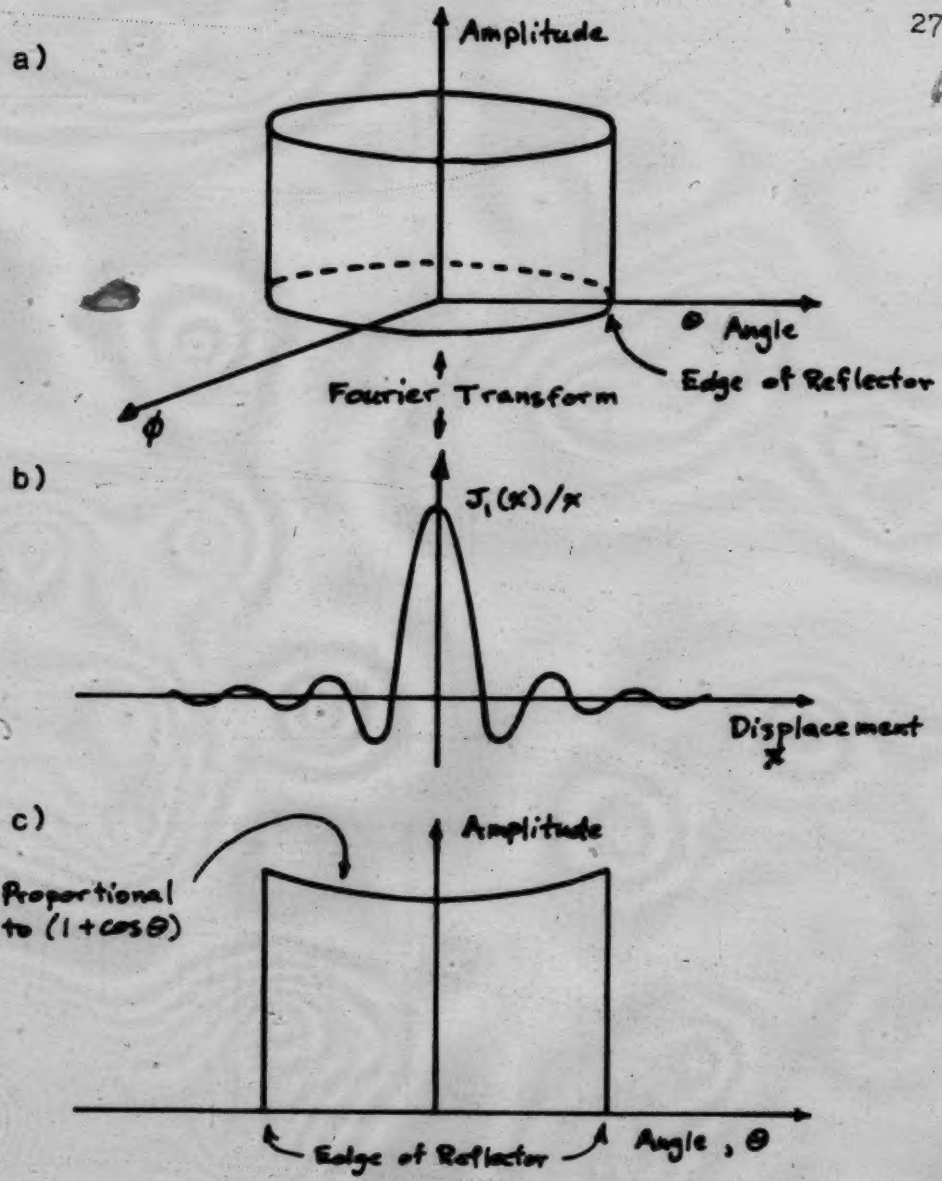

Fig. 2.2 (a) Feed radiation pattern to uniformly illuminate a shallow reflector. (b) Cut through aperture distribution needed to produce (a). (c) Cut through feed pattern for a deep parabolic reflector antenna with uniform illumination.

dimensional function is shown in Fig. 2.2b. This focal plane distribution is known to optical astronomers as Airy's rings.

There are a number of reasons why this aperture distribution is not optimum for radio telescopes. The most significant difference between optical telescopes and radio telescopes is the operating wavelength which makes radio telescopes very small when measured in terms of wavelength. Thus an optical telescope captures many of the higher order rings which often can't be used with a radio telescope without blocking a significant portion of the reflector area. Elimination of the higher order rings results in a smoothing of the sharp cutoff of the radiation pattern and the appearance of spillover lobes. Since the edge of the dish is no longer illuminated at full intensity, the illumination efficiency drops.

Another deviation from this ideal field distribution occurs because the distance from the feed to the reflecting surface is not constant; it is proportional to $1+\cos\theta$ with θ being the off-axis angle. (This is also true with optical telescopes, but not to the same extent.) Thus the radiation pattern must also increase by the same factor to maintain the uniform aperture distribution, as illustrated in Fig. 2.2c. Minnett and Thomas (1968) have attacked this problem with much more rigor and have obtained equations describing the fields at the focal space of reflector antennas.

Although $J_1(x)/x$ is not a precise description of the fields at the focus, it is accurate enough to be a starting point for a design to be experimentally optimized. Koch (1973) and Scheffer (1975) describe feed horns developed in this way. Scheffer explains how this field distribution is obtained by superimposing several coaxial waveguide modes in the horn. A more simplistic explanation is that the main central lobe is supplied by the central circular waveguide, and the first ring lobe is generated in the large coaxial cavity, which is coupled to the waveguide across the narrow coaxial cavity. In practice, the proper coupling was achieved by varying the height of the two inner coaxial rings in a systematic fashion and measuring the feed horn pattern. The criteria for optimum adjustment were steep skirts, low edge illumination of the reflector, and a flat or concave main beam.

Later, in the modification of the feed for 408 MHz operation, another ring was placed around the outside of the horn to create an additional narrow coaxial cavity. The depth of this cavity is almost $\lambda/4$ at 408 MHz, so it presents a high impedance at the open end. This cavity is approximately $3\lambda/4$ deep at 1420 MHz, so it acts as a choke at that frequency as well. The total width is slightly less than the width of the focus box so the shadowing of the reflector was not changed.

This feed has been configured to receive both hands of circular polarization. The coaxial transmission line to waveguide transition is at one end of the 14.95cm circular waveguide. This transition consists of two spatially orthogonal monopoles - one for each hand of circular polarization - in front of a short circuit plane at the end of the waveguide. The separation of the two senses of polarization is obtained with a quarter-wave-plate placed between the transition and the horn.

Antenna patterns at 1420 MHz are shown in Figure 2.3. The illumination at the edge of the dish (±60°) is -15 dB for the E plane and -17 dB for the H plane with respect to the on-axis (0°) intensity.

C. Modification for 408 MHz Radiating Structure

A number of different methods were tried in an attempt to add 408 MHz reception capability to the new 1420 MHz feed. Various designs were tested and discarded either because of distortion of the 1420 MHz radiation pattern, or because of inferior 408 MHz radiation patterns. Elementary array theory will show that an array of 408 MHz radiators whose first nulls lie at 60° or beyond must have the phase centres of the elements within the 1420 MHz horn. One such array that was tried consisted of four dipoles arranged in a square above a ground plane and is called a boxing ring antenna. Dipoles were placed in front of the feed to form this type of feed. This design was rejected because of

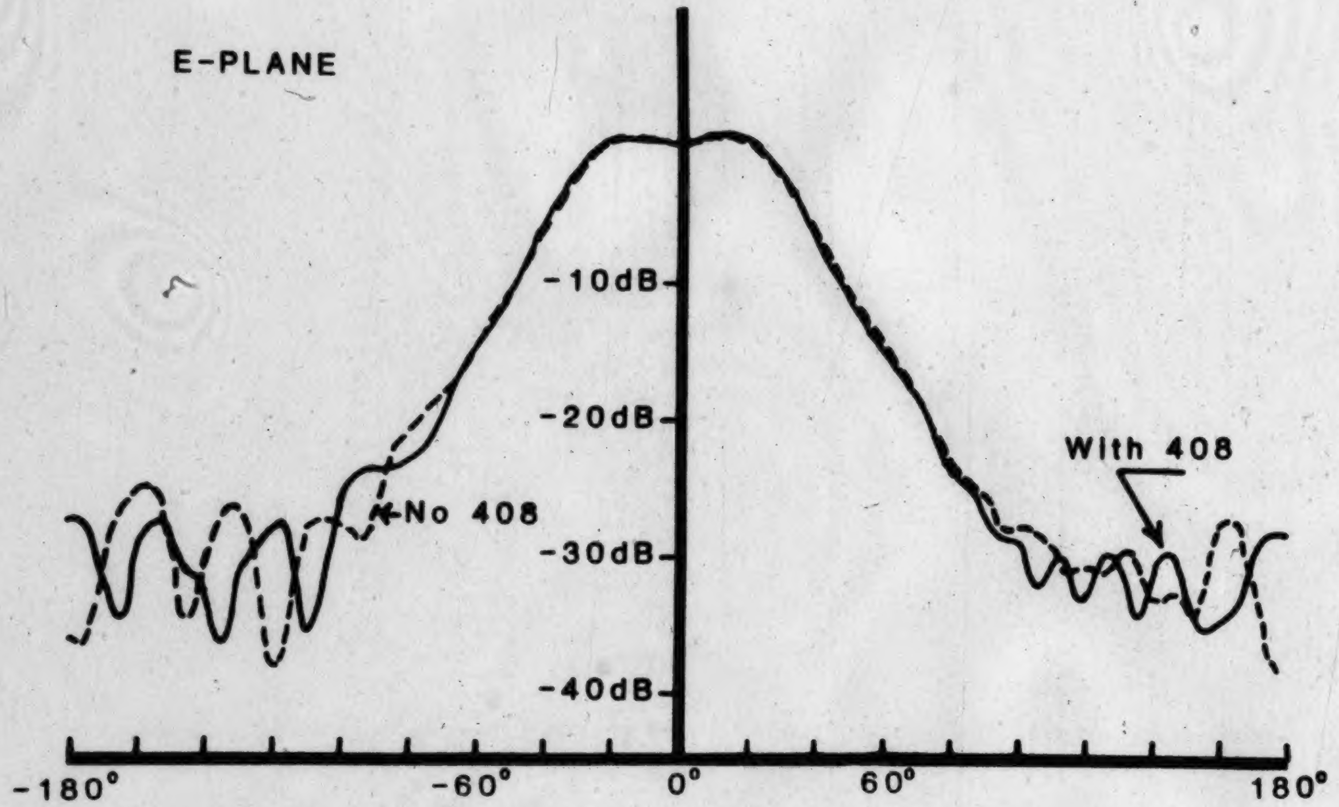

Radiation Patterns of Feed Horn at 1420 MHz

Figure 2.3a

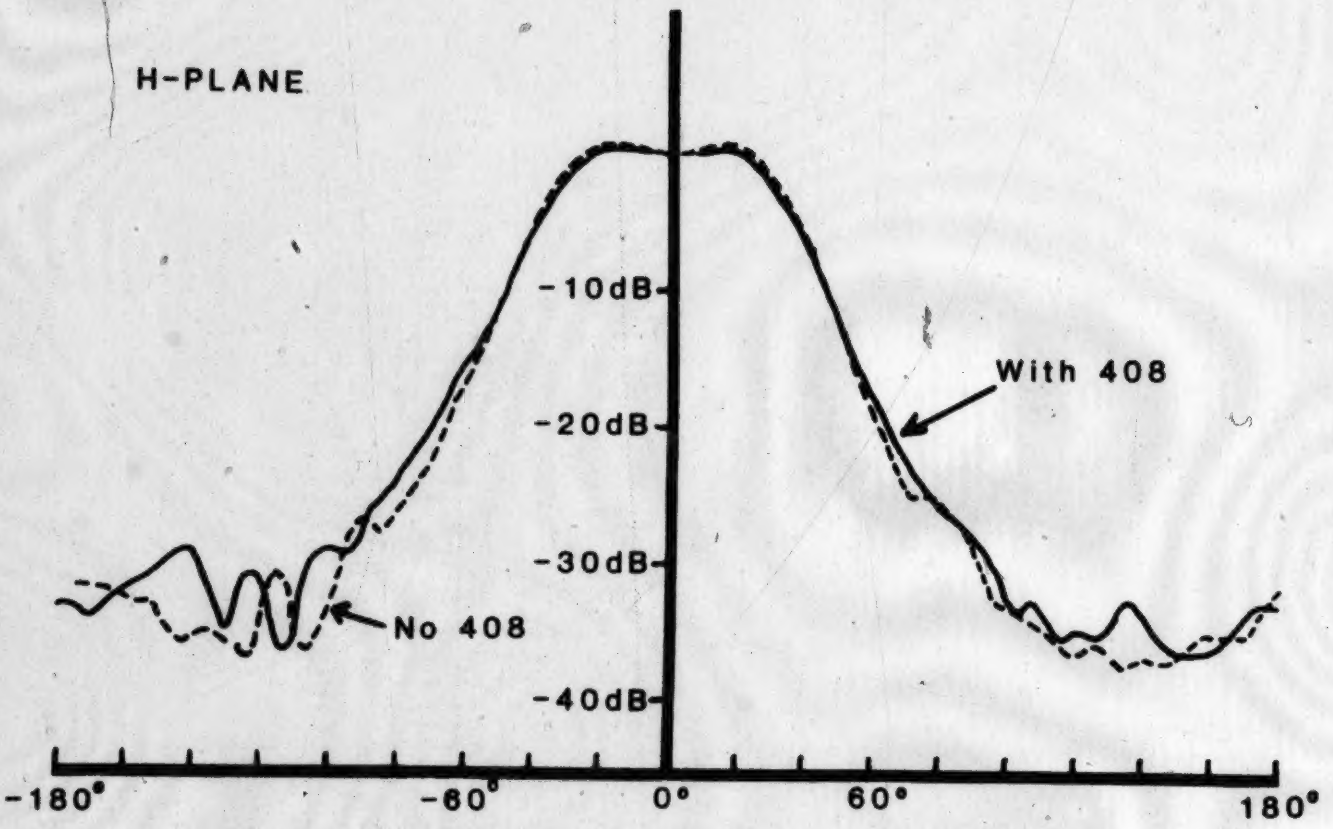

Radiation Patterns of Feed Horn at 1420 MHz

Figure 2.3b

large distortion to the 1420 MHz radiation pattern. Also, because the feed horn was a very crude approximation to a flat ground plane, the 408 MHz radiation pattern did not approach the predicted pattern. An array of cavity backed slots formed using the outer choke ring was also considered, but this idea was discarded because the maximum array element spacing was exceeded. The method finally chosen involves exciting the large cavity and using it as a waveguide horn. These modifications produced a feed with adequate performance at 408 MHz with negligible effect on the 1420 MHz operation.

From these experiments it was concluded that the method selected was the only practical method of adding a second frequency to the 1420 MHz feed horn.

The diameter of the large cavity is big enough to support TE_{11} modes at 408 MHz. Several other dimensions, however, are less than optimum. The cavity forms a coaxial waveguide over much of its length, and its length is short. These two factors together prevent an equal field from being established on the side of the horn opposite to the exciting structure. This would cause the beam to be steered off-centre. The solution to this was to use pairs of diametrically opposed radiators.

The radiators used are monopoles mounted one third the distance from the back of the cavity to the open end. Experiments with the feed horn at 1420 MHz had shown that radial structures within the horn had no measurable effect on the radiation pattern. This was true even if a short circuit was connected across the large ring-cavity.

Measurements at 408 MHz were made with movable monopoles that could be moved towards either the front or the back of the horn. It was found that unless the monopole probes were very close to the open end or the back wall the radiation patterns were independent of the probe positions. What did depend upon the probe position was the input impedance which became smaller as the probe was placed nearer to the back wall. The position used was selected because it placed the probes well away from the mouth of the horn, which ensured that interaction with 1420 MHz was minimized, and also kept the radiation resistance large enough to be useful.

At this location the radiation resistance is low, typically 23Ω, and has a large capacitive reactance associated with it. The technique used to transform this radiation impedance to 50Ω is very similar to "gamma match" devices used on some Yagi antennas. The base of the monopole is connected to a ground plane (actually the wall of the large cavity), and the feed point is moved part way up the monopole. The radiator is fed through a parallel conductor running from near the base to the feed point, where it is joined to the monopole. The other end of the parallel conductor is attached to the centre of the coaxial transmission line through a small inductance chosen to cancel residual capacitances. The construction details are shown in fig. 2.4. The theory of operation of the matching structure can be explained as follows (ARRL 1977). Three things occur simultaneously. First, the monopole is fed away from its base. This multiplies the base impedance by a factor $1/\cos^2\Theta$ where Θ is the distance from the base expressed in units of angle. Second, the parallel rods form an impedance transformer, just like the parallel conductors in a folded dipole. Since the conductors are equal diameter, the step-up ratio is 4:1. And finally, the parallel conductors form a balanced transmission line with a short circuit at the end. This places a shunt impedance across the output terminals. These three factors together determine the probe impedance.

The probe dimensions were obtained in the following manner. A prototype probe was constructed out of ¼" copper tubing and brass shim stock with the total probe length and position of the bridge piece being variable. This was installed in the feed horn with three dummy probes made of single pieces of copper tubing. The impedance of the prototype was measured with a network analyzer, and the two variables were adjusted to move the real part of the impedance near the 50Ω circle. The imaginary part was measured at the center frequency and this determined the required series reactance to make the load resistive. An inductance was required, and was formed with a short piece of semi-rigid coaxial line with a short circuit at one end. The probes installed in the horn had fixed inductance and bridge pieces,

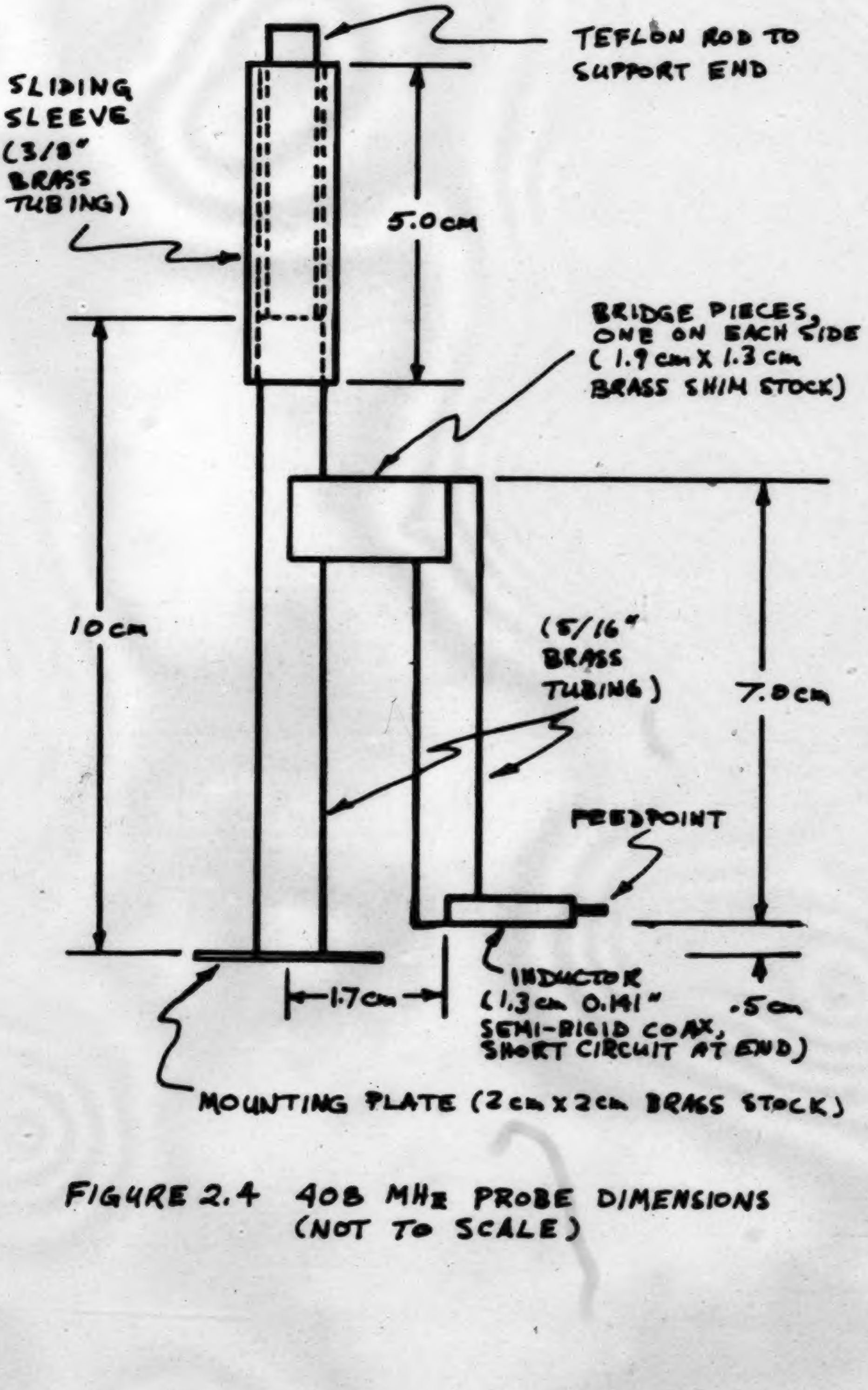
TEFLON ROD TO SUPPORT END
SLIDING SLEEVE (3/8" BRASS TUBING)
5.0cm
BRIDGE PIECES, ONE ON EACH SIDE (1.9cm X 1.3cm BRASS SHIM STOCK)
10cm
(5/16" BRASS TUBING)
7.0cm
FEEDPOINT
INDUCTOR (1.3cm 0.141" SEMI-RIGID COAX, SHORT CIRCUIT AT END)
1.7cm
.5cm
MOUNTING PLATE (2cm x 2cm BRASS STOCK)

FIGURE 2.4 408 MHz PROBE DIMENSIONS (NOT TO SCALE) and the probe length was left adjustable to compensate for component and structural variations.

The adjustment of one probe in the horn affected the adjustment of the others due to mutual coupling. Thus the probes all had to be tuned together, in an iterative sequential manner. The horn was pointed at the sky with the network analyzer connected to one probe and all the others terminated with 50Ω. This probe was adjusted for maximum and broadest return loss. An adjacent probe was then measured and adjusted. This process was continued around the horn until the probes had similar and maximum return losses. The adjustments were then fixed with solder.

Each probe was connected to a short length of semi-rigid coaxial cable that runs through the back wall of the feed to a type-N connector.

This telescope was being modified to observe broadband continuum radiation in a 4 MHz bandwidth centred on 408 MHz. In anticipation of man-made interference, the receiver was made tunable with the front-end filter spanning 403 to 413 MHz. The measured return loss of a probe over this range is at least 15 dB. Plots of return loss versus frequency are shown in fig. 2.5.

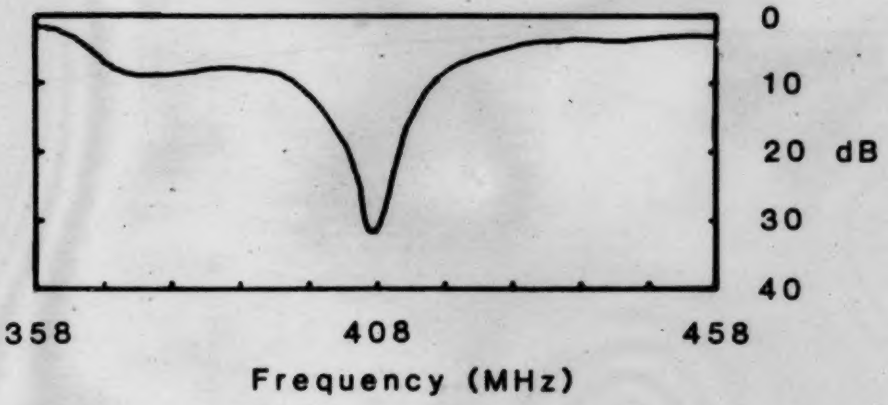

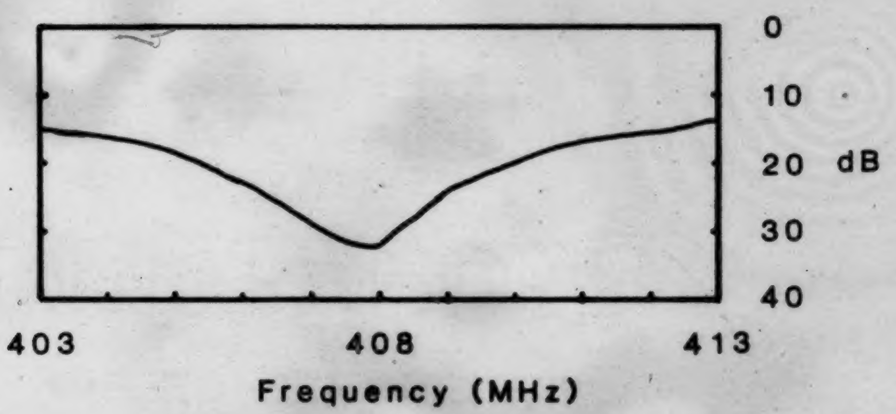

Figure 2.5 Return loss of one probe measured with the other probes tuned and terminated

The complete dual frequency feed is illustrated in Plate 2.1. Typical radiation patterns at 408 MHz are shown in fig. 2.6. The shape of these radiation patterns is simple compared to the 1420 MHz patterns, since the horn is smaller at 408 MHz (in terms of wavelengths) than at 1420 MHz. The patterns show that the choke ring reduces the amplitude of the back lobe while leaving the main lobe virtually unaffected. This is because the high impedance of the choke reduces the currents flowing on the outside of the horn, while having little effect on the aperture (LaGrone and Roberts 1966). The patterns were also measured at 400 and 420 MHz. The variation in the main beam was less than ½ dB. The back lobe varied less than 3 dB over this range.

The feed patterns are quite symmetrical and have edge illuminations (±60°) of -10 dB in both principal planes. The back lobes are less than -20 dB. It should be realized that in practice the radiation patterns near 180° will be modified by the focus box, and these measurements give an inaccurate description of the actual patterns at these angles.

It is interesting to compare the antenna patterns of the 408 MHz feed horn with a cylindrical waveguide horn and a dipole array. The radiation patterns for a cylindrical horn with the same diameter as the dual frequency horn were calculated based on theory presented by Silver (1949). The calculated patterns are similar to those in Figure 2.6,

Plate 2.1

This photograph shows a dual frequency feed horn prior to installation on the dish. The outer choke ring is clearly seen. The four 408 MHz probes are within the large cavity. They are supported at each end, with the inner end insulated from the metal with a Teflon rod. The two inner rings set up the proper coupling at 1420 MHz between the flared waveguide and the large cavity for the optimum 1420 MHz radiation pattern. The innermost ring is connected to the circular waveguide.

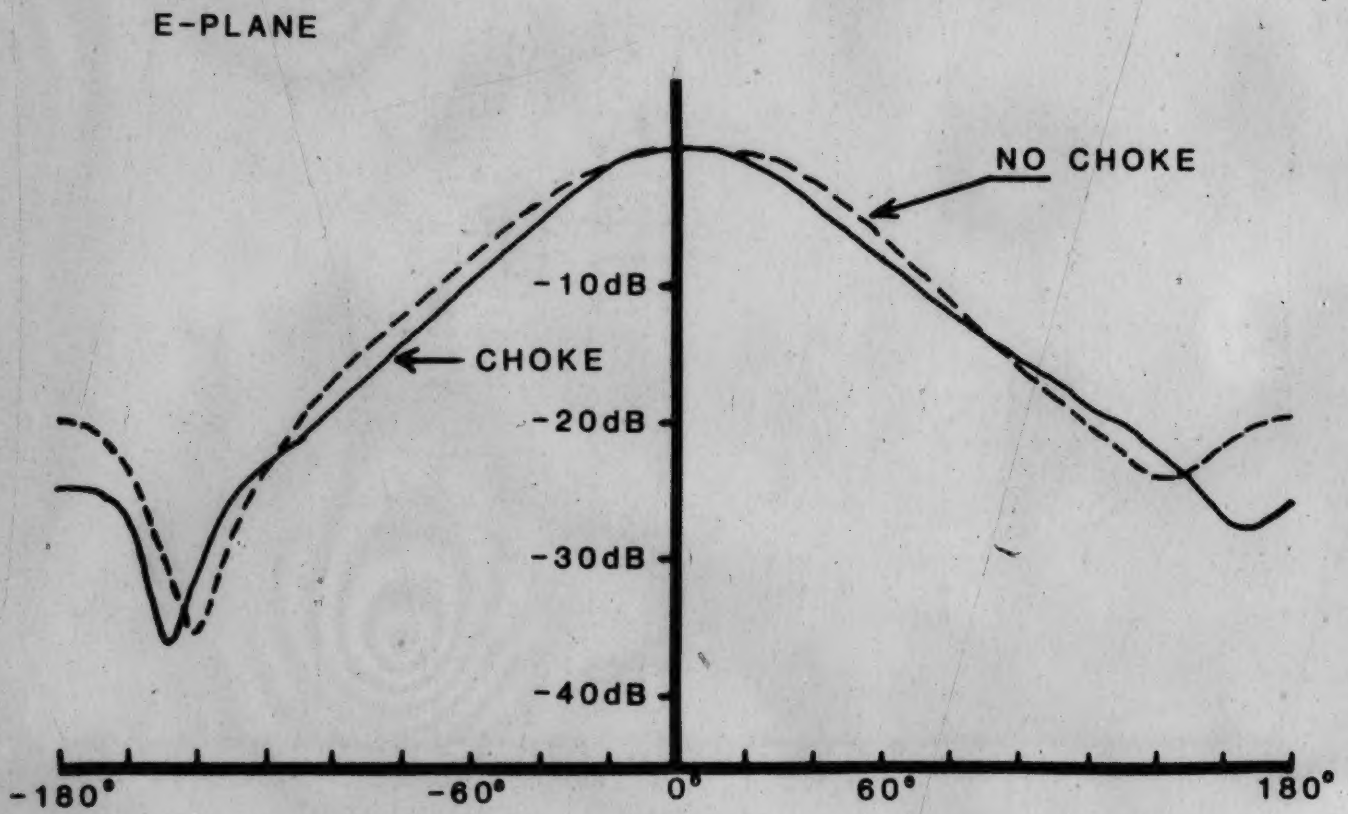

Radiation Patterns of Feed Horn at 408 MHz

Figure 2.6a

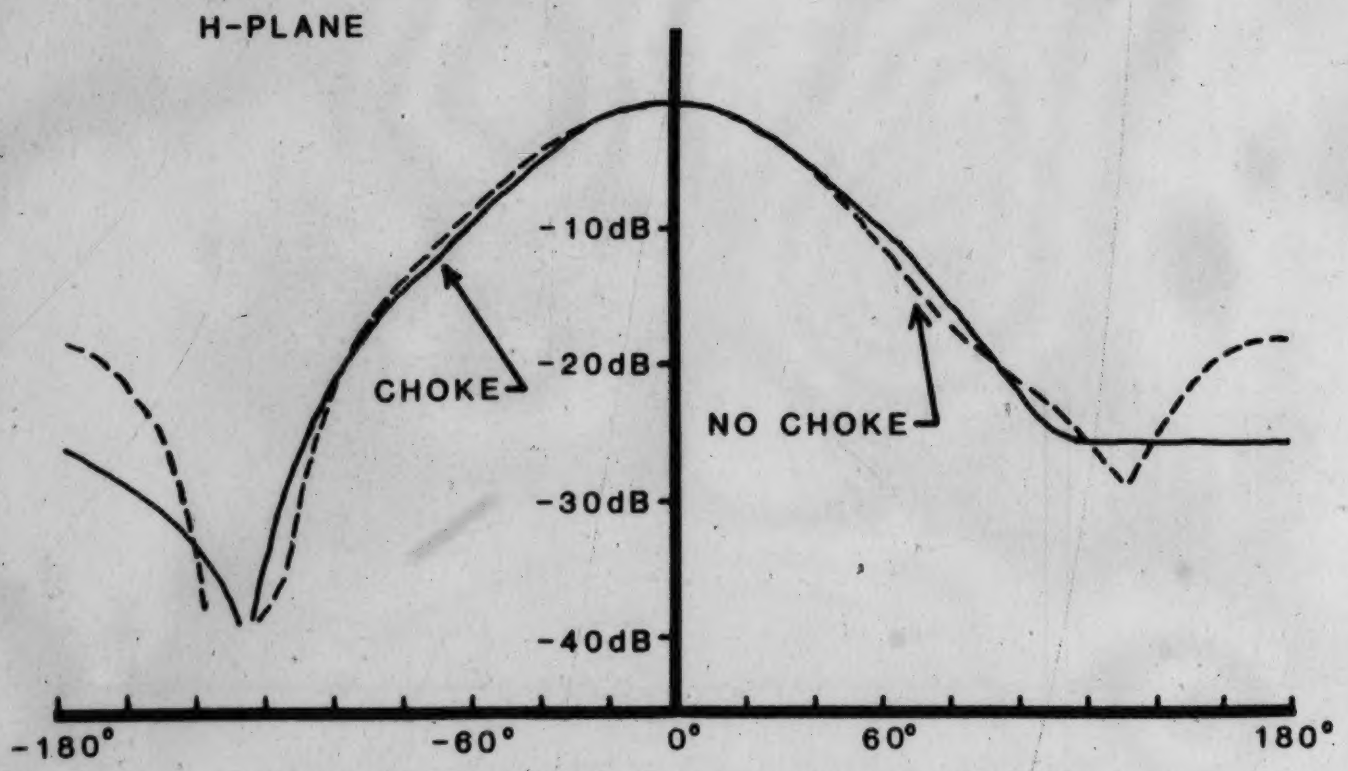

Radiation Patterns of Feed Horn at 408 MHz

Figure 2.6b

except that the edge illumination is greater: -6 or -7 dB compared with -10 dB. A boxing ring antenna also has a similar simple pattern, but edge illumination is between -18 (E plane) and -12 dB (H plane). It appears that the dual frequency horn is a compromise between a cylindrical horn and a boxing ring array. This is reasonable because the cavity is so short that the structure is in a transitional stage between a pure antenna array and a pure waveguide horn.

D. Combining Network

The last component of the feed to be discussed is a combining network that phases the four probes properly. Opposing probes must be fed in antiphase so that the electric field vectors set up in opposite sides of the feed cavity are coparallel, and the phase difference between orthogonal probes must be 90° so that circular polarization is received. A six-port device described by Saleh (1981) was used.

This network has appealing structural symmetry and simplicity; ten $\lambda/4$ 50Ω transmission lines are arranged in a ladder structure. The load impedances are also 50Ω. The four junctions on one side of the ladder are the antenna ports, and the junctions at the two corners on the other side are the receiver ports. The phase difference between two adjacent antenna ports is 90°, and the sign of the phase depends upon the receiver port used. Thus one port supplies right-hand circular polarization, and the other supplies left-hand circular polarization. The phase and amplitude characteristics of this device are summarized in fig. 2.7.

There are several subtleties in the operating characteristics of this device that should be mentioned. This device is really a special four-way power splitter/combiner. Power applied to a receiver port is equally divided among the 4 antenna ports, with 90° phase steps from port to port. Power applied to a single antenna port is also split equally four ways. Each receiver port receives 1/4 of the power, as do each of the adjacent ports, but with equal phase. If independent sources are attached to all of the antenna ports, this power division scheme remains true. Thus if each source supplies equal power then each receiver port receives that same amount of power, namely one quarter of the power from each of four antenna ports. The remaining power is dissipated in the sources. This is significant because it means that if four independent, equal intensity sources are connected to the four input ports, the output is the same as if the network had only one source and one input. This is an important result for the noise measurements to be described later.

Sources in the sky provide coherent sources. Opposing probes supply signals with a 180° phase difference to two ports separated by a third port. This middle port receives an equal fraction of the power from the two other ports, which each undergo identical phase shifts, and arrive out of phase. Therefore the signals cancel. This power

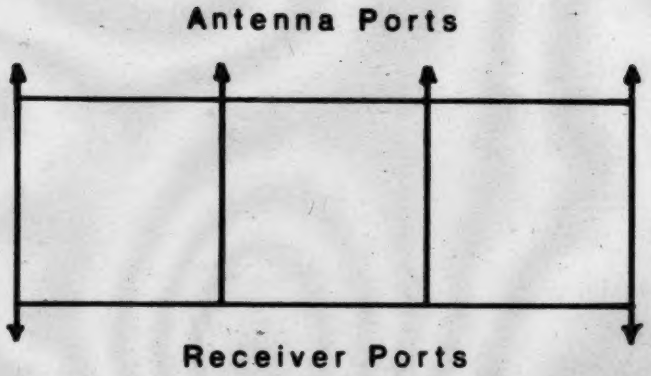

All coaxial cable lengths between junctions are λ/4. Cable characteristic impedance equal to load impedances. At junctions, centre conductors joined together and shields joined together.

Combining Network Construction

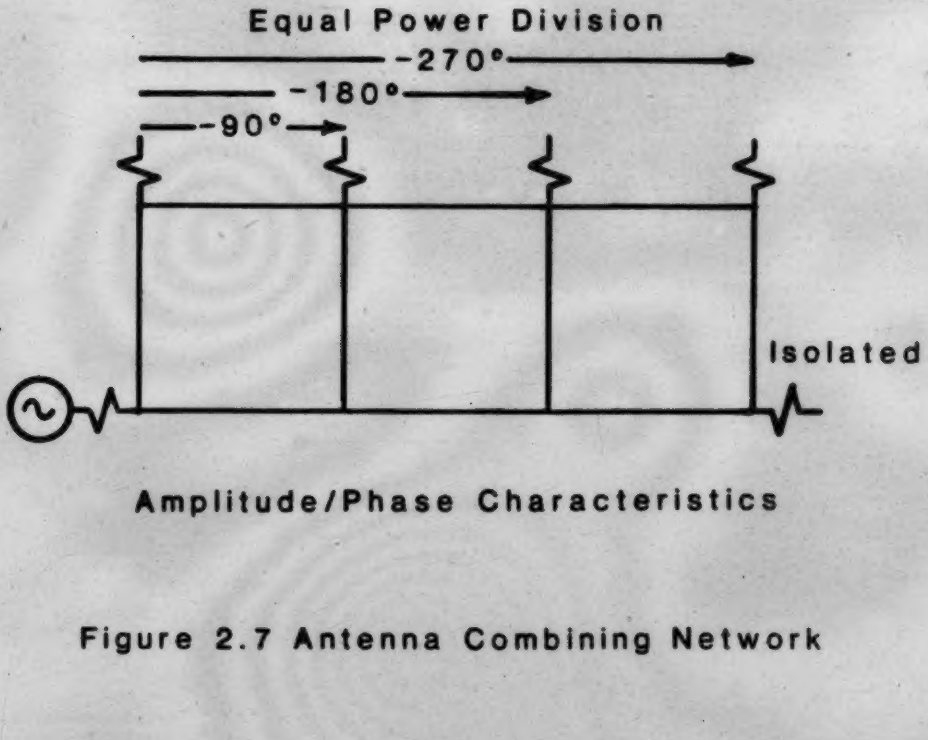

Amplitude/Phase Characteristics

Figure 2.7 Antenna Combining Network

appears in the receiver ports. The distribution of the power between the two receiver ports will depend upon the polarization characteristics of the celestial source. With a randomly polarized source or linearly polarized source, the power is equally divided between the two receiver ports, since the wavefront can be decomposed into two circularly polarized components of equal intensity. If the source is partly or wholly circularly polarized, then one port receives more power than the other.

The network was constructed of ¼" diameter semi-rigid coaxial cable. Since phase shifts were obtained through time delays, the network was frequency sensitive. In addition, because of slight variations in cable lengths and network construction, the phase differences between pairs of antenna ports were not the same, nor precisely 90°. The lengths used were therefore cut by an iterative process.

Deviation from 180° between opposing probes results in steering the feed radiation off axis. Using trigonometry and invoking a $\sin(x) \approx x$ approximation, it can be shown that this phase or delay error (d) slews the antenna pattern by:

$$\theta \cong 11 \frac{d}{s} \; [\text{ degrees}]$$

If the spacing, s, between the probe feed points, is 55 cm, the equation becomes:

$$\Theta \equiv \frac{d}{5} \text{ degrees}$$

with the phase error d expressed in degrees. The worst measured error at the band edge was 5°, which means that the feed will be pointing about 1° off centre. This is a trivial amount since the reflector subtends 120° at the focus.

The accuracy of the 90° phase shift determines the feed's response to circularly polarized radiation. The most common description of circular polarization uses two electric field vectors, both temporally and spatially in quadrature. Mathematically this can be written:

$$\begin{aligned} E(t) &= A \cos \omega t \, \mathbf{a}_x + A \cos (\omega t - 90°) \, \mathbf{a}_y \\ &= A \cos \omega t \, \mathbf{a}_x + A \sin \omega t \, \mathbf{a}_y \end{aligned}$$

with $\mathbf{a}_x$ and $\mathbf{a}_y$ designating orthogonal unit vectors perpendicular to the direction of propagation. Now suppose that there is a phase error of ε. This error can be evenly distributed between the x and y components:

$$E(t) = A \cos(\omega t - \frac{\varepsilon}{2}) \quad \mathbf{a}_x \quad + A \sin (\omega t + \frac{\varepsilon}{2}) \quad \mathbf{a}_y$$

Using trigonometric identities and rearranging:

$$E(t) = A \cos \frac{\varepsilon}{2} \, [\cos \omega t \;\; \mathbf{a}_x + \sin \omega t \;\; \mathbf{a}_y \,] + A \sin \frac{\varepsilon}{2} \, [\sin \omega t \;\; \mathbf{a}_x + \cos \omega t \;\; \mathbf{a}_y \,]$$

The left hand term represents a counter-clockwise rotating vector, and the right hand term represents a clockwise rotating vector. For small errors the relative response of the feed to the unwanted sense of polarization is

$$R = \frac{\sin\frac{\varepsilon}{2}}{\cos\frac{\varepsilon}{2}} \cong \sin\frac{\varepsilon}{2} \cong \frac{\varepsilon}{2}$$

$$\cong \frac{\varepsilon[\mathrm{deg}]}{120}$$

If the error is 5°, then the ratio of the field amplitudes is 1/24 or about 0.04 or -27 dB. In practice this ratio will be better, since the above worst-case value is only a spot value at the edge of the band. The receiver uses broadband noise and spot values away from this band edge will have a smaller R.

So far only the phase response of the combining network has been discussed. The amplitude response, or the network losses, are also very significant since the signal power is multiplied by a factor α, and noise power equal to $(1-\alpha)kTB$ is added. By measuring the noise added to the network by a resistive noise source, the loss was determined.

A Dicke total power receiver was used to measure the losses of the combining network and the cables that join this network to the feed horn. A well matched termination immersed in liquid nitrogen was used as a noise source. This load was used because its noise temperature was not excessively large compared with the increase in noise due to the device under test. Consider the measurement of the losses in the coaxial cable (0.73 metres of RG-214) that runs from a probe to the network. First, the temperature of the load alone was measured with the Dicke receiver. Next the cable was placed between the load and receiver and the temperature measurement was repeated. The loss of the cable was then determined using this set of equations:

$$T_1 = T_{load}$$

$$T_2 = \alpha T_{load} + (1-\alpha)T_{ambient}$$

Each of these cables has 0.09 dB of loss and thus adds 6K of noise. To measure the losses of this network, it was necessary to connect cold loads to each input. Since these are independent noise generators, these 4 ports with 4 loads behave like a single port and a single load, and the measurement technique is the same as with the piece of cable. The loss of the network was found to be 0.04 dB, which increases the noise temperature by 3K. The total contribution of the network and cables is 0.13 dB or 9K.

These numbers are similar to those obtained by multiplying the cable lengths by the specified loss per unit length. For both RG-214 cable and ¼" O.D. semi-rigid coaxial cable the loss is 0.15 dB/metre. The calculated loss for 0.73m cable is 0.11 dB. The combining network is made of 10 pieces 0.13m long, so the average path length from antenna port to receiver port is $10 \times 0.13/4 \cong 0.3$m and the average loss is 0.05 dB.

The feed and combining network have so far been treated separately; now they will be considered as a unit, for the characteristics of one device can be affected by the properties of the other. A good example of this is the isolation of one receiver port from the other, which depends upon the quality of the match of the loads on the antenna ports. With 50Ω resistive terminations on the antenna ports, the isolation is greater than 35 dB from 400 to 418 MHz. However, the feed probes do not have as high a return loss as the loads, nor do they have a high level of mutual isolation. These result in power being reflected back into the network. One way to understand what occurs with a reflection at the base of the probes is to replace this feed with an ideal feed behind a partially reflective plane. A circularly polarized wavefront is generated by transmitting through the antenna. Part of this wave is reflected, and the reflection changes its hand of polarization, thus the reflected power must end up in the port other than the one connected to the transmitter. The measured isolation is greater than 10 dB between 398 MHz and 412 MHz and averages 13 dB in a 4 MHz band centred on 408 MHz. This means that the system temperature of a receiver connected to one port will increase by a fraction of the equivalent noise temperature of the load on the other port. 13 dB translates to a power ratio of 1/20, so an ambient temperature load increases the system temperature by 300/20 or 15K, and a GaAsFET low noise amplifier ($T_{input} \cong 70K$ measured) used as a load (Frater and Williams 1981) produces an increase of 70/20 or 3.5K.

This effect also makes the match to the probes appear better than it actually is. This is because the network tends to divert power reflected by the loads away from the source, as explained above. The measured return losses for the feed horn with combining network is shown in Fig. 2.8 for both hands of polarization. Comparison to the single probe return loss in Fig. 2.5 will show the dramatic improvement in matching due to the network.

E. Frequency Independence Measurements

One of the most important specifications for the dual-frequency modification was that degradation of the primary frequency characteristics was unacceptable. A number of measurements indicate that the 408 MHz modifications have no significant effect on the 1420 MHz performance.

To determine if the 408 MHz feed structure modified the 1420 MHz field distribution, the 1420 MHz radiation patterns were measured with and without the 408 MHz probes. Small changes in the edge illumination were observed, but the magnitude of these changes was of the same order as the difference between repeated pattern measurements, with identical feed configurations.

Another way to measure the interaction between the two sets of probes is to measure the transmission from one set to the other set. The attenuation at 1420 MHz for a signal path from the 408 MHz probes through the 408 MHz combining network into the 1420 MHz probes was greater than 26 dB. Thus noise from the 408 MHz system will be reduced by at least a factor of 500 when it reaches the 1420 MHz receiver. At

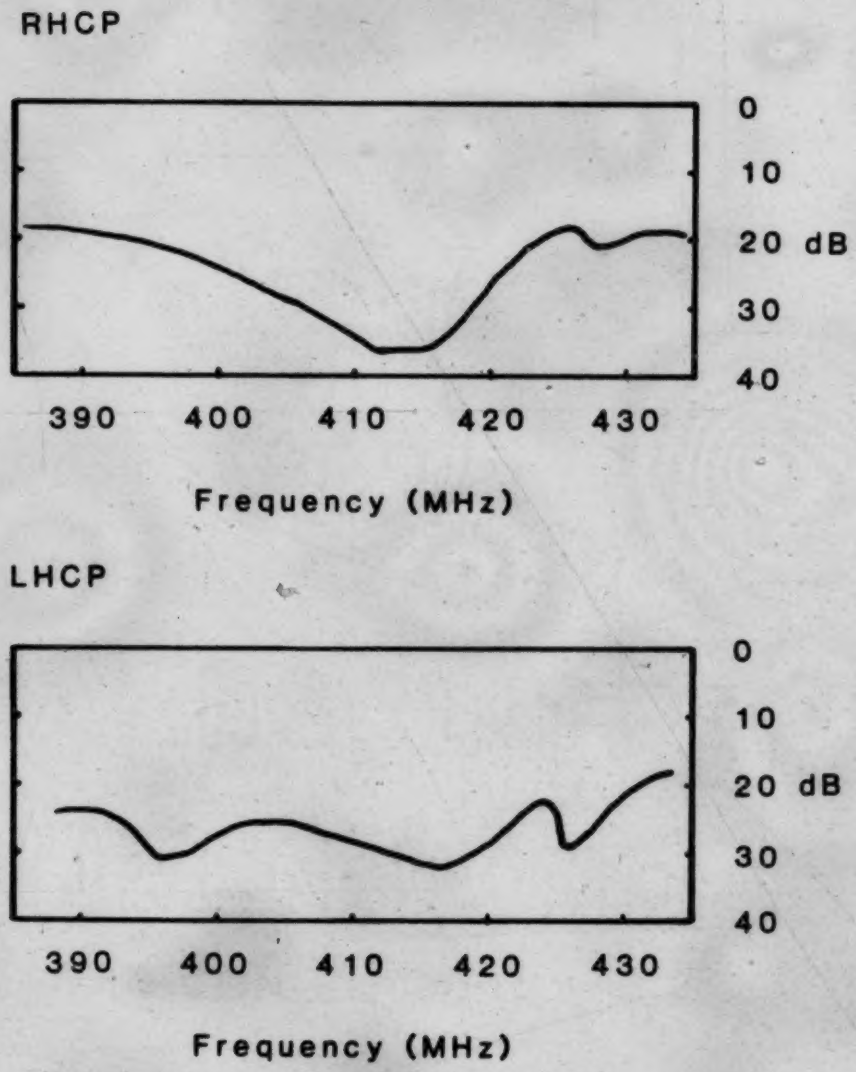

Figure 2.8 Return loss of entire feed system: feed horn, cables, and combining network. Each receiver port was measured with the other port terminated.

1420 MHz, the effective noise temperature of a 408 MHz GaAsFET LNA input is about room temperature and the increase in system temperature should be less than 0.6K.

Another way that coupling can occur is if waves coming out of the waveguide are reflected back into the waveguide by the 408 MHz probes. This possibility was tested by injecting a signal into one 1420 MHz probe, and measuring the coupling into the other probe. Because of the quarter-wave plate, a circularly polarized wave is launched, and any reflection would change the sense of rotation and emerge from the other probe. The coupling was measured both with and without the 408 MHz probes in place. This was found to be -18 dB and -19 dB respectively which is an insignificant change.

So far no mention has been made of coupling from the 1420 MHz probes into the 408 MHz probes at a frequency of 408 MHz. Since this frequency is below cutoff for the 14.95cm diameter waveguide, this interaction should be extremely small.

F. Performance on Dish

The most important test of a feed is to place it on a reflector antenna (see Plate 2.2) and to measure the performance of the combination. Characteristics that can be measured are the antenna pattern, aperture efficiency and spillover. The antenna pattern or primary pattern determines the area of the sky -

known as the field of view - that can be mapped in one survey. The aperture efficiency is a measure of the sensitivity of the dish. This is determined partly by the radiation pattern of the feed antenna. Spillover is response of the antenna to sources outside the main beam (primarily thermal radiation from the ground) via a direct path to the feed that does not include the reflector surface. These measurements were made using standard techniques involving a Dicke switch total power receiver and astronomical sources.

1. Dish Radiation Patterns

The antenna patterns were measured in two principal planes: declination, which involves scanning the dish in a north-south direction; and right ascension, which requires either mechanically scanning the dish east-west, or allowing the earth's rotation to sweep the beam through the test source. The test sources were Cassiopeia A, a supernova remnant which is a bright centimeter-wave source, and the sun. The large signal-to-noise ratio for these sources permitted the pattern to be measured rapidly and accurately. The half-power points were found to be separated by 5.3° in both right ascension and declination planes. The power response of the Far West dish in the declination plane is illustrated in Figure 2.9.

PLATE 2.2

FOCUS BOX

This box contains the receiver electronics. In front of the box, at the prime focus, is the feed. The box is insulated and temperature controlled to keep the electronics at a constant temperature. On the right-hand side of the box is the thermoelectric heater/cooler device. Several cables can be seen running from the back side of the horn into the focus box. These carry the signals from each 408 MHz probe to the combining network inside the box. The 1420 MHz signals enter the box via the circular waveguide. The cables running along the support legs to the side of the box carry LO and IF signals as well as power and monitoring signals.

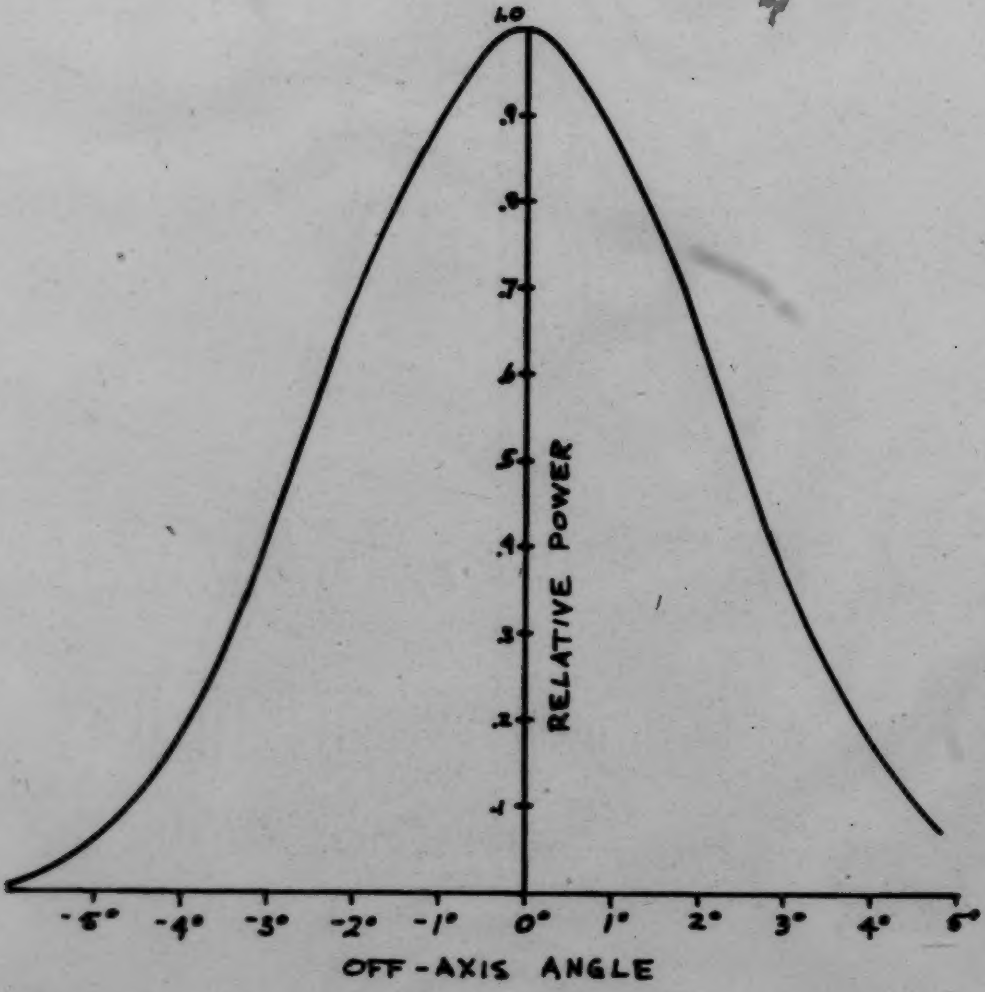

Figure 2.9 408 MHz Primary Radiation Pattern

2. Aperture Efficiency

The aperture efficiency is simply the ratio between the power out of a receiver connected to the actual antenna and the power out of the same receiver connected to an ideal antenna of the same cross-sectional area that delivers all the energy that it intercepts to the receiver. Again, Cas A was used as a test source. The flux was calculated using information from Baars et al. (1977). The efficiency was found to be 60% at 408 MHz and 54% at 1420 MHz.

The relatively high efficiency at the low frequency is probably another result of the shape of the feed pattern. At 408 MHz, the edge of the dish is illuminated more strongly than at 1420 MHz, so more of the collecting area is utilized and the higher efficiency results. The 1420 MHz efficiency is very close to that measured with a prototype feed without the 408 probes. This is further confirmation of the isolation between the two receiving frequencies.

3. Spillover

The spillover measurement involved an absolute measurement of the power out of a combining network antenna port with the antenna pointing at the zenith (at empty sky). The temperature scale of the receiver output was calibrated with precision 50Ω terminations at liquid nitrogen (78K) and boiling water (373K) temperatures. Then known losses and sources of noise were subtracted to obtain the amount of noise due to spillover. This calculation follows:

T_{zenith} (typical)		85K±1K
Galaxy (typical) (Pauliny-Toth and Shakeshaft 1962)		-21K±2K
Antenna Losses:		
Unused port	15K±1K	
Combining network	3K±1K	-24K±2K
Cables	6K	
Solar noise		-10K±5K
Spillover		30K±10K

In practice the zenith antenna temperatures will be lower than those given here. The load on the unused receiver port couples to the receiver input via the combining network, increasing the system noise temperature. When these measurements were made, this port was terminated with a 50Ω dummy load at ~300K, but it is now terminated with a room temperature GaAsFET amplifier. The effect of this amplifier is the same as that of a termination at 70K. Thus the contribution of the unused port will drop from 15K to 3.5K, and the zenith temperature will be at least 73K.

The antenna temperature was also measured at elevation angles ranging from near zero (pointing at the horizon) to 90° (pointing at zenith). The sky contribution to the antenna temperature obtained from Pauliny-Toth and Shakeshaft (1962) was then subtracted at each of these points. The antenna temperature was constant within ±3K until the antenna beam neared the horizon, where it began to increase. When the dish was stopped by the horizon limits in the pointing mechanism, the antenna temperature had risen by 3K.

G. CONCLUSION

The 1420 MHz feed horn has been successfully modified to simultaneously receive 408 MHz radiation. This was done without noticeable degradation of 1420 MHz performance.

The performance of the antennas at 408 MHz can be summarized:

HPBW = 5.3°

Antenna temperature (less sky) = 52K±4K

Spillover = 30K±10K

Aperture efficiency = 60%

Bandwidth ≅ 20 MHz

CHAPTER 3: 408 MHZ RECEIVER

A. The General Problem

The problem that was set before me was to develop four parallel receivers that are sensitive enough for radio astronomy applications and also stable enough to be used to produce images of the sky. The need for sensitivity is obvious: the receiver-generated noise must not be large enough to overwhelm the signals from weak sources in the sky. The stability - amplitude and phase - requirement is necessary because of the way that the images of the sky are made. As explained earlier, the sky is sampled by the interferometer fringes. The visibilities or Fourier components not only depend upon what is in the sky, but also the amplitude and phase characteristics of the receivers. When the image is formed by summing the Fourier components, if the amplitudes and phases of the receivers are not what one believes them to be, the image will not be constructed correctly. Each of these areas of concern - sensitivity, gain stability, and phase stability - will be discussed separately and explained below.

First, the major building blocks of a radio astronomy receiver will be outlined. A very basic receiver is shown in fig. 3.1. Remember that an interferometer requires at least two of these receivers. The problem is to make each receiver operate in a very similar manner with respect to all the others. What makes the

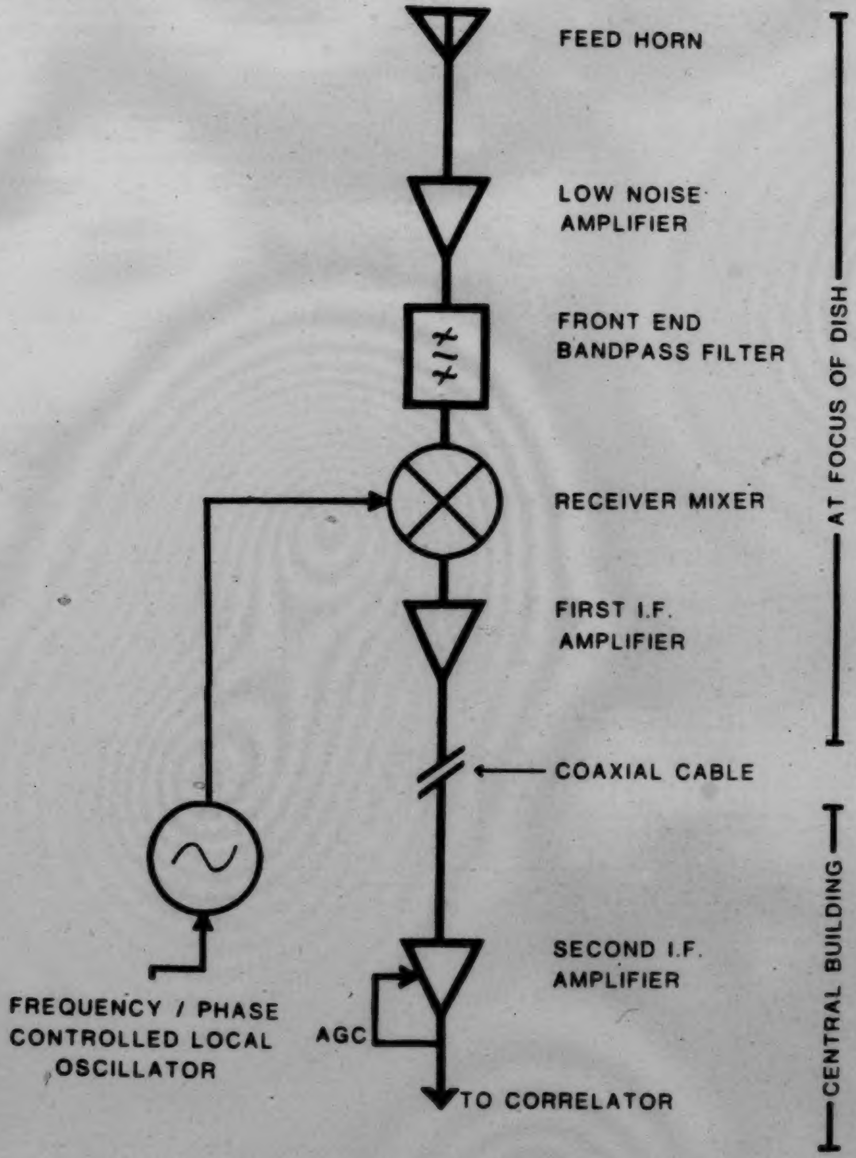

BLOCK DIAGRAM OF A RADIO ASTRONOMY RECEIVER SUITABLE FOR USE IN AN INTERFEROMETER

Figure 3.1

situation more difficult is that the receivers are in separate enclosures and run from separate power supplies. In spite of this, several control systems can be used to stabilize the receiver. These circuits were one of the main areas of interest of this project.

After the signals from the sky are collected by the feed horn, they are amplified by a low noise amplifier (LNA). Contrary to common communications receiver design principles, the front end bandpass filter follows the first stage of gain. It is very important to maintain a high signal to noise ratio, and loss before the first stage of gain would result in an increase of noise. Communications receivers often place filters preceding any gain because they are tuned to frequency bands that have many strong carriers. Without the filter, the front end amplifier might be pushed into saturation by a strong signal. This could desensitize the receiver or produce spurious signals through intermodulation in the amplifier. The increase in system noise is often not as important with communications receivers, because of the greater signal levels of man-made radio sources. Near the 408 MHz observing band are several frequencies used by both terrestrial users and satellites. For this reason the design of the front end had to take into consideration potential man-made interference.

Following the LNA and filter is a mixer which converts a band of signals centred on 408 MHz to a band centred on 30 MHz, the intermediate frequency (IF). A commercial double balanced diode mixer was used here.

The IF amplifier frequency is 30 MHz. The signal frequency is nominally 408 MHz, so an LO frequency of 378 MHz was chosen. A signal at 348 MHz will also produce a 30 MHz output, but the input filter rejects this "image" frequency.

A tuned IF preamplifier follows the mixer. Commercially available amplifiers are used since some very high quality units are available, and considerable effort would be required to build an amplifier that would be equal in performance. The IF preamplifier is placed preceding the cable to compensate for the cable losses and hence maintain a low system temperature.

After travelling down the transmission line to the Synthesis Telescope building, the IF signal is again amplified. This IF amplifier has higher gain and a narrower passband than the previous stage. In addition, its gain can be controlled with a voltage. A portion of the output is sampled and rectified, and processed to provide a voltage to adjust the gain to keep the output power constant. If the input power to the receiver is constant, a reasonable assumption since the dishes point at the same area of the sky during the entire observation, then this automatic gain control (AGC) circuit will keep the receiver gain constant. The amplified IF signal is then passed to the Digital Signal Processor (DSP) where it is correlated with signals from the other receivers (Lo 1982).

Local oscillator (LO) circuitry is located at both ends of the cable. This system makes the signal phase from sky to correlator entirely independent of the length of the coaxial cable connecting the antennas to the central receiver. This device is very important since the cable is not in a controlled environment like the rest of the receiver. It is subject to large and sometimes rapid temperature variations which change the cable length. Designers of other synthesis telescopes either attempted to control the cable temperature or else used a local oscillator that produced a constant phase to the mixer. This local oscillator is the first known system to stabilize the phase to the IF output. Because the Digital Signal Processor does the fringe derotation after correlation, the LO phase does not have to be continuously variable. It is switched in 180° steps to reject common mode errors. It is also switched 90° for calibration of the real and imaginary channels of the correlator.

The system design specifications for the 408 MHz receivers should now be stated:

- centre frequency of 408 MHz, tunable ±3 MHz to avoid interference;
- 4 MHz IF bandwidth;
- low system temperature

- low susceptibility to man-made interference;
- very stable gain;
- stable phase characteristics;
- LO phase controllable in accurate 90° steps;
- subsystems must share a single coaxial line between antenna and centre of interferometer.

Now the design philosophy used will be set forth:

- the system engineered is not an experiment, it is a permanent addition to a research instrument, and was constructed with this point in mind.
- the new system must use existing observing and map production software with a minimum of modification.
- commercially available devices such as amplifiers and filters were purchased unless there was a definite advantage in constructing the device. The wheel has been invented one too many times.
- the use of necromancy was avoided, since the equipment will be repaired and possibly duplicated without my attention.
- everything was made as simple as possible, but not simpler (Einstein).

The development of this receiver will be discussed in four parts:

- the front end, the mixer and receiver sensitivity;
- the IF amplifiers and receiver gain stability;
- the local oscillator system and receiver phase stability;
- system tests.

The LO system design is unique and therefore many pages will be devoted to its development. Other subsystems are more conventional and were either commercially built or were developed by other workers, and thus will be covered in less depth.

B. Receiver Front Ends

The 408 MHz front ends consist of two stages of low noise amplification separated by a bandpass filter. In the development of the front ends, low noise figure and good large-signal handling capabilities were of prime concern. This arrangement gives a system temperature of about 104K, 50K of which is due to the low-noise amplifiers.

Commercial low noise amplifiers (LNAs) constructed with bipolar transistors were originally purchased for the 408 MHz receivers. The specified noise temperature of these amplifiers was 120K, but all the units were tested and the noise temperature was found to be about 180K. This was too large to be acceptable. Unfortunately a manufacturer of a superior amplifier could not be found. However, 400 MHz is high enough that 1/f noise becomes insignificant in gallium arsenide field effect transistors (GaAsFET) (Cooke 1982). At least one semiconductor manufacturer claimed to make GaAsFET devices with a noise figure of 0.5 dB or 35K at 400 MHz. In addition to the superior noise performance, GaAsFETs are much more linear than bipolar transistors and are thus less prone to intermodulation. A design existed for amplifiers built with GaAsFETs (Galt, personal communication) so it was decided to have a technician construct and adjust a set of amplifiers. This circuit is shown in Fig. 3.2.

In the adjustment of these amplifiers several factors and variables had to be considered. Of course minimum effective noise temperature and maximum gain were desired. The amplifiers also had to be stable for the loads that they would be attached to. To satisfy these requirements, the drain current and drain voltage were varied, as well as the input and output matching networks. As suggested by Weinreb et al (1982), a small inductance was placed between the source leads and ground to improve the input match (Anastassiou and Strutt 1974). With these particular LNAs the improvement was minimal.

One major problem encountered with this design was a tendency for the amplifier to oscillate in the vicinity of 4 GHz. The solution was to place a small piece of conductive foam near the input inductance. The foam is carbon impregnated and is often used to protect integrated circuits from static damage. The foam was kept small to minimize

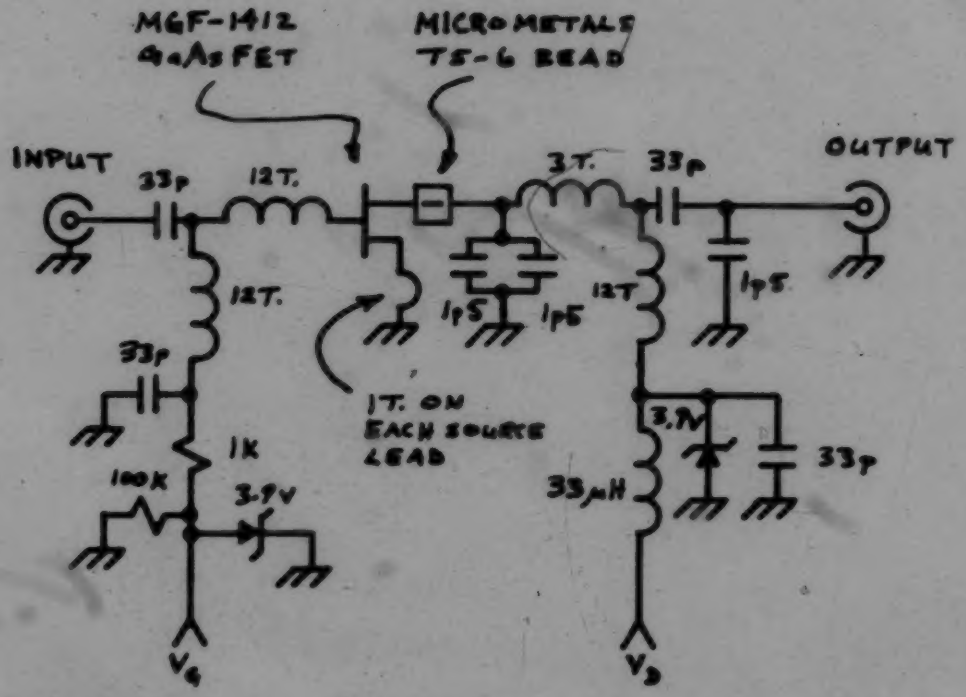

ALL INDUCTORS #30 WIRE ON 0,215 cm FORM.

Figure 3.2 GaAsFET Low Noise Amplifier

losses at 408 MHz, yet large enough to reduce the gain at the higher frequencies, stopping the oscillations. This lossy foam technique is akin to the use of ferrite beads, and other workers have had to resort to this method of amplifier stabilization. After this was done, I_D and V_{DS} were adjusted for optimum noise figure and gain. The stability was verified by subjecting the LNA to various loads that could be encountered in the receiver as well as open circuits and short circuits.

After discussion with the Department of Communications, and some interference monitoring, it became apparent that there would be man-made signals near the observing band. Thus the receiver was deliberately designed to be less sensitive to interfering signals with very little reduction in sensitivity to radio astronomy sources.

Traditionally, radio astronomy receivers have been built with the LNA following the antenna and preceding the front end filters. If a loss precedes the LNA that attenuates the input signal by a factor α, the increase in noise temperature is $(1-\alpha)T_a$ where T_a, is the physical temperature of the lossy device. T_a is usually about 300K. Most filters have an insertion loss of several decibels. Suppose that the loss is 2 dB or 0.63, then the increase in system temperature due to the loss is 110K, which is not acceptable for low noise receiving systems. Thus radio astronomy receivers usually have no filters before the LNA save for the frequency selectivity of the antenna. This unfortunately makes the front end very susceptible to out-of-band interfering signals.

The type of interference that was of most concern was intermodulation distortion. In a non-linear device, many possible combinations of these intermodulations are produced, and the danger is that two out of band carriers may generate a third signal within the observing band.

The noise figure was compromised slightly to obtain better protection from interfering signals by placing a filter between the two amplifier stages. The gain preceding the filter is 15 dB, and the increase in temperature due to the 2 dB filter loss is about 3K. Although the first stage of amplification is subject to a wide band of signals, perhaps including strong man-made signals, the second stage receives only a select fraction of this spectrum, hopefully without interference. Without the filter, out-of-band signals may be amplified to a level by the first stage sufficient to cause intermodulation distortion in the second stage.

The question now arises concerning the amount of increase of noise that can be afforded. What is important is not simply the absolute increase, but the increase relative to other noise sources in the system. The system temperature, including the minimum galactic contribution, was found to be about 125K. If the location of the filter has resulted in a change of 3K, then the signal to noise ratio has been reduced by 2½%. It was felt that the slight increase in system noise due to the front end configuration was worth the added interference protection.

The performance of the front end low noise amplifiers consisting of two amplifier stages connected through a 408 MHz bandpass filter was measured. The typical noise temperature of these units at 408 MHz was 50K±10K. The bandwidth between the points where the noise temperature rises to 80K was typically 15 MHz. The gain of the sets of amplifiers varied between 25 and 33 dB, depending on the unit tested. The return loss of the input and output ports averaged 14 dB.

An interesting property of low noise amplifiers is that the equivalent noise temperature of the input can be lower than the physical temperature of the device (Percival 1939, Frater and Williams 1981, Forward and Cisco 1983). The noise power emerging from the inputs of the LNA's was measured and found to be equivalent to a resistive load at 70K. Extra amplifiers were constructed and used as loads on the unused receiver port of the feed combining network. Since the amount of coupling between the used and unused receiver ports is 1/20, changing the load temperature from 300K to 70K has reduced the noise added to the system from 15K to 3.5K. With a system temperature of 104K, this means that the signal to noise ratio has been improved by about 10%.

A readily available commercial mixer was used for the receiver mixer. The device is a double balance mixer with a ring of four diodes. The conversion gain is about 1/4 or -6 dB with a local oscillator signal power of 5 mW or +7 dBm. The IF output of the mixer goes to the IF preamplifier stage.

The sensitivity of the synthesis telescope to a point source is an important statistic. Napier and Crane (1982) show how the following relation is obtained:

$$\Delta S = \frac{2\sqrt{2}\, k\, T_s}{\sqrt{Btc}\; n_c n_a A_a}$$

ΔS = noise power

k = Boltzmann's constant = 1.38×10^{-23} Joule/°K

T_s = system temperature = 104K

B = receiver bandwidth = 4 MHz

t = observing period = 12 hr.

c = number of correlations = 140 (for full survey)

n_c = correlator efficiency = 0.89

n_a = aperture efficiency of antenna = 0.6

A_a = antenna area = $\pi(4.5\text{m})^2$

For a full survey (140 spacings or 35 days) the rms noise is 2.4 mJy/beam.

C. Automatic Gain Control

Each visibility measurement of the sky consists of two numbers: the amplitude of the correlated signal; and the phase difference. If there is an error in the amplitude of the visibilities, then the strength of the mapped sources will not be known for certain. If this error varies with time, then the noise level of the map will increase since the Fourier components (or visibilities) will not add together in a way that tends to cancel the side lobes. Thus for the best map, the visibility amplitudes must be well known which is ensured if the receiver gains are kept constant.

The maximum allowable error in the gain should be determined. Experienced interferometrists at Cambridge (Baldwin and Warner 1979) state that most interferometers are capable of a gain stability ($\Delta G/G$) of 1%, and that better amplitude stability would not be useful because it would be hidden by phase errors.

One way to control the receiver gain is to receive a signal of constant intensity, and adjust the gain to keep the output level constant. Fortunately, there is one such signal that is inherent to the system: the system noise. The receiver noise originates from many sources: the receiver mixer; the low noise amplifiers; losses in the cables to the horn, the combining network, and the horn itself; spillover; the galactic background; and the source being mapped.

Assuming that these stay constant, and that a reference voltage level stays constant, then a difference amplifier can compare the output level to the reference level and adjust the IF amplifier gain to counteract any changes in gain between the antenna and the IF amplifier's output.

The AGC circuit used is shown in Fig. 3.3. The IF amplifiers used have two outputs: an intermediate frequency output and a video (or rectified) output. The IF output goes to the correlator and the video output is used by the AGC amplifier. The amplitude of the video output represents the output signal level. This signal is filtered in an R-C circuit and is applied to the inverting input of an operational amplifier. The non-inverting input is connected to a voltage reference formed by an adjustable resistance wired into a voltage divider. The difference between these two inputs is amplified and is applied to the gain control voltage input of the IF amplifier. Thus this closed-loop tends to minimize the difference between the reference and the video output, keeping the IF output level constant.

The AGC itself creates a problem. It keeps the output power of the receiver constant irrespective of the brightness of the region being mapped. Thus the system gain will be different for sources that produce a different antenna temperature. This multiplies the source brightnesses in the map by a factor that is constant across the map. The intensity scale of the map can be calibrated by multiplying the map

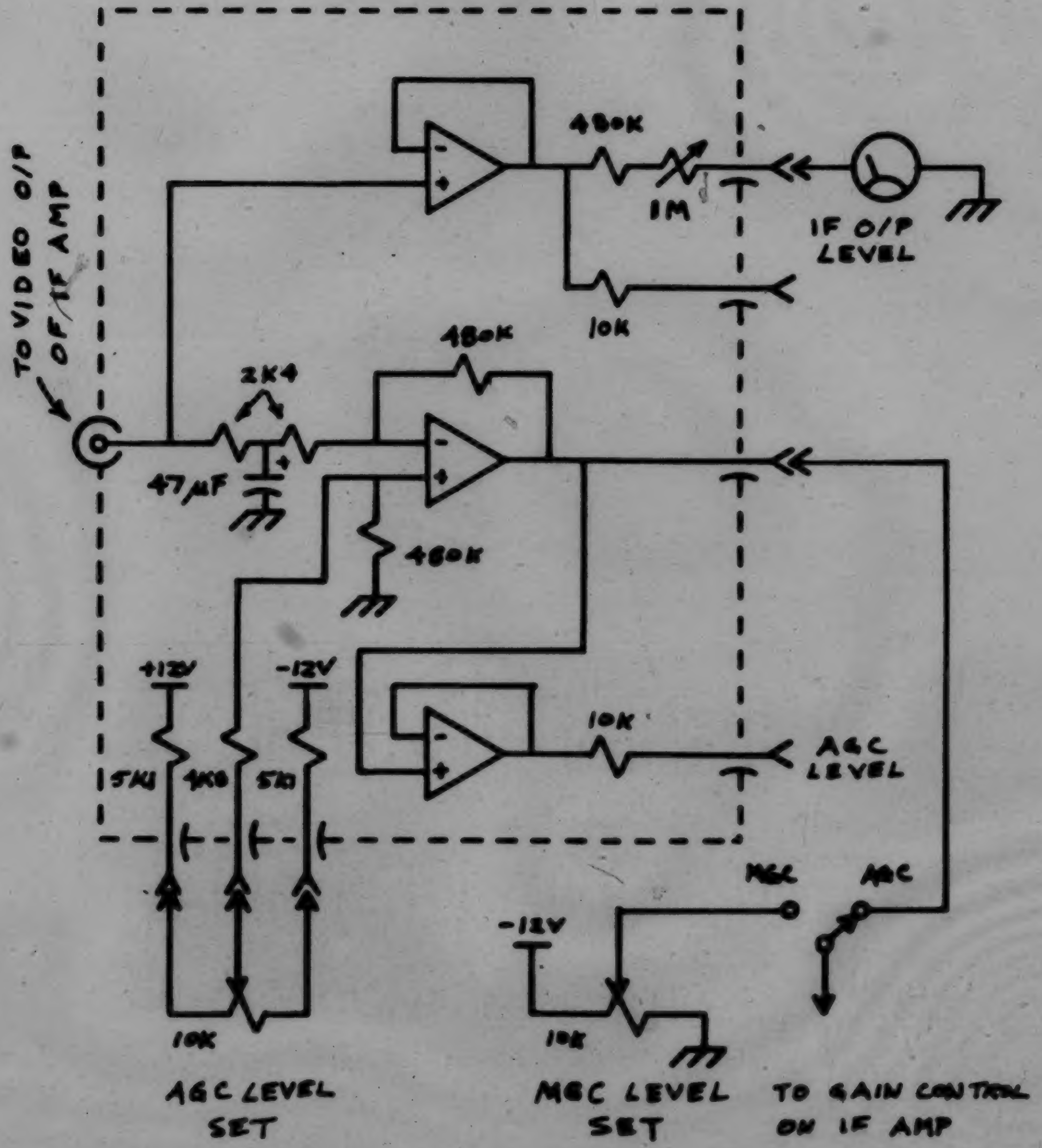

OP-AMPs: μA741

Automatic Gain Control

Figure 3.3

by the system temperature correction. This correction factor can be obtained by dividing the system temperature with a dish pointed at a region of the sky with a known temperature by the system temperature of the dish pointed at the mapped region.

Another reason to use an AGC circuit is to keep the rms input levels to the analog-to-digital conversion circuits, known as quantizers, constant. The input signals are quantized to one of three possible levels. The decision levels are fixed, so for meaningful quantization, the input must not be too large nor too small.

D. The Local Oscillator System and Phase Stability

1. Need for Phase Stability

Phase stability is essential for an interferometer of this type, for without it images of the sky with correct absolute positions of sources cannot be made. The prime source of phase error is changes of length of the coaxial cable transmission line due to temperature changes. The system developed controls the phase from the output of the LNA to the output of the IF amplifier in the Synthesis Telescope building. With this system the change in IF phase for a change in transmission line length is at least 7 times better than would be expected for a system that only stabilizes the LO phase, and at least 90 times better than a system with no phase stabilization.

The relative phase between receivers making up an interferometer determines the position of the fringes in the sky. A phase error changes the position of the fringes and results in a position error of the Fourier components that form the the map. Since a point source is actually the sum of many Fourier components, random phase errors will tend to blur the point source. Equally important, at locations where there is no source, the components must add to zero, but errors may lead to a non-zero sum, which means that the noise level of the map has risen. An equivalent way of looking at this is that the synthesized beam has been broadened and reduced in amplitude and that the side lobe level has been raised. This kind of phase error with a synthesis telescope is analogous to errors on the reflecting surface of a filled aperture radio telescope and the effects are the same.

The question of specifying the maximum phase error now arises. One might get an estimate by considering filled aperture radio or optical telescopes. The maximum allowable rms error with these instruments is often specified as $\lambda/10$. This corresponds to a maximum rms phase error of 72°. Before this is applied to a synthesis telescope, one very important point should be kept in mind. That is, in a filled aperture each spacing is effectively measured many times, while with most synthesis telescopes there is no redundancy and each spacing is measured only once. Thus in a filled aperture telescope, many measurements are added together and the phase errors tend to cancel, while with a synthesis telescope, there is only one opportunity to measure the phase for one spacing, so the phase had better be right. Rahmat-Samii (1983) has calculated the radiation patterns for reflector antennas with random surface errors of various magnitudes. His results show a surface with λ/10 errors has a reduced main beam amplitude, -6dB in his examples, and increased sidelobe levels. He also shows that to maintain the correct sidelobe amplitude, the surface accuracy must be much better than λ/10. Dragone and Hogg (1963) have done a similar study, but out to higher order sidelobes. They show that to keep these sidelobe levels to within 3 dB of the ideal pattern the surface accuracy of the dish should be ±0.01λ or ±7° in phase. This suggests that the peak-to-peak phase error in a synthesis telescope should be smaller than 14° to produce a beam with sidelobes that have small deviations from their ideal values.

It is useful to consider the phase stability requirements for other synthesis telescopes. Based upon experience at Cambridge, Baldwin and Warner (1979) have plotted expected phase error due to the ionosphere verses frequency and baseline. For a 600m baseline at 400 MHz, their expected rms error is about 1°. For the design of the Very Large Array in New Mexico, Napier et al. (1983) specify a phase error of 1° rms per gigahertz. Based upon considerations such as these, it was decided to make the phase of the 408 MHz receivers as accurate as possible, preferably less than 1° rms.

Larger phase errors can be acceptable if adaptive-optics techniques are used. This is done to produce maps from Very Long Baseline Interferometers consisting of antennas scattered around the world (Steer 1984). However, these methods rely upon a large number of simultaneous correlations and a small number of uncomplicated source structures in the field mapped. The 408 MHz system has only four simultaneous correlations and will be used to map complicated objects that fill the field so these image construction techniques are not appropriate. In addition, one of the original specifications for this system was that it would use the same observing techniques and data reduction programs as used for 1420 MHz observations which depend on accurate phase.

2. Sources of Phase Instability

It should be clarified here that the phase stability that is of concern is the differential phase between antennas. There are a large number of potential sources of differential phase errors in the interferometer - virtually every component. Filters, amplifiers, mixers and transmission line, all change the phase of signals passing through them. On the short term, the phase characteristics of these devices are stable. As they age, these characteristics may change, but these changes are corrected by the routine calibration observations. One source of rapid phase changes is rapid temperature change. If all parallel sets of components undergo the same temperature change, and if all the components have similar characteristics, the differential phase will not change. To establish this situation, all components were either constructed as similarly as possible, or specified to be phase tracking when ordered. In addition, the components were placed in constant temperature environments at the focus of the dishes and in the Synthesis Telescope building. The temperature control in the focus boxes is held to within 1°C of 25°C, and to within several degrees in the Synthesis Telescope building.

The coaxial cables running from the receivers on the dishes to the central Synthesis Telescope building are not at a controlled temperature, and the characteristics of different cables may not be exactly the same. Although the phase temperature coefficient is larger for the short lengths of RG-214, the phase change will be dominated by the much longer Heliax cable. For a one degree increase in temperature, the phase of the output of the total cable length will change between -6° and -12° at 378 MHz, and it will change between -½° to -1° at 30 MHz. (The uncertainties are due to uncertainties in the manufacturer's specified phase temperature coefficient.) The frequency of 378 MHz was chosen because it is the ultimate local oscillator frequency. Even if a subharmonic of this frequency is sent down the cable, the phase gets multiplied along with the frequency when 378 MHz is generated, so the change in phase is the same as if 378 MHz were used. 30 MHz was also used in this illustration because it is the intermediate frequency. The phase change due to temperature would be unimportant if all the cables were always at the same temperature and the cables all had the same phase temperature coefficient. In that case the phases would all change by the same amount.

These two conditions are probably not met. According to the cable manufacturer's catalog, the phase temperature coefficient can vary by a factor of two. Although cables from the same lot probably have uniform coefficients, cables from different batches may have different coefficients. This variation is probably due to changes in the mean bubble size in the foam dielectric. Thus it cannot be guaranteed that pairs of cables will track each other in phase as the temperature changes.

It is also not a good assumption that all the cables are at the same temperature all of the time. Although the cables are buried except for about 50m (¼ of total length), the soil can be extremely dry at times, reducing the thermal capacity of the ground. This would make the ground a less effective filter to the daily temperature variations at the surface. The surface temperature can change rapidly and over an extreme range because of the observatory's location in a semi-arid mountain valley. Because of the large extent of the array (600m), the surface temperatures at one end of the array may differ by several degrees from the other end.

From these considerations it was decided that the cables alone did not have sufficient phase accuracy to distribute a local oscillator signal. Although at times the cables may be stable enough to be used in an uncontrolled fashion, there are times when phase errors would be unacceptable. The telescope is intended to be used all year round for many years, so a closed-loop local oscillator system was designed to ensure that these errors are always at acceptable levels.

3. Phase Stabilization Techniques used with other Telescopes.

This problem of obtaining adequate phase stability is not unique to this observatory: all synthesis telescope builders have had to face it and have come up with a variety of solutions. These will be mentioned briefly before describing the solution developed for the 408 MHz telescope.

With the Westerbork Synthesis Radio Telescope in the Netherlands the designers decided to attack the source of the problem - temperature fluctuations. The cables were carefully thermally insulated before burial. This telescope is located near the sea and experiences a less severe climate. The water table is also quite high which increases the specific heat of the soil. All of these factors make the temperatures experienced by the cable less extreme and more uniform along the length of the cables. The stability of that instrument is better than 1°. Since the 408 MHz cables for the Synthesis Telescope have been in place for a number of years, it is too late to implement this solution.

A method of generating signals with identical phase at any number of points along a transmission line was originally considered for local oscillator signal distribution at the Very Large Array (NRAO 1967), and has been used on interferometers (Little 1969) including a 100 GHz interferometer (Archer 1977). This method places oscillators at each end of the cable that send signals of the same frequencies down the cable in opposing directions. These signals are sampled at any point along the cable and go to a mixer that adds the two frequencies together and adds the phases together. The phase of each signal is proportional to the distance from the oscillator. Since the sum of the distances to the two oscillators always equals the total cable length, the phase produced is always the same, wherever the mixers are placed. This system has a form similar to the 408 MHz LO if only one mixer is used, and it is placed adjacent to one of the oscillators. There is one important difference though, this method supplies signals of equal phase to all the receivers attached along the same line but the 408 MHz system does the same for receivers attached to separate transmission lines.

A more sophisticated method involves sending a signal up and down the line to measure the line length. The phase of the master oscillator can then be adjusted to oppose any length changes. This method was originally described by Swarup and Yang (1961). The 1420 MHz local oscillator system in the Synthesis Telescope is based on this technique (Shimozawa 1968, Landecker and Vaneldik 1982) as is the LO system at the VLA (Napier, Thompson and Ekers 1983).

4. Theory of 408 MHz Local Oscillator

It was decided not to copy the 1420 MHz LO design for several reasons. First, some features of the 1420 MHz system were not required at 408 MHz, and hence the system did not have to be as complicated. One feature not needed was the continuously variable phase to stop the fringes. At 408 MHz fringe derotation is done in the Digital Signal Processor. Another reason is that the 1420 MHz system does not correct for IF phase uncertainty. This can be significant since it may be as large as one degree of phase per degree of temperature differential. This amounts to 8% of the total instrumental phase error. When various LO schemes were being investigated, a method that corrects for the IF phase was discovered and it was decided to implement this design.

The 408 MHz local oscillator does not deliver a signal whose phase is independent of line length to the receiver mixer. On the contrary, this phase is very dependent upon the line length, but it changes with transmission line length in an amount and sign so that it cancels the phase that the IF signal acquires travelling down the transmission line. Thus, in contrast to other systems, this system delivers an IF phase independent of the line length. The theory and design of this system will be detailed below.

I will explain the theory of operation of the 408 MHz local oscillator in step-by-step manner beginning with a very simple circuit in the top half of Fig. 3.4. This circuit has an oscillator attached to a transmission line. The notation used is [frequency]$\underline{/[\text{phase}]}$. The output undergoes a time delay due to the transmission line which, for a single frequency, is equivalent to a phase shift.

In the lower part of fig. 3.4, a phase locked loop is built around the transmission line. The voltage controlled oscillator (VCO) is at one end of the line and the phase detector is at the other end. The VCO frequency depends upon the loop filter output voltage. The loop filter tries to force the VCO frequency (and phase) to a value so that the output of the phase detector is minimized. The output of the phase detector is a function of the frequency difference of the two inputs or, if the frequencies are equal, the phase difference. For this illustration, assume the output is minimized when the inputs are equal. Now suppose that this negative feedback loop has arrived at the point where the frequencies are equal. It will now attempt to make the phases equal. Referring to the diagram, this requires $\phi=\alpha-\omega\ell/c$ or $\alpha=\phi+\omega\ell/c$.

It becomes obvious what must be done to make the output phase independent of line length: combine the two signals in a mixer and select out the sum with a filter. The output then has a frequency and phase: $2\omega\underline{/2\phi}$.

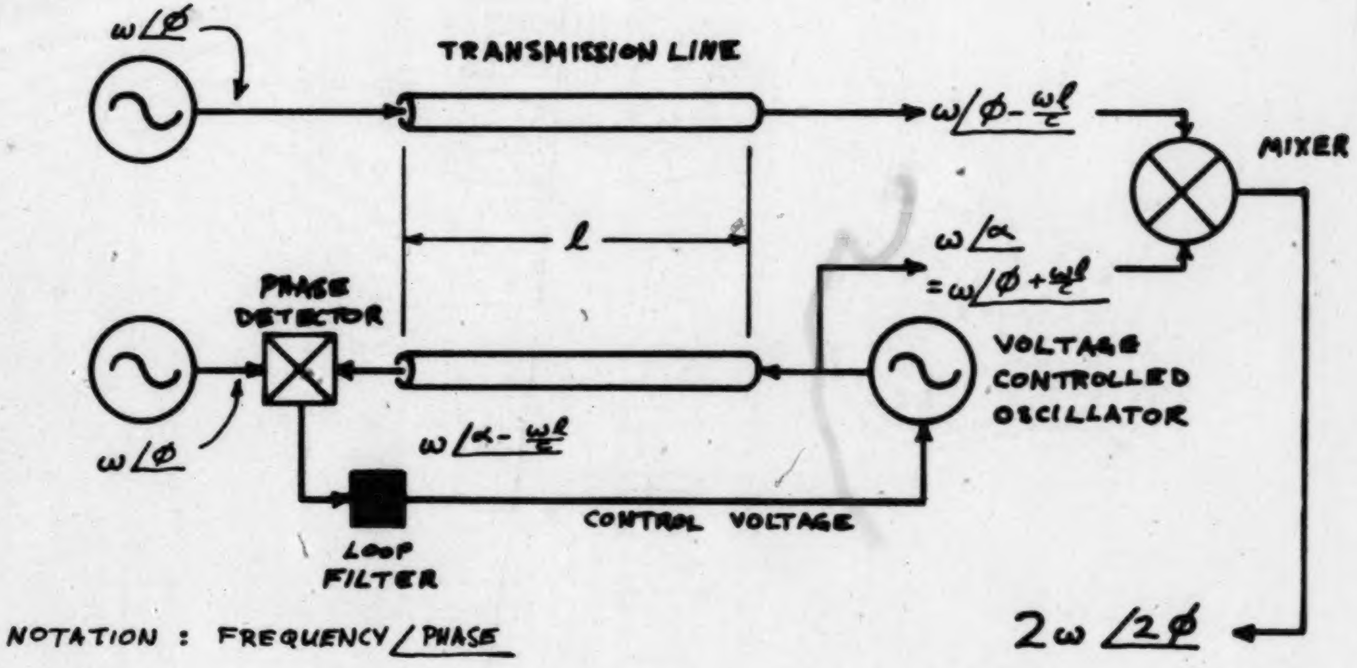
$\omega \angle \phi$
TRANSMISSION LINE
$\omega \angle \phi - \frac{\omega l}{c}$
MIXER
l
$\omega \angle \alpha$
$= \omega \angle \phi + \frac{\omega l}{c}$
PHASE DETECTOR
VOLTAGE CONTROLLED OSCILLATOR
$\omega \angle \alpha - \frac{\omega l}{c}$
$\omega \angle \phi$
CONTROL VOLTAGE
LOOP FILTER
NOTATION : FREQUENCY / PHASE
$2\omega \angle 2\phi$

Figure 3.4 Elementary Phase Stabilized Local Oscillator

The similarity to the original VLA LO scheme is apparent: we have two oscillators of equal frequency at each end of a transmission line and their outputs are combined in a mixer to produce a signal with double the frequency. The difference between this design and the earlier designs is that the remote oscillator is phase locked to the local oscillator. This means that parallel systems on different lengths of cable have identical output phase. Without the phase locked oscillator, only mixers along the same line have the same phase.

Above, it has been implied that the separate signals now use a common transmission line. This would cause difficulties in the implementation of this design. With "ideal" mixers, the output frequency and phase are the sum and difference of those of the two input signals. In a real mixer, there is a small amount of coupling from one input to the other. This means that a signal can mix with itself and double its frequency and phase. If this occurs, then there are three output signals with a frequency 2ω with the following phases: 2ϕ; $2\phi-2\omega\ell/c$; $2\phi+2\omega\ell/c$. To make the output independent of length, the last two signals must be of equal amplitude if they are to cancel exactly. The amount that these undesired signals must be suppressed is large. Consider a desired signal vector with an undesired signal vector placed at the end. The greatest angle that the resultant makes with the desired vector occurs when the desired vector and the (small) undesired vector form a right angle. If an error of 1° is acceptable, the ratio of the lengths of the two vectors is 0.017 or -35 dB. -50 dB results in a 0.2° maximum error.

Another way that this problem could arise is with reflections from impedance discontinuities (such as connectors or bends) along the transmission line. Reflection errors cannot cancel in the same way that spurious coupling errors can because there is the phase due to the extra path length added to one of the error signals which isn't present in the other. In anticipation of difficulties such as these, the design was modified by offsetting the two frequencies.

Suppose an offset oscillator and a mixer are added to the system. They can shift one of the signals either up or down in frequency depending on whether the sum or difference frequency is selected. To preserve phase, this offsetting frequency must be sent down the cable along with the shifted signal. At the other end of the cable, the offsetting frequency restores the shifted signal to its original frequency. By carefully choosing the order in which the three signals are mixed together, the problems discussed previously can be reduced or eliminated.

The offset oscillator will make the system more complicated. Now three RF signals travel up and down the cable, as well as the VCO control voltage and the IF signal. One way to reduce the number of signals on the coaxial line could be to divide one of the frequencies by two at one end. Then the shifted signal and the offsetting signal are the same. With this configuration one would have to make certain that all the components in the system are very linear, so that the halved signal is not doubled before the doubler and interferes with the other signal.

There is another way to apply an offset to the two signals that doesn't require that the offsetting signal be sent down the coaxial line. Instead of shifting only one of the signals, both are shifted equally in opposite directions. The offset cancels when these two signals, $\omega+\omega_{off}$ and $\omega-\omega_{off}$, are mixed together to produce a sum, 2ω. A block diagram illustrating this circuit complete with signal frequency and phase is shown in fig. 3.5. Notice that the length-dependent phase terms do not cancel exactly and produce a phase error $-2\omega_{off}\, \ell/c$. There are two ways to deal with the error: reduce the size of the offset until the error is insignificant or make the error do something useful, that is, cancel another error.

It was decided to use this phase error to cancel the length dependent phase that the IF signal gains as it travels down the transmission line. If the LO frequency is below the reception frequency, the LO phase changes sign upon mixing, and the sign of the phase added to the IF signal as it travels down the coaxial line is negative. Thus to obtain cancellation, the following must be true:

$$\omega_{IF}\ell/c = 2\omega_{off}\ell/c$$

$$\text{or } \omega_{off} = \omega_{IF}/2$$

The offset frequency must be one half the IF centre frequency. This is the basic principle of operation of the 408 MHz local oscillator system. Fig. 3.5 is a very simplified block diagram of the system showing key elements and frequencies and phases. Many essential devices such as filters and amplifiers have been left out for clarity. Another deviation from the actual circuit for clarity is the use of a separate transmission line for each signal; in reality they are multiplexed onto a common transmission line. The actual frequencies used are:

$$\begin{aligned} \omega_s &= 408 \text{ MHz} \\ \omega_{IF} &= 30 \text{ MHz} \\ \omega &= 189 \text{ MHz} \\ \omega_{off} &= 15 \text{ MHz} \end{aligned}$$

Figure 3.6 is a different kind of block diagram. Here the actual components that make up one local oscillator are shown with signal frequencies. A number of subsystems common to all local oscillators have been left out, namely the following signal sources: 15 MHz, 189 MHz, and 204 MHz.

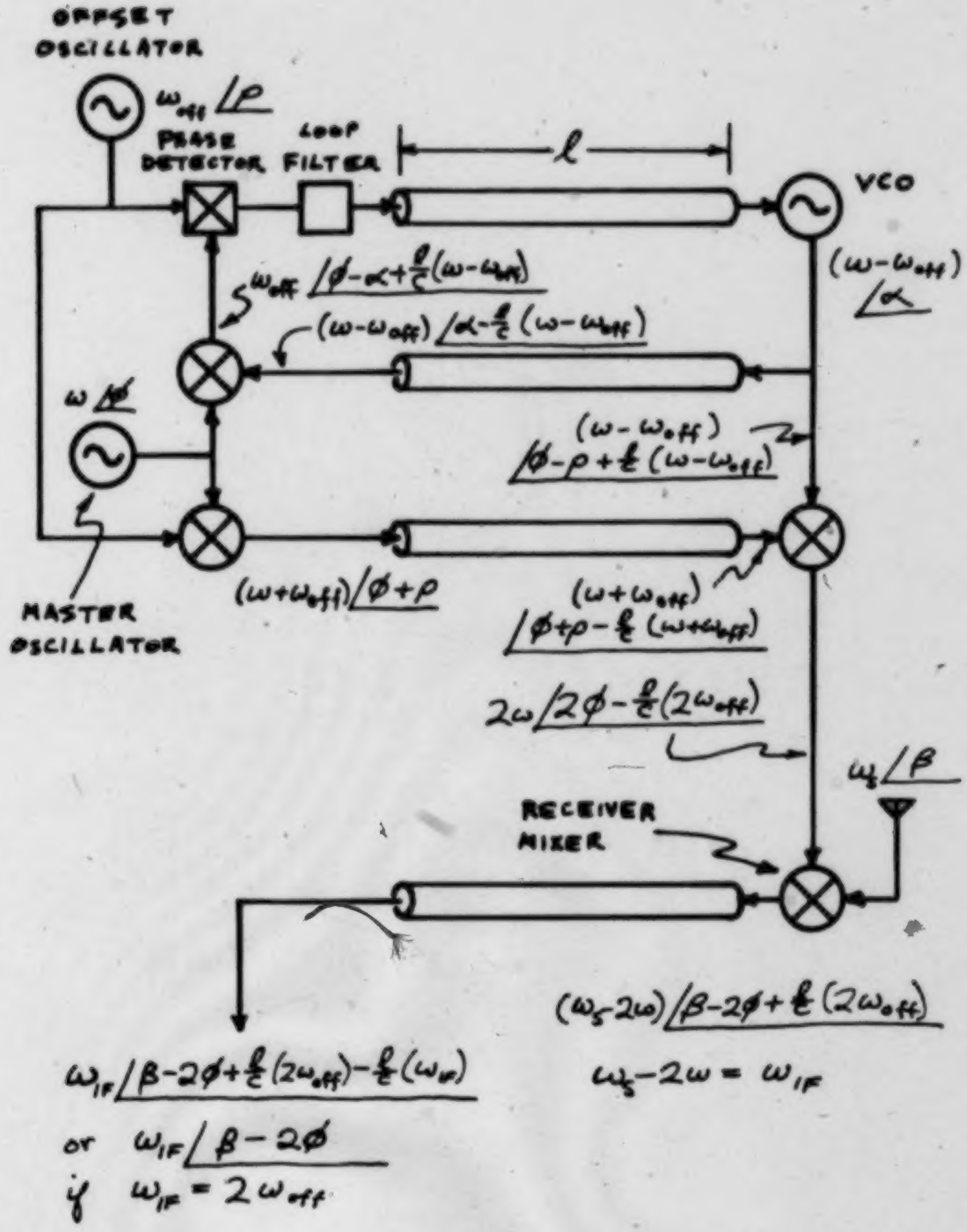

Frequency/Phase Scheme of Local Oscillator System

Figure 3.5

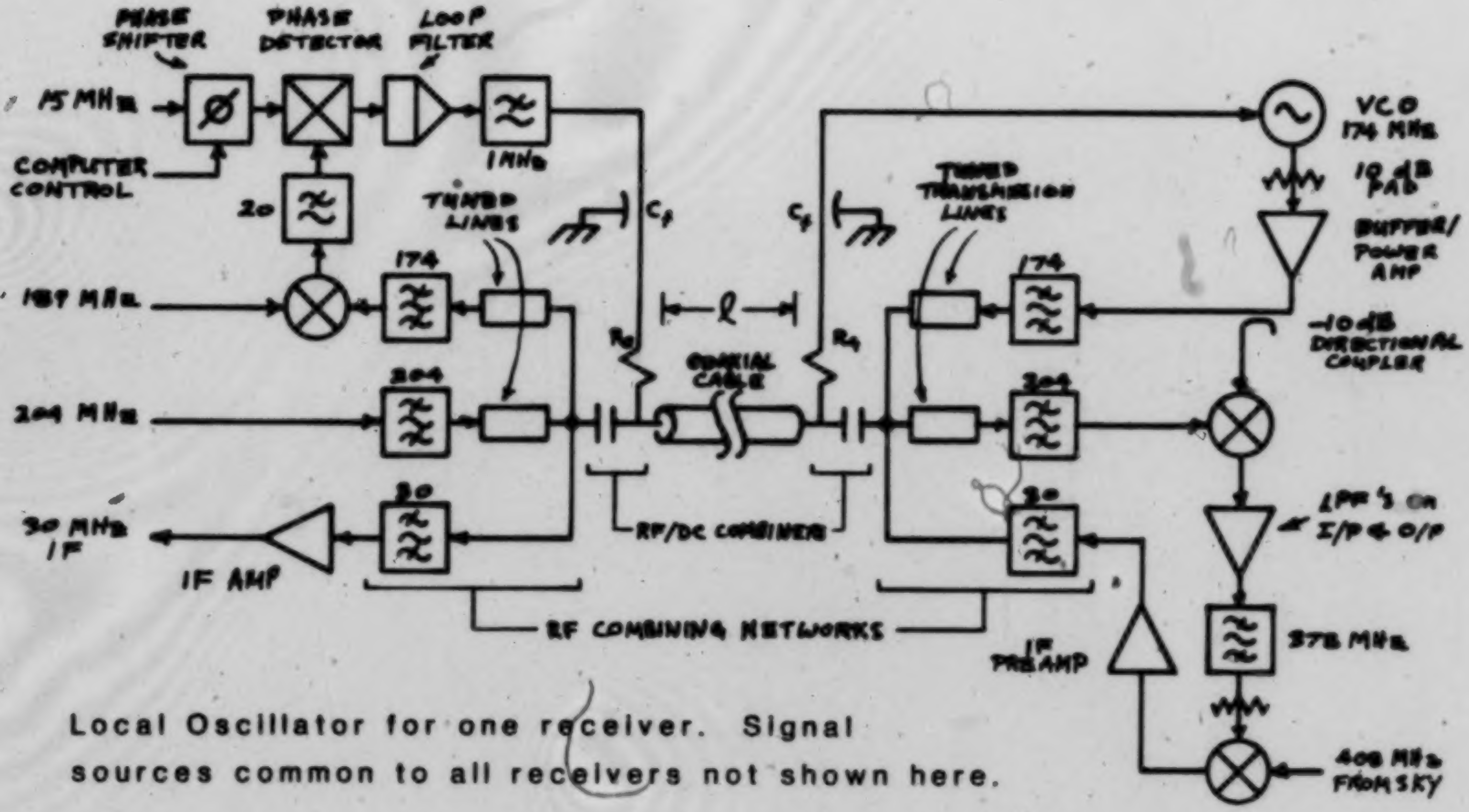

Local Oscillator for one receiver. Signal sources common to all receivers not shown here.

Figure 3.6

5. Design of 408 MHz Local Oscillator

Here I will describe how a system was designed and constructed that fulfilled the requirement outlined in the previous sections. The design required that signal levels be at optimum levels and that spurious signals be minimized.

Sources of Error

First, several sources of error that influenced the design will be discussed. These are spurious signals, phase errors due to reflections and crosstalk between signals, and phase errors due to dispersion.

In the explanation of the theory of operation of this system, it has been assumed that the electrical length of the transmission line is the same at all frequencies. That would be true if the dielectric of the coaxial cable was a vacuum, but is incorrect for any other dielectric. Referring to fig. 3.5 and using the following substitutions: $\omega-\omega_{off} = \omega_{174}$

electrical length at 174 MHz = ℓ_{174}

$\omega+\omega_{off} = \omega_{204}$

electrical length at 204 MHz = ℓ_{204}

The phase error of the IF can be written as:

$$c\epsilon = \omega_{IF}\ell_{IF}-(\omega_{204}\ell_{204}-\omega_{174}\ell_{174})$$
$$= \omega_{IF}\ell_{IF}-(\omega_{204}\ell_{IF}-\omega_{174}\ell_{IF}+$$
$$\omega_{204}(\ell_{204}-\ell_{IF}) -\omega_{174}(\ell_{174}-\ell_{IF}))$$
$$= \omega_{IF}\ell_{IF}-(\omega_{204}-\omega_{174})\ell_{IF}+$$
$$\omega_{204}(\ell_{204}-\ell_{IF})-\omega_{174}(\ell_{174}-\ell_{IF}).$$

Since $\omega_{204}-\omega_{174} = \omega_{IF}$,

$$c\epsilon = \omega_{204}(\ell_{204}-\ell_{IF})-\omega_{174}(\ell_{174}-\ell_{IF}).$$

If the dispersion was zero, all the electrical lengths would be the same and the error would be zero. The significance of this error is determined by taking the derivative with respect to ℓ_{IF}

$$c\frac{d\epsilon}{d\ell_{IF}} = \omega_{204}\left(\frac{d\ell_{204}}{d\ell_{IF}}-1\right)-\omega_{174}\left(\frac{d\ell_{174}}{d\ell_{IF}}-1\right)$$

To assume $d\ell_{204}/d\ell_{IF} \cong d\ell_{174}/d\ell_{IF}$ is reasonable since 174 MHz and 204 MHz are similar in frequency relative to 30 MHz. Now suppose that the relative change in length at the high frequencies is 0.99 of that at 30 MHz. (Experimental measurement of the dispersion showed that the actual value is closer to one.) Using these values, the phase error per unit length is

$$\frac{d\epsilon}{d\ell_{IF}} = \frac{360°\text{x}30\text{x}10^6/\text{sec}}{300\text{x}10^6\text{m/sec}}(.99-1)$$
$$= -.36°/\text{m}$$

The actual error is probably much less than this since the dispersion is much less and the differential length change will be much smaller than 1m. Thus it is safe to ignore effects of dispersion in the transmission line.

Spurious signals were a serious problem that was discovered with the prototype LO system and required the circuitry to be modified. One type of spurious signal was due to mixing of 174 MHz and 204 MHz in certain devices to produce 30 MHz in the middle of the IF band. This signal was generated in the devices that combined the different signals onto the coaxial cable. Non-linear characteristics in ferrite devices caused a small amount of mixing to occur. Using combining techniques that do not use these components reduced this interference to very low levels. These methods will be described later.

Another type of interference was phase modulation of the 174 MHz VCO by voltages induced on the center conductor of the coaxial cable by the AC power lines running to the antennas. Minimization of the VCO gain (i.e. change in frequency for a change in control voltage) and optimization of the loop filter parameters reduced this phase modulation to barely measurable and insignificant levels.

Although solid shield coaxial cable should have extremely good isolation from external electromagnetic fields, this cable was installed with both ends grounded and this impairs the low frequency shielding characteristics. For maximum shielding of a conductor, the current return path should be parallel to and as close as possible to the current forward path. This makes the current loop as small as possible and reduces the number of magnetic flux lines intercepted. When both ends of the coaxial cable shield are grounded, part of the current returns via the ground, increasing the area of the current loop greatly, and increasing the coupling to external fields. Although it may have been possible to improve the shielding by isolating one end from ground, it was decided to design the phase locked loop so that it had immunity to this source of error. Ungrounding one end might not be permanent since it could easily and unknowingly be grounded again, degrading the system.

The unwanted signal induced on the cable is composed of 60 Hz with numerous harmonics. The induced voltage was measured with an oscilloscope and was found to be 3 mV peak to peak. The phase locked loop counters this error signal so that the output phase error of the VCO is 1° peak to peak. The rms error is much less since these phase error peaks occupy only a small part of the 60 Hz period.

The last source of error to consider is due to partial reflections along the coaxial transmission line. Reflections are due to variations in the transmission line's characteristic impedance which can result from bends, damage, or connectors. There are two ways in which these reflections can cause errors. First, suppose the line has at least two sources of reflection separated by a length of cable. Now the signal can travel to the other end of the cable via a direct path or by a zig-zag path which involves at least two reversals of direction due to reflections. These two signals add vectorially at their destination and could have nonzero phase with respect to the ideal situation without reflections. This is because the two signals have travelled different distances and hence have unequal phases. The relative phases will change if the cable expands or contracts since one signal traverses the length of cable between the reflections three times, while the other passes through only once. Since phase stabilized local oscillators always have signals travelling in both directions in the transmission line, the error can be minimized by making the two signals close in frequency so that they are each affected by the reflections in the same way and the differential phase error approaches zero (Thompson 1981). Errors can also be minimized by reducing or eliminating reflections by using high quality connectors and minimizing the number of connections. Distributed line attenuation will help by reducing the relative amplitude of the reflections.

In this LO system, single reflections are also a potential source of phase errors. If part of the 204 MHz signal is reflected back to the central unit, part of this may leak through the skirts of the 174 MHz filter and mix with 189 MHz to produce 15 MHz which would interfere with the 15 MHz signal produced from the 174 MHz signal. The phase of the 174 MHz signal carries information on the length of the line and is thus important. This type of interference can also occur at the remote end of the transmission line by 174 MHz leaking into the 204 MHz path. The problem is less severe here because the 204 and 174 MHz signals are mixed and a 174 MHz signal entering via the wrong port of the mixer is a small error. This source of error was controlled through careful specification of the filters so that the filter skirts attenuate the unwanted signal by a sufficient amount. Details of filter selection are in the section on filters.

Voltage Controlled Oscillator

The voltage controlled oscillator (VCO) is one of the key components in the local oscillator system. It is part of the phase locked loop and its frequency is controlled by the voltage from the loop filter. What makes this device so important and useful is that the phase is also determined by the control voltage. This is because a VCO is a perfect integrator; the output phase is proportional to the time integral of the control voltage. The phase relative to another oscillator is set by initial conditions and can be adjusted by modulating the control voltage momentarily. For this reason the VCO is used to adjust the LO phase to compensate for coaxial line length changes.

The voltage controlled oscillator part of the system actually consists of the VCO itself followed by an amplifier which isolates the oscillator from its load and provides power gain. The oscillator is a simple common collector Clapp design. The frequency is determined by a voltage-variable capacitor (varactor diode). Although it is possible to use a simple oscillator to drive resistive loads, this device must be attached to a filter which is a complicated load. A load like this will make the frequency of oscillation unpredictable near the passband because it becomes part of the frequency selecting circuit and its impedance changes rapidly with frequency. To ensure a constant load, a 10 dB attenuator is attached to the oscillator output and is followed by a high gain commercial hybrid amplifier (Motorola type MHW-591). This arrangement provides enough isolation so that the oscillator operates predictably.

The oscillator schematic is shown in figure 3.7. The oscillator is built around a medium power UHF transistor (2N5109). This transistor is used in the 1420 MHz LO and has proven to be very reliable there. Neglecting biases and power supplies, the circuit is very simple. The inductor with the two variable capacitors form a parallel L-C resonant circuit. C_4 and C_5 also contribute to the parallel capacitance across the inductor, but their primary function is to form a reactive voltage divider that provides the correct feedback ratio for the circuit to oscillate. The ratio of C_4 and C_5 to C_4 determines the step-up ratio from the emitter to ground to base to ground. There are two frequency adjustments: the coarse frequency setting and the control voltage. In each case the reverse bias on a varactor diode is adjusted. A series capacitance establishes the range of the variable capacity. The output power is coupled by an inductor in parallel with the tuned circuit inductance.

DC bias voltages are applied to the circuit through radio-frequency chokes consisting of single layer solenoids of #22 enameled

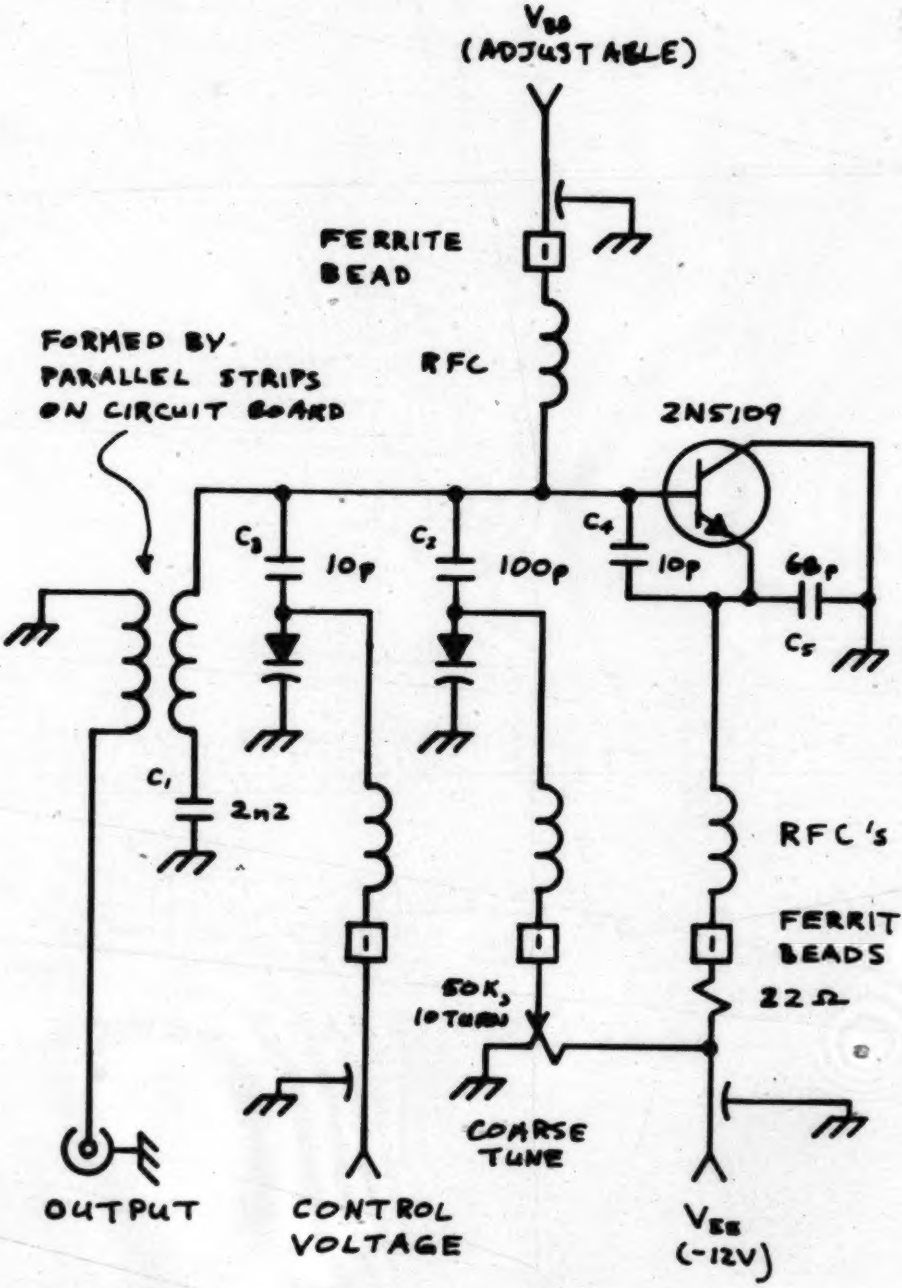

VARACTORS : MV3102
FERRITE BEADS : 3B
RFC's : SINGLE LAYER #34 WIRE ON
LARGE VALUE 1/4 W RESISTOR.

Figure 3.7 Voltage Controlled Oscillator

wire wrapped around large value ¼ watt resistors with ferrite beads on one lead. The base and emitter bias voltages are set inside a shielded box external to the oscillator chassis and enter this box through feedthrough capacitors. The control voltage also enters through a feed through capacitor.

Although the circuit is relatively simple, printed circuit boards were used to try to make the VCO easy to build with repeatable results. In spite of this, oscillators had to be individually adjusted to make them oscillate properly. The size of C_3 sets the tuning range or the gain of the VCO. In some cases C_4 and C_5 were adjusted so that the feedback ratio was large enough for the oscillator to be self-starting, but not so large that the output was distorted. The coarse tuning potentiometer was adjusted to centre the tuning range on 174 MHz and V_{BB} was adjusted so that the emitter current was 100 mA.

The output power of the oscillators is about 1 mW. This was increased to 500 mW by the buffer amplifier. The second harmonic was -35 dB with respect to the fundamental although the fourth harmonic was only -20 dB down. For this reason a filter follows the amplifier. The average gain of the five VCO's produced is 0.7 MHz/volt or 4.3×10^6 rad/sec/volt.

Phase Detector and Loop Filter

The phase detector and loop filter are essential elements of the local oscillator. These devices set the VCO frequency and also control the VCO phase. What has made the design of the loop filter interesting is that it is separated from the VCO by a long cable which has a time delay and associated capacitance. Poles due to the frequency multiplexing circuitry made the design even more challenging. The loop has good performance: no false lock frequencies are known; phase noise errors are less than 1° peak-to-peak; and the transient response is adequate with damped oscillations due to a phase step shorter than 0.2 ms. A computer program has been developed that predicts the loop stability as well as frequency response.

The phase detector used is a Motorola MC12540 emitter coupled logic (ECL) phase/frequency detector (PFD). This device, or its equivalent in other logic families, is now widely used for phase locked loops. What makes it so attractive is its simplicity: besides the detector and loop filter, all that is required are devices to convert the input signal levels to ECL levels. Additional frequency acquisition circuitry is not required, because when the loop is unlocked, the PFD automatically produces a frequency sweep. Additional circuitry is included for lock detection and indication, and display of VCO control voltage. The phase detector and loop filter are shown in Fig. 3.8 and the lock detector is shown in Fig. 3.9.

The PFD has an almost linear voltage output versus phase transfer characteristic over a range of phase from -2π to $+2\pi$. The PFD contains a flip-flop triggered by the rising edges of the two input wave trains. The output is a pulse whose width is equal to the time delay between the two rising edges. Two complementary outputs are provided: one has pulses if the phase difference is positive, the other is triggered if the difference is negative. Thus one output is active from a time delay slightly greater than zero to just less than one period. The other output is active on the other side of zero delay. This is how the device has a range of ±2π. In practice, for small phase differences the pulse width is so narrow that the rise and fall times reduce the gain causing a departure from the ideal linear transfer characteristic.

The PFD behaves in a similar manner if the input frequencies are different. The sign of the difference determines which output is activated. The manufacturer's data sheet claims that the active output has a DC level, but this is not true. Experiment has shown that the output waveform is actually the beat frequency. The waveform shape is not important as long as a signal appears on the correct output to tune the VCO in the right direction.

The complementary outputs of the PFD are connected to the differential inputs of the loop filter. The loop filter uses a low noise, high gain operational amplifier. An active design was chosen because it is a closer approximation to an ideal integrator due to its high low frequency gain and thus reduces the static phase error needed

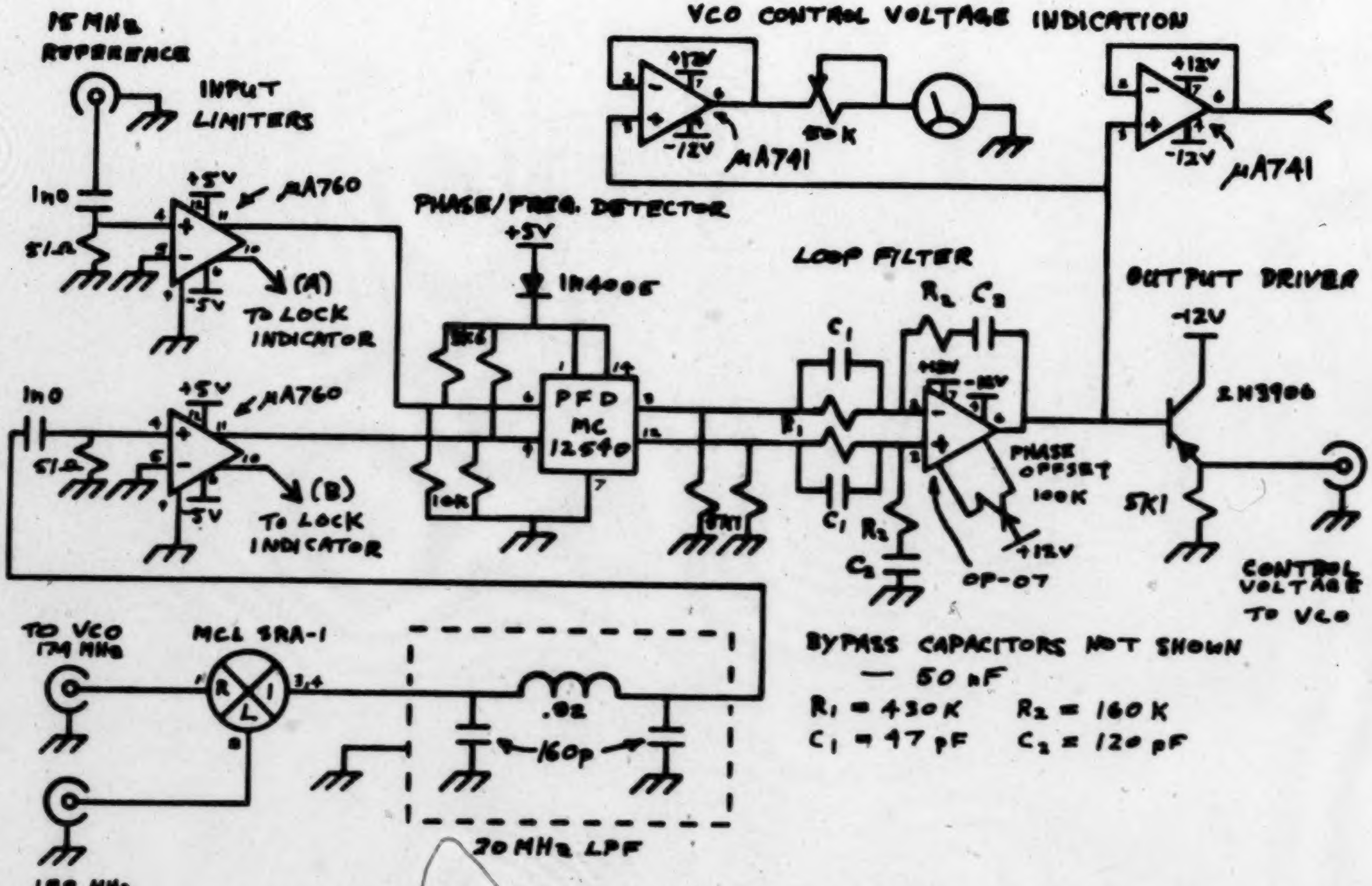

Figure 3.8 PLL Phase Detector and Loop Filter

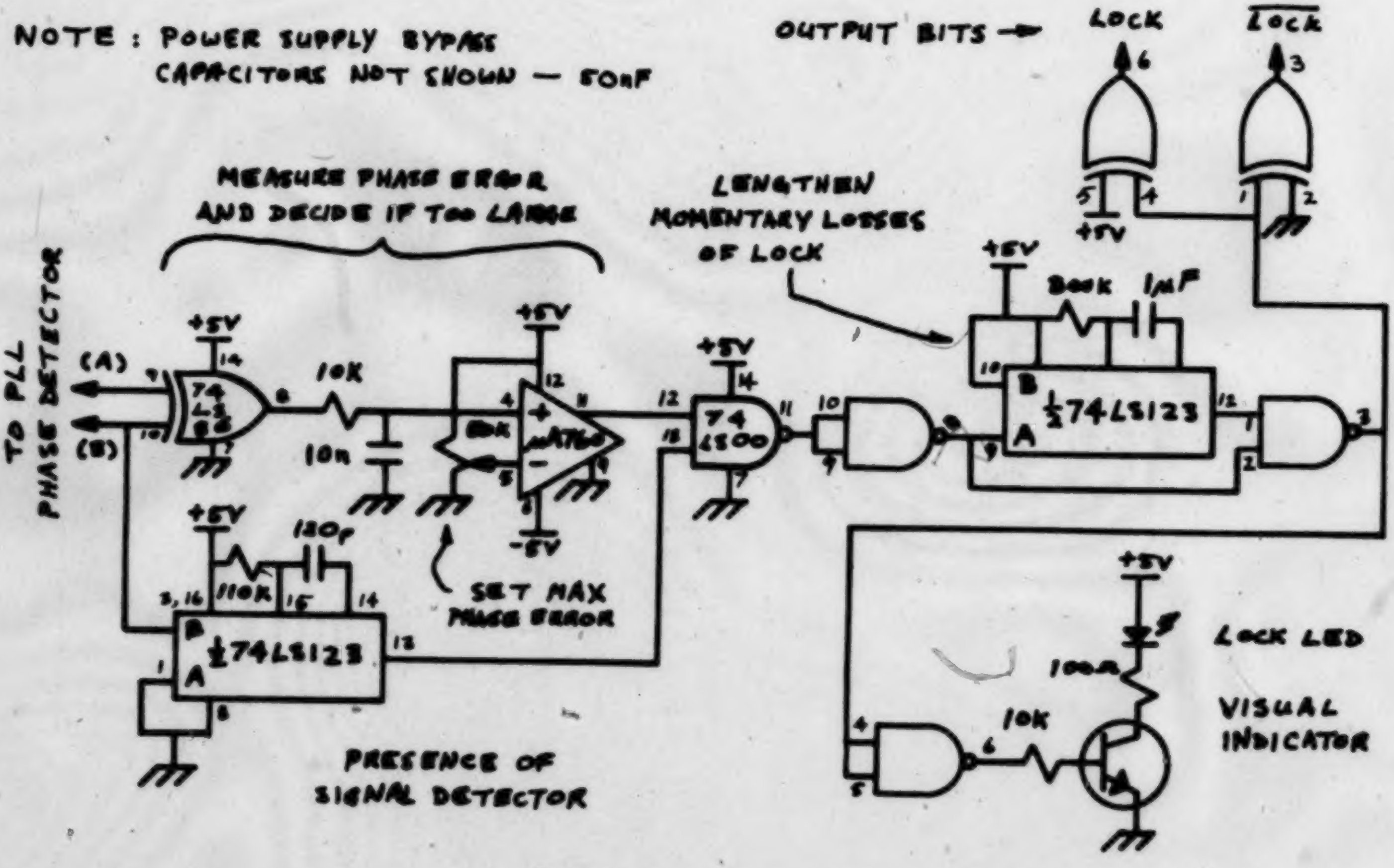

Figure 3.9 PLL Lock Detector

to produce the VCO tuning voltage. The resistors and capacitors determine the filter transfer function which is dependent upon the transfer functions of other components in the PLL. An emitter follower drives the coaxial line. This transistor steps up the load impedance so that the line capacity does not degrade the filter's characteristics.

High speed voltage comparators convert the input sinusoids to square waves at TTL levels. A DC block and a voltage divider change this to ECL levels. On the same circuit board is the mixer that converts the 174 MHz signal from the VCO to 15 MHz. The mixer output is filtered to remove the sum product.

Many of the components on the phase detector and loop filter circuit board are for indication of loop operation. Two op-amps are wired as voltage followers and are connected to the control voltage. One drives a front panel meter and the other buffers a front panel test point. An auxiliary phase detector is made with an exclusive-or gate and is part of the lock indicator. The output of the gate is filtered and compared with a decision voltage level to determine if the phase error is too great. In parallel with this circuit is a missing pulse detector to determine if signals are present, since if both signals are missing, the input phases are equal and the detector would falsely indicate a locked state. A second missing pulse detector lengthens momentary losses of lock so that they may be observed. The lock detector drives an LED indicator.

Synthesizers

All frequency sources are locked to the Observatory frequency standard. A commercial frequency synthesizer was purchased for the 189 MHz source and a simple synthesizer was designed and constructed to generate 15 MHz.

The SST frequency standard provides signals at 10 and 1 MHz. Neither of these can be used to produce 15 MHz easily. Rather than building a PLL synthesizer, a simple low cost synthesizer using standard low-power Schottky TTL devices was constructed. The circuit is shown in Fig. 3.10. The input (10 MHz) sine wave is converted to a square wave by a high speed comparator. The signal is split, one part is divided by two in frequency (5 MHz) by a D flip-flop, and this is mixed with the other part (10 MHz) to produce 15 MHz which is filtered before the output. An alternate method of generating 15 MHz would be to take the 5 MHz square wave and filter out the 15 MHz component. The former method was chosen because the mixing is done in a way so that the output waveform is a square wave at 15 MHz. This technique places the desired signal about 16 dB above the unwanted frequencies, improving the output spectral purity.

To maximize the 15 MHz component in the output, the output of the digital mixer must be as close as possible to an ideal 15 MHz square wave. To accomplish this, the pulse width of the 10 MHz square waves is shortened to that of 15 MHz pulses and the relative timing of the two wave forms is adjusted by a string of inverter gates before mixing in an exclusive-or gate.

Two stages of filtering follow the digital circuitry. A band-pass filter selects the wanted component and three carefully tuned notch filters enhance the rejection properties of the band-pass filter skirt. One advantage of this synthesizer design is that the spurious signals are all at predictable frequencies - multiples of 5 MHz. In this set of filters, two shunt notch filters (at 5 MHz and 20 MHz) are separated by a series notch filter (at 10 MHz).

There were a number of important considerations in the implementation of this design. Careful shielding was required to prevent the many harmonics of 5 MHz generated by the synthesizer from being radiated. The synthesizer circuitry, band-pass filter, and set of notch filters were each placed in individual boxes which in turn were shielded within the chassis so that all the circuitry was double shielded. The synthesizer was built using wirewrap techniques which is appropriate for building one of a kind devices like this and is suitable for use at 15 MHz. It also allows for easy circuit changes, such as in the adjustment of the digital delay line. The filtered

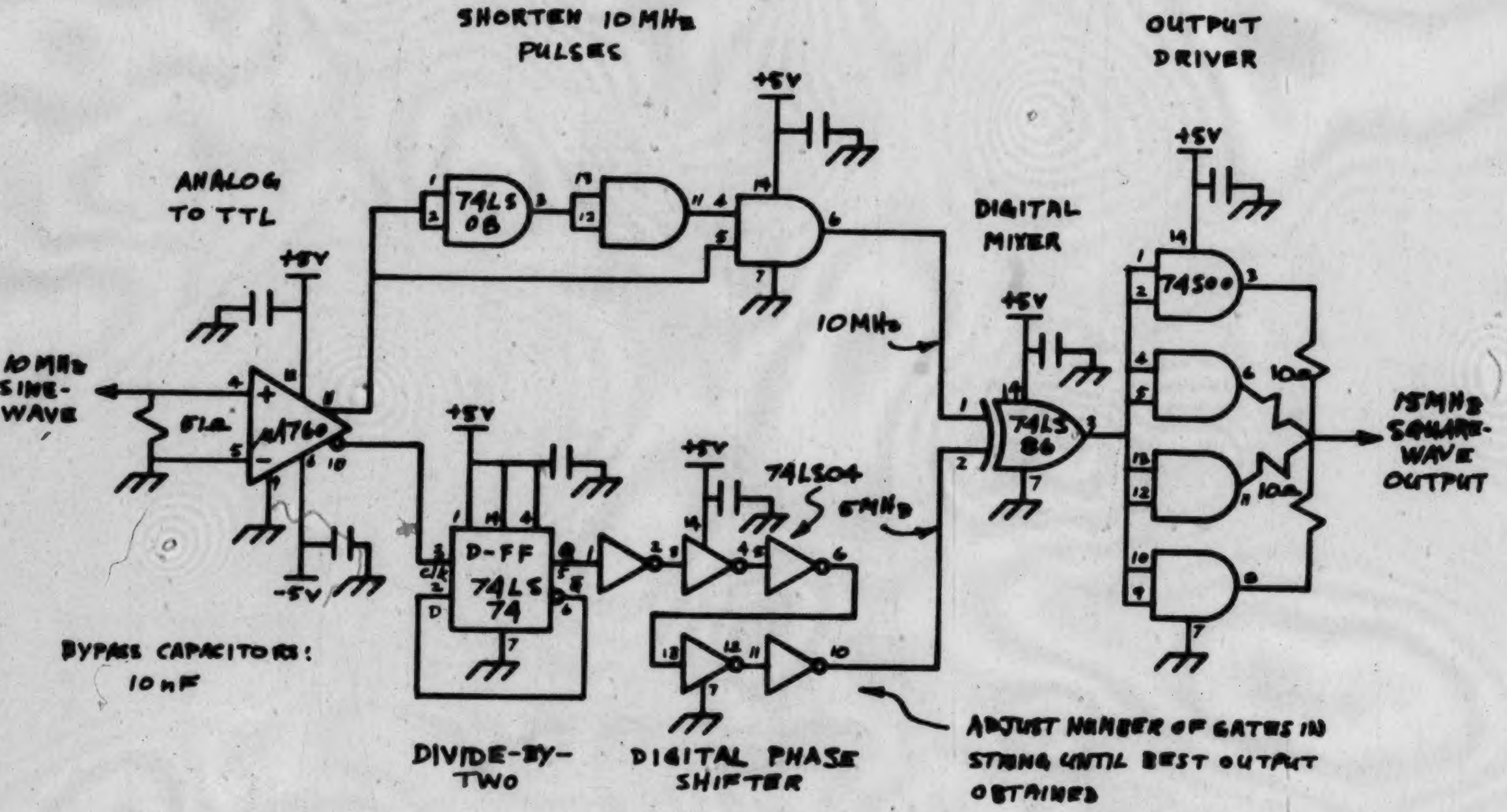

Figure 3.10 15 MHz Digital Synthesizer

output is connected to a 10 dB directional coupler and an eight-way power splitter to provide a 15 MHz signal for the 204 MHz source, and eight identical front panel outputs. At the present, only four outputs are required, but additional outputs were provided in anticipation of the addition of more dishes to the Synthesis Telescope.

One problem with this synthesizer is that there are random 180° phase jumps in the output. The source of this is not understood. The flip-flop changes state without the proper corresponding input. This stage continues to operate correctly, but with phase shifted 180°. The mean time between these glitches is on the order of several minutes. Fig. 3.5 shows that the phase of the 15 MHz synthesizer cancels in the generation of 378 MHz and is therefore unimportant. The phase locked loop follows the phase jump without becoming unlocked. The effects of this problem are therefore not apparent beyond the output of the synthesizer and could be ignored.

204 MHz Source

A 204 MHz signal is sent up each cable to each focus box and is mixed with the 174 MHz signal to produce the 378 MHz LO. A 204 MHz signal is generated by mixing 189 MHz and 15 MHz together and filtering the sum. This signal is then split eight ways and is amplified before being sent up the coaxial transmission line. Eight outputs were provided to accommodate future expansion of the Synthesis Telescope.

This subsystem was constructed with commercial components. The components were placed in a shielded chassis to prevent spurious signals, especially the second harmonic of 204 MHz, from being radiated. Leakage was measured with a UHF receiver and a small loop antenna in very close proximity to the chassis. Signals were barely detectable with this setup and it was decided that these signals would be too weak to interfere with the radio telescope.

Phase Shifter

One unique feature of the 408 MHz Digital Signal Processor is that fringe derotation is performed after correlation, and not with the local oscillator as is the usual practice. However, 90° shifts in the local oscillator phase are required during calibration to establish the real and imaginary channel gains and the orthogonality between these two channels. In addition, 180° phase shifts are required for phase switching, which cancels out constant-level offset errors along the signal path from the receiver mixer to the correlator. For these reasons, a method of obtaining computer controllable 90° and 180° phase shifts had to be devised.

The method selected was to control the phase of the 15 MHz reference used by the phase locked loop phase detector by switching in lengths of transmission line. The phase shifting is done at 15 MHz rather than 189 MHz so that the desired accuracy (less than ~2°) can be obtained without excessively small tolerances for the cable lengths. This method is superior to other methods, such as lumped-value component networks or digital circuits, because of its easy adjustment, high accuracy and long term stability.

The switch driver circuit is shown in Fig. 3.11. Two TTL level signals - one for 90° and one for 180° - are sent from the Digital Signal Processor for each receiver. Thus two switch drivers are required for each of four antennas. The control signals are sent down a long (~300m) twisted pair cable from the main building to the Synthesis Telescope building. They are received by U_1 through a voltage divider. U_1 is a high speed voltage comparator whose reference level is set at 1.7V by a voltage divider. Two complementary outputs are available on this integrated circuit, and they are at TTL levels. One output controls the switch driver, and the other controls the LED display driver. Q_2 and Q_3 are a complementary pair of emitter followers that provide ±4V drive to the switch board at about 40 mA. Q1 and associated components act as an interface between the single ended TTL output of U1 and the double ended drive required by Q_2 and Q_3. Q_4 and Q_5 switch current through the indicator LEDs. Q_4 is also an inverter for the input signal to Q_5.

One switch section is shown in Fig. 3.12. PIN diodes have a low resistance if forward biased and a high resistance if reverse biased. If the switch drive is positive, then the delay line is connected to

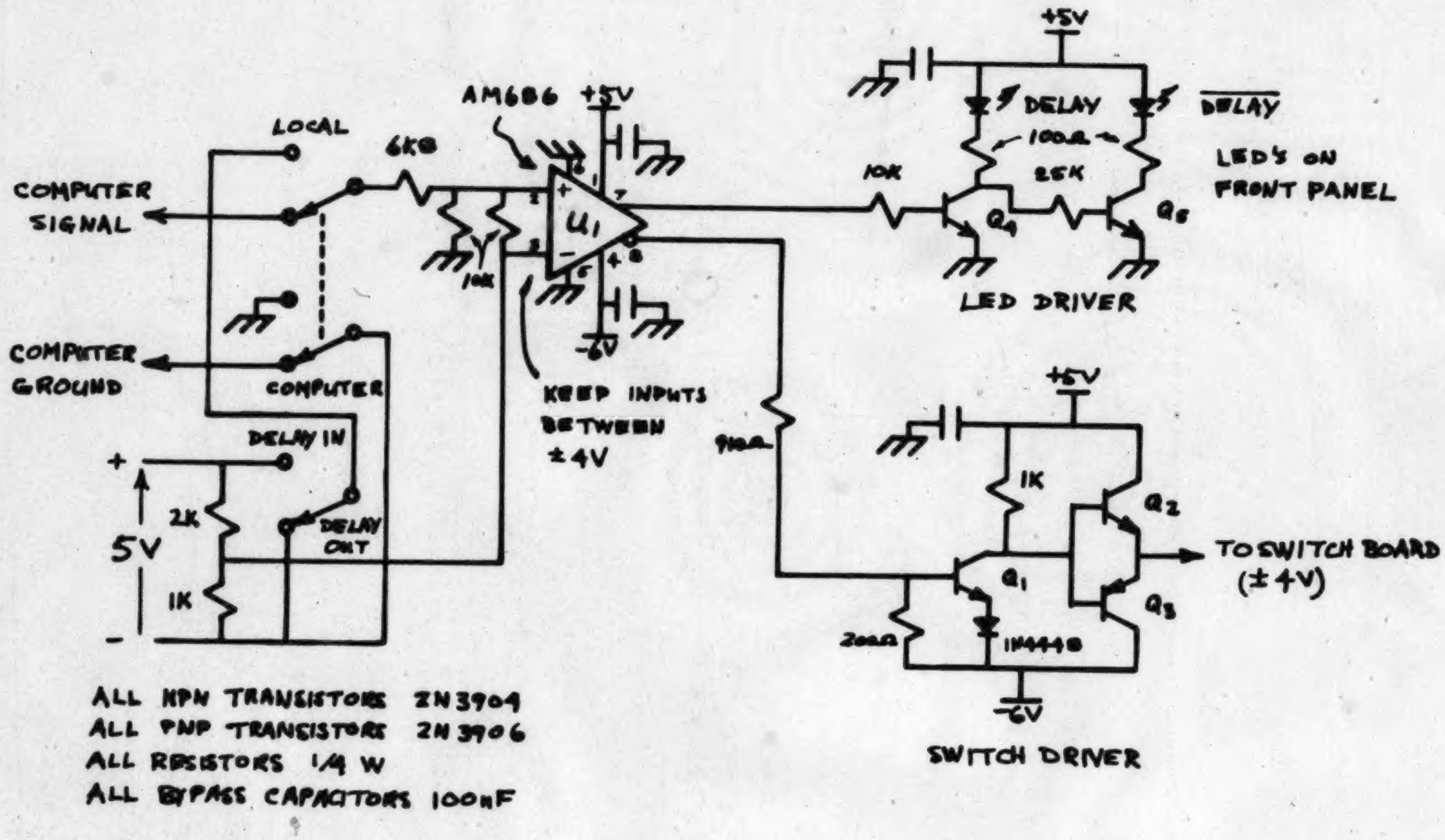

ALL NPN TRANSISTORS 2N3904
ALL PNP TRANSISTORS 2N3906
ALL RESISTORS 1/4 W
ALL BYPASS CAPACITORS 100nF

Figure 3.11 Phase Shifter Switch Driver

the input and output through the forward biased PIN diodes and the short circuit is grounded. If the drive is negative, then the delay line is isolated and the short circuit section is switched in. The forward bias current of the PIN diodes is about 10 mA.

RF/DC Combining Network

Since the coaxial cable to the antennas carries both radio frequencies and DC, a circuit was developed to combine and separate these two types of signals. The device is simple; consisting of a capacitor, resistor, and a feedthrough capacitor inside a shielding box with connectors and is shown in Fig. 3.13. The development of the device was not so simple, since it involves not only the separation of very low and high frequencies, but also phase locked loop stability, phase noise suppression, and spurious signal generation.

This device provides two signal paths, one through a DC block and the other through an RF block onto the common coaxial line. The RF block should have the smallest DC resistance possible, otherwise low-pass filters are formed in the VCO control line due to the series resistance and either the coaxial line capacitance or the feedthrough capacitance in parallel. These poles have a detrimental effect upon the phase lock loop stability. The original design had several turns of wire through a ferrite bead which satisfied this requirement. Unfortunately, the ferrite material has non-linear characteristics

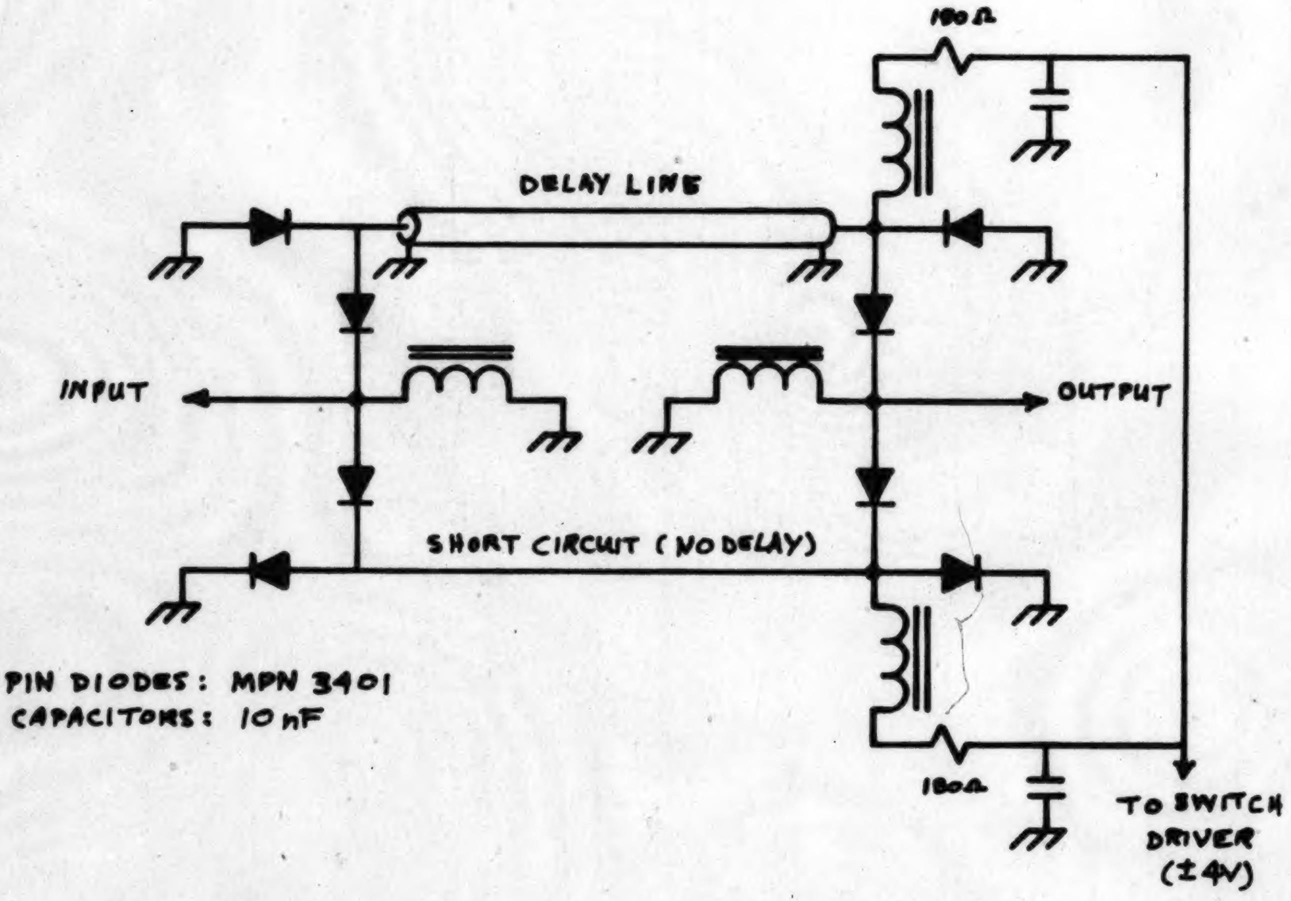

Figure 3.12 Phase Shifter PIN Diode Switch

which mixed the 204 MHz and 174 MHz signals together to form a 30 MHz interference signal. An inductor with a large enough reactance could not be constructed without ferrites at these frequencies. For this reason, a resistor had to be used. A small 2.2 nF Phillips ceramic plate capacitor was used for the DC block. The DC feedthrough capacitor has a value of about 2.5 nF.

Two conflicting requirements made selection of the resistance difficult. For phase locked loop stability, any poles should be far away from the origin when plotted on the complex frequency or s-plane. This resistance is in series with the VCO control voltage, and always has a shunt capacitance following it, forming a simple R-C low pass filter. The pole location is inversely proportional to the resistance value, so to move the pole away from the origin the resistance must be made smaller.

The phase locked loop can be made to lock for a number of different series resistances, but the open loop gain must be reduced as the poles are moved closer to the origin to maintain loop stability. The consequence of lower open-loop gain is that output phase noise due to noise on the VCO control voltage is suppressed less. Therefore, to have a stable feedback loop with good noise rejection, the values of the decoupling resistances should be made as small as possible.

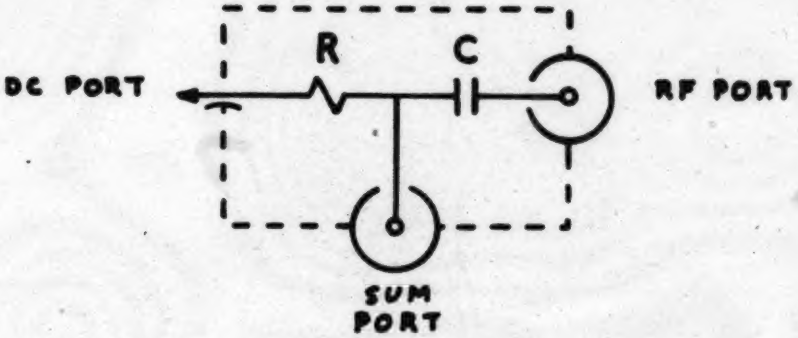

Figure 3.13 RF/DC Combining Network

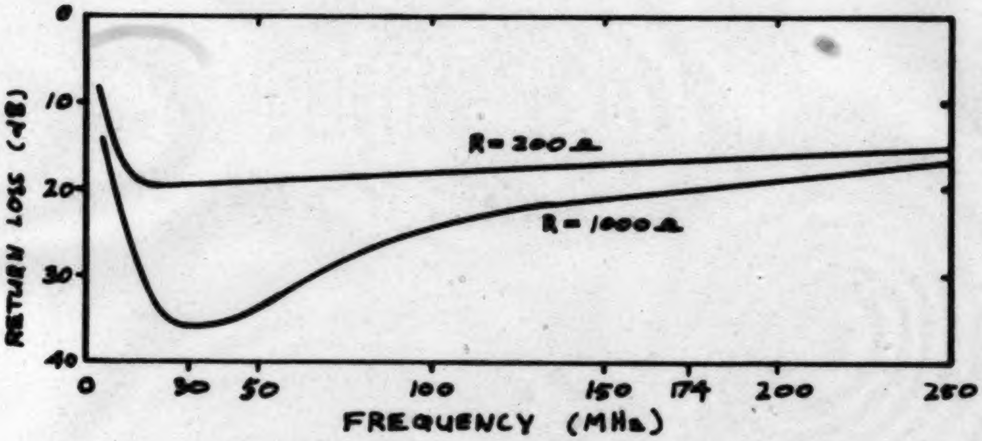

Figure 3.14 RF/DC Combining Network

Return Loss vs. Frequency

At radio frequencies, the end of the resistor connected to the DC port is effectively connected to ground by the feedthrough capacitor. Thus it appears as a shunt resistance across the junction. Immediately we can see that the resistor must be as large as possible, to minimize interaction with the other circuits. If we assume that all other loads are 50Ω at their frequency of operation, the mismatch due to this parallel resistor is easy to calculate. This is tabulated below with measured values at 200 MHz in parentheses:

R	R//50Ω	VSWR	Reflection Coeff.	Return Loss
100Ω	33Ω	1.50	0.20	14 dB
200	40	1.25	0.11 (0.16)	19 (16)
300	42.9	1.17	0.077	22
1000	47.6	1.05	0.024 (0.11)	32 (19)

Of course, these calculations are only a crude approximation to the actual values because it was assumed that the components were ideal and without parasitic capacitances or inductances. The numbers in parentheses were obtained from measurements of an actual combining network with a network analyzer. The RF port was terminated with 50Ω, the DC port was unterminated, and the return loss was measured through the sum port. The return losses were plotted for 200Ω and 1000Ω in Fig. 3.14. At 200 MHz, the return loss for the 1000Ω combiner was 19 dB instead of 32 dB, and for 200Ω it was 16 dB instead of 19 dB. Thus parasitic elements degrade the performance, especially when large values of resistance are used. In fact, the 1000Ω combiner is only 3 dB better than the 200Ω combiner.

In light of the two conflicting design specifications upon the decoupling resistances, and also the practical limitations on the network performance, it was decided to construct the RF/DC combining networks using a 200Ω resistor in the network at the local end of the cable, and a 1000Ω resistor at the remote end. The large value can be used at the remote end since the capacitance following the resistor is much smaller (~2.5 nF) than the capacitance following the resistor at the local end (~33 nF). Since it is the product of R and C that is to be kept small, if one is reduced, then the other can be increased. The performance in this configuration is good: the network is no longer a source of interference; the mismatch is small enough that there is no adverse effect upon the high frequency circuits; and the noise rejection characteristics of the phase locked loop are good.

RF Combining Network

Three radio frequency signals are multiplexed onto the coaxial transmission lines running from the dishes to the Synthesis Telescope building: the IF band of 28 to 32 MHz, 174 MHz, and 204 MHz. These three signals must be combined and separated in such a way that each subsystem appears to be independent of the other two. The simplest way to do this was to purchase a commercially built three-way power combiner which provides a high degree of isolation between the inputs. However, mixing occurred between the 174 MHz signal and the 204 MHz signal producing an interfering carrier at 30 MHz in the center of the IF band. These combiners depend upon ferrites to obtain their broadband characteristics, and the non-linear characteristics of the ferrites can make them into mixers. For this reason a combiner was designed and constructed that did not depend upon ferrites. The design of this device will be explained below.

After the commercial three-way combiners were rejected, a "T" junction was evaluated. A simple parallel junction will work if the impedance of the off-resonance devices is large compared to the resonant device. A length of transmission line can be used to transform the off resonance impedance of a filter to something more desirable, without affecting the pass-frequency behavior. Tuned lengths of transmission line are a satisfactory solution because this junction is not broad band: it has to work at only three frequencies. The final circuit is shown in Fig. 3.15.

The first step in the design procedure was to measure the terminal impedances of the filters. The 30 MHz filter had not been constructed at this point, since its design depended on the higher frequency components. The input impedance of the 204 MHz filter was measured at 174 MHz, and the 174 MHz filter was measured at 204 MHz. Since these filters were not of a symmetrical design, the impedance of each port

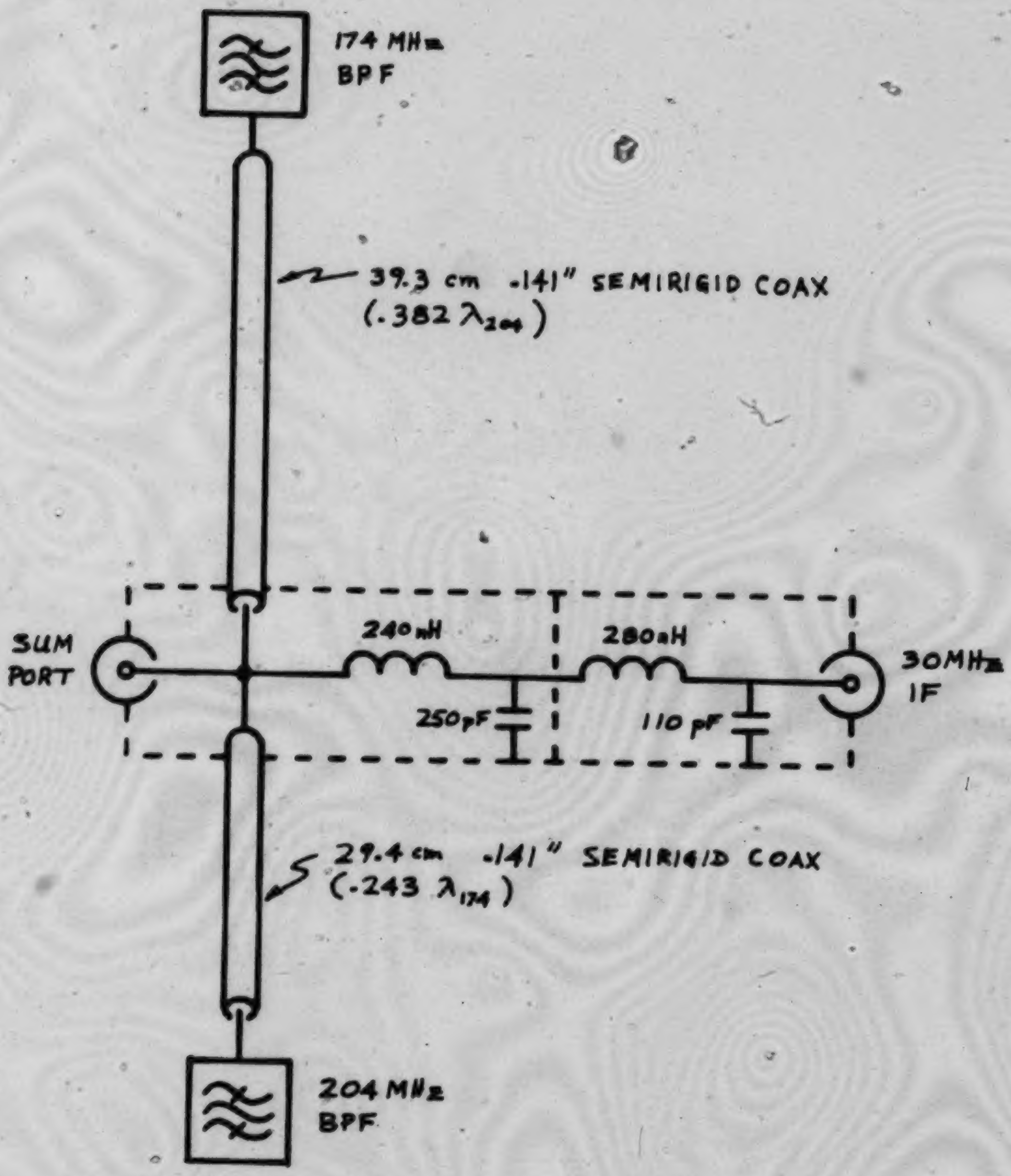

Figure 3.15 RF Combining Network

was different, and both ports were measured. These impedances were plotted on a Smith Chart (Fig. 3.16) along with the output impedance of the IF preamplifier and the input impedance of the IF amplifier. Attaching a length of transmission line to an input moves its apparent impedance along a constant radius in a clockwise direction about the centre of the chart. The desired destination for this point is the region of very high impedance. In selecting which end of the filter to use, the end that required the shortest length of transmission line was used. Another consideration was the variation of impedance with frequency: ports with the least variation were preferred. These coincided with the ports requiring the minimum length of cable.

The effect of these filters and their transmission lines at 30 MHz was determined next. The parallel combination of the two filters through the coaxial lines was found to be -j40Ω. This information is important in the design of the filter that prevents the high level 204 MHz and 174 MHz signals from getting into the IF amplifiers. This parallel impedance modified the necessary value of the first element in the filter.

It was decided to build a three element low-pass filter rather than a more complex band-pass filter. The first design was a third order Butterworth design for a 50Ω load and with a half-power frequency of 40 MHz. This was not a practical design since to obtain the correct value for the first shunt element, an inductor would have had to be

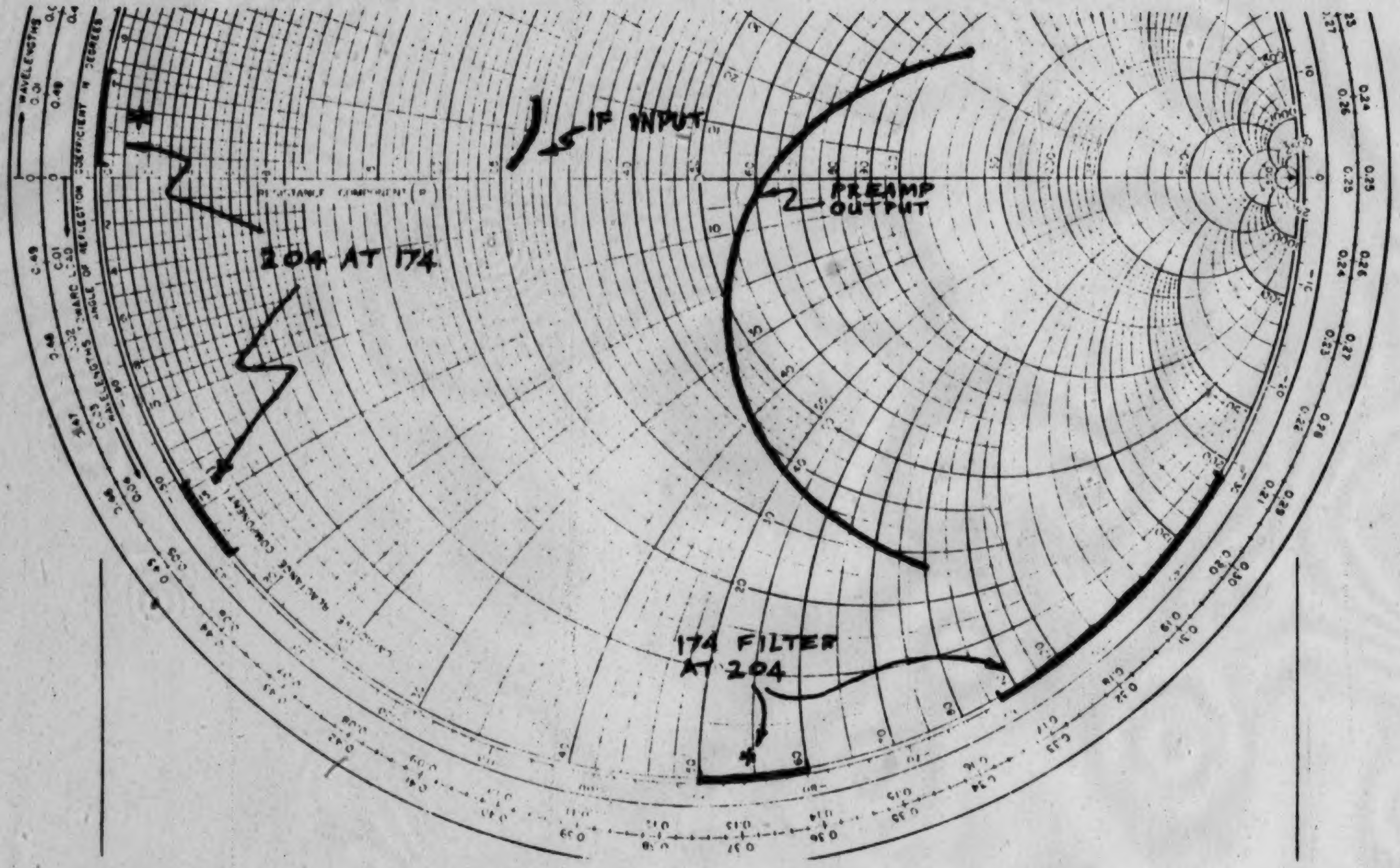

Input Impedances of the Components Connected to the RF Combining Network

Figure 3.16

used instead of a capacitor because of the large capacitive admittance of the high-frequency filters. The problem with this inductor was that its value was so large that a ferrite core inductor would have had to be used, and ferrites have the ability to produce interference at this point. There are two things that could be done to reduce this inductance value: change the characteristic impedance of the filter and/or change the cut-off frequency. The cutoff frequency was not changed since a lower frequency would bring a pole nearer to the IF passband, and a higher frequency would reduce the attenuation of high frequencies. The output of the preamplifier varied so greatly that any filter impedance would be wrong. The IF amplifier input was better behaved, staying near 27Ω. This suggested that a lower filter impedance might be suitable.

It was found that no input shunt element was required other than the impedance of the two high frequency filters, if the filter impedance was changed to 30Ω. Then the calculated value for the capacitors was 133 pF, which is -j40Ω at 30 MHz and is the same impedance as presented by the off-resonance high frequency filters. The inductance required had a reasonable value - 0.24 μH - and could be constructed with an air core. At 200 MHz, this filter looks like a series L-C circuit and has an impedance of about +j300Ω. Thus it has little effect upon high frequency operation.

To improve the rejection of the high frequencies, a second low-pass stage was added. This one was also a Butterworth design with a cutoff frequency of 40 MHz, but with an impedance of 35Ω. To minimize coupling, the two stages were shielded from each other, although the parallel capacitors were combined into one unit.

The performance of this device was satisfactory since it does not produce 30 MHz interference. It is superior to the three-way splitter in another way: the transmission losses are much lower and are primarily due to the filters themselves. The network's transmission loss and return loss are plotted in Figure 3.17.

Coaxial Line

Three semi-rigid coaxial transmission lines run from the Synthesis Telescope Building to each of the antennas. Two cables are dedicated to the 1420 MHz receiving system and the third was originally a spare, but is now used by the 408 MHz receiver. The cable is an integral part of the system, and its characteristics were important in the design of the receiver.

First, the physical characteristics of the cable will be mentioned. The cable consists of 370 metres of Heliax semi-rigid coaxial line with a 24 metre length of RG-214 flexible coaxial cable running from the tower base to the focus box. RG-214 has two braided

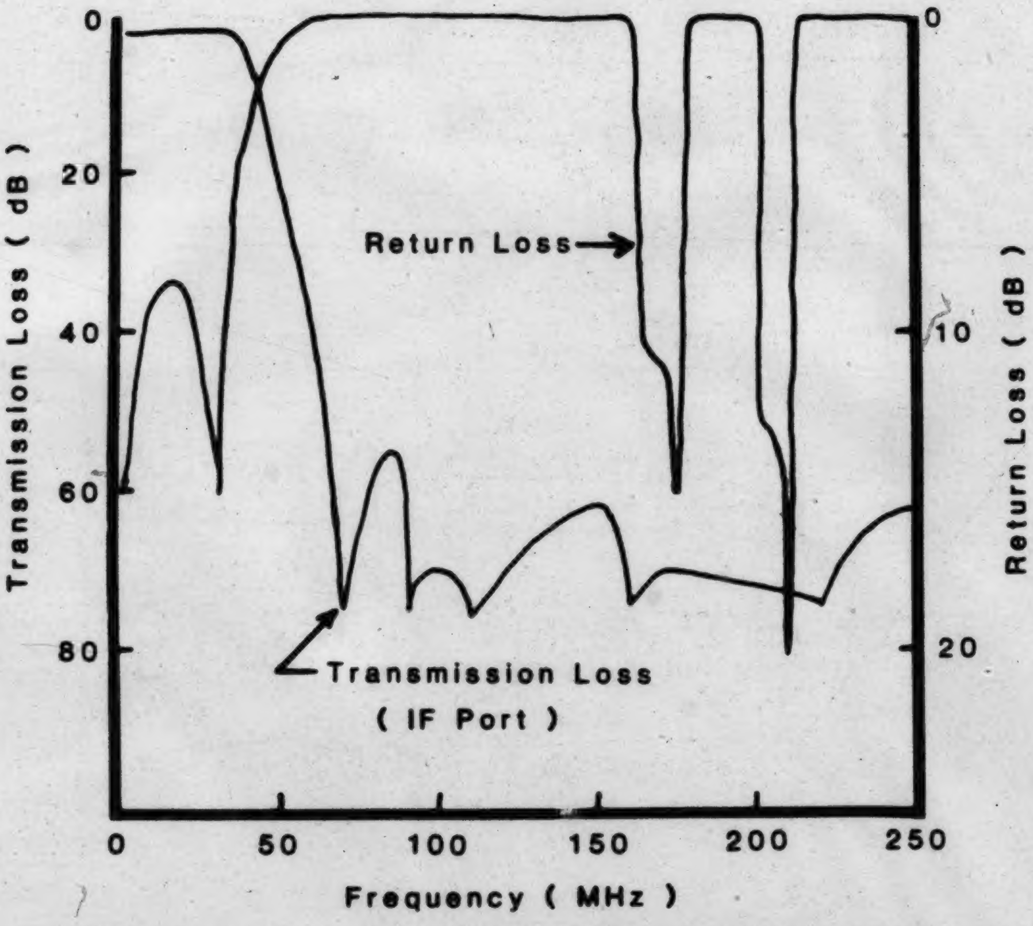

High Frequency Combining Network Characteristics:
Transmission from Sum to IF Port;
Return Loss of Sum Port

Figure 3.17

copper shields (nominally 0.8 cm dia.) so that the cable is very flexible. The dielectric between the shield and center conductor is solid polyethylene. The Heliax is type FHJ4 with a diameter of 1.3 cm. The shield is solid copper with helical corrugations that give the cable limited flexibility. The dielectric material between the inner and outer conductors is polyethylene foam.

The characteristic impedance is 50Ω for both types of cable. Because of the large cross-section and composition of the Heliax cable, it is a low-loss cable. Typical values of attenuation are: 1.4 dB/100 m at 30 MHz; 4 dB/100 m at 200 MHz; and 6 dB/100 m at 400 MHz. The cable velocity factor is 0.78. The RG-214 has more loss: 10 dB/100 m at 200 MHz; 15 dB/100 m at 400 MHz. This cable has a velocity factor of about 0.7.

The line capacitance is important because it affects the phase-locked loop performance. It was measured to be 33 nF.

The round trip time delay due to the cable was also required for the phase locked loop design. This number was obtained by taking the line length measured in wavelengths, and dividing it by the frequency to give the time delay, which was found to be 3.2 microseconds.

The phase temperature coefficient is also important, since it specifies how much the line length (and phase) will change due to temperature variation of the cable. The copper in the cable expands with temperature. However, this is counteracted by a decrease in dielectric constant with temperature of the polyethylene dielectric. The net result is that the length of the cable appears to shorten with temperature. The cable manufacturer specifies a phase temperature coefficient (D) of -36 to -72 ppm/°C for Heliax. The coefficient for RG-214 is on the order of -100 ppm/°C.

The change of phase can be calculated as follows:

$$\frac{360[\mathrm{deg}]F[\mathrm{MHz}]L[\mathrm{m}]\Delta T[^\circ\mathrm{C}]D[\mathrm{ppm}/^\circ\mathrm{C}]}{3\times10^{8}[\mathrm{m/s}]}$$

Phase Locked Loop design

The phase locked loop (PLL) has been analyzed with the guidance of Gardner (1979), Landecker and Vaneldik (1982) and Carpenter (1973) as well as with the aid of a pocket computer (HP-41CV). The parts of the LO within the loop are along the path from the PFD to the VCO and back to the PFD and are shown in Figure 3.18. A number of methods exist for stability analysis of control systems. The root locus method was chosen because it is more reliable than other methods (such as open loop frequency response) since the root locations are directly related to the transient response. Programs were written that calculated the root loci, closed-loop transfer function, and the loop response to undesirable signals on the VCO control voltage. The development of these programs will be outlined below. As is often the case in control system analysis, the system to be modelled will be treated as an essentially linear system in order to greatly simplify the computations.

For control systems such as the one shown in Figure 3.18, the closed-loop transfer function in the complex frequency domain is

$$\frac{\Phi_o(s)}{\Phi_i(s)} = \frac{KG(s)}{1+KG(s)}$$

where G(s) is the open-loop transfer function and K is the loop gain. The denominator is called the characteristic equation and its roots (called poles) are a function of K. A stable system is one whose output (in the time domain) remains bounded at all times for a transient input. A fundamental rule of control theory is that a closed-loop pole located on or to the right of the imaginary axis of the complex frequency or s-plane makes the system unstable. More generally, the further to the left of the imaginary axis the pole is located, the faster the response decays exponentially, and the further to the right, the faster the growth. The sinusoidal oscillations that are modulated by this exponential term have a frequency of oscillation proportional to the distance from the pole to the real axis. The details of the transient response can be determined by multiplying the transfer function by the Laplace transform of the transient, and then performing an inverse transform (Ogata 1970).

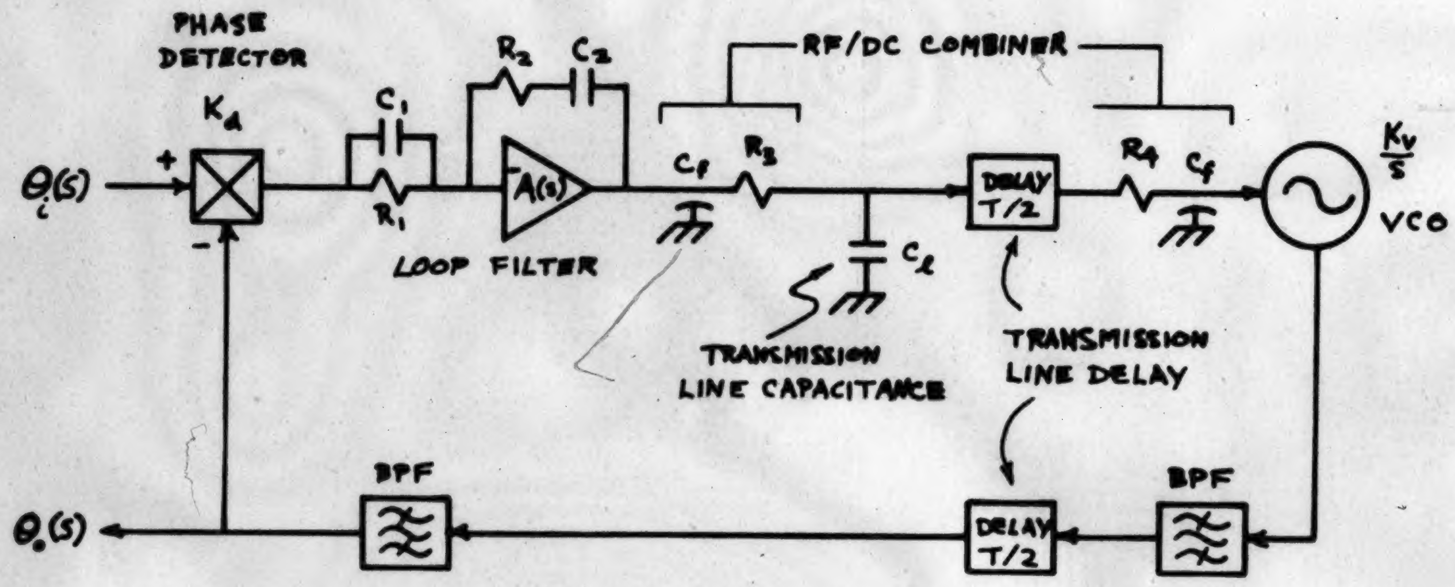

Phase Locked Loop Simplified for Control System Analysis

Figure 3.18

The root locus method involves plotting the roots of the characteristic equation on the s-plane as the gain is varied from zero to infinity. Traditionally graphical construction techniques have been used, but here a computer was used to solve rapidly for the roots while using a more accurate expression to describe the transmission line delay and the op-amp non-ideal gain characteristics. To calculate the roots, 1/G(s) was evaluated and the imaginary part of s was adjusted until the phase was 180°. A value of s for which this is satisfied is a root location and the magnitude of 1/G(s) for that same value of s equals the gain, K.

Figure 3.18 was used to derive G(s). This diagram does not show the frequency conversion since this involves the addition of a constant phase which was moved outside of the loop and simply added to the reference phase. The single transmission line has been separated into two signal paths. The line capacitance and time delay were considered as lumped elements. The delay for each direction is shown separately, but were combined in the computation. Filters have frequency dependent phase characteristics which were considered as additional delays. Resistors R_3 and R_4 are components of the RF/DC combining networks. Using this model the behaviour of the loop was predicted and optimum loop variables were selected.

The total time delay up and back down the transmission line is 3.2 μs. The Laplace transform of a transport delay is e^{-sT}

(Ogata 1970). This transcendental function makes the use of traditional control system analysis techniques, such as root locus, difficult and most people (Carpenter 1973, Hertz et al 1984) have instead used the truncated series expansion:

$$e^{-sT} \cong 1 - sT.$$

This expression is valid only if the product sT is much less than one, which is the case if the magnitudes of the loop poles and zeros are each much smaller than 1/T. This condition was not satisfied with the 408 MHz LO, so the exact expression was used. Since the calculations were done with a computer, this presented no difficulties. The effect of this delay on the root locus was to bend the branches towards the right side of the s-plane as though there were a large number of zeros at positive infinity. This effect degrades the system stability since root loci which do not cross the jω-axis with no delay may be made to cross, and loci that normally cross may cross at a lower gain.

The bandpass filters were ignored in this analysis because their delay was small compared with that of the transmission line delay. Carpenter shows that the delay of a filter can be approximated by the slope of its phase transfer function. From measurements of a 174 MHz bandpass filter this was calculated as follows:

$$\frac{2\pi}{2\pi \times 14\ \text{MHz}} = \frac{1}{14 \times 10^6}\ \text{sec} = .07\ \mu\text{s}.$$

The coaxial cable degraded loop stability in another way. It has a large value of capacitance which forms a low-pass filter with R_3. If R_3 is small, the filter pole is far from the origin of the s-plane and would have little effect. However it is desirable to make R_3 large to isolate the RF and DC paths and this moves the pole inwards. This additional pole reduces the maximum stable loop gain. Another low-pass filter is formed through R_4 and the feedthrough capacitor, C_f. The output impedance of the loop filter is low (because of the emitter follower transistor) so the pole formed was distant from the origin and was ignored. The transfer function of R_3, R_4, C_ℓ, and C_f is:

$$\frac{V_{o(s)}}{V_{i(s)}} = \frac{1}{s^2 R_3 R_4 C_\ell C_f + s(R_3 C_\ell + R_3 C_f + R_4 C_f) + 1}$$

The loop filter gain and band shape determine the static and dynamic error response of the loop. The DC gain should be made as large as possible so that the phase error is small. At a glance, it can be seen that this condition is satisfied by the filter configuration used since C_2 effectively removes R_2. The bandwidth of the filter should be large so that lock time is small and so that noise induced sidebands on the VCO output are suppressed. As well, the filter phase should be such that the open loop phase is not an odd multiple of π which would result in positive feedback and oscillations.

This type of loop filter is often used in PLLs. The inclusion of C_1 is not so common (Landecker and Vaneldik 1982). Its purpose was to add another zero to the circuit and pull back the root locus branches that are drawn to the right side by the delay. This capacitor short circuits R_1 at higher frequencies, widening the loop bandwidth.

If the loop filter's operational amplifier is assumed to have infinite gain at all frequencies, then the voltage transfer function is the feedback impedance divided by the impedance of the input elements:

$$\frac{V_{o(s)}}{V_{i(s)}} = \frac{(R_2+1/sC_2)}{\left(\frac{1}{1/R_1+sC_1}\right)} = \frac{(sR_1C_1+1)(sR_2C_2+1)}{sR_1C_2}$$

This assumption works for most cases but fails when more gain is demanded than the op-amp can supply. This happens at very low frequencies where the ideal gain approaches infinity and the op-amp has a flat, finite gain. At the gain crossover point a pole will appear. Actually this is the pole at the origin from the ideal case (the 1/s term) which has now moved to the left along the real axis. Thus the loop filter is not an ideal integrator. Rather, it exhibits limitations resulting from the finite gain of the amplifier. Since the op-amp gain drops at 20 dB/decade with frequency, another gain crossover may occur at a higher frequency to create another pole.

The op-amp manufacturer claims the typical gain is flat at 115 dB to 1 Hz, where it begins to drop at a rate of 20 dB/decade. Thus the gain can be modeled as:

$$A(s) = \frac{A_o}{1+s/\omega_c}.$$

Millman and Halkias (1972) give the following expression for negative feedback amplifiers with finite gain elements:

$$\frac{V_{o(s)}}{V_{i(s)}} = \frac{Z_2(s)}{Z_1(s)} \frac{1}{1+(1+Z_2(s)/Z_1(s)/A(s)}.$$

In this equation $Z_1(s)$ is the impedance of the elements in series with the input and $Z_2(s)$ is the impedance of the feedback elements. If $|A(s)|$ is large enough, this equation tends towards the previous equation for voltage gain.

These more exact expressions were used in the calculations because large bandwidth and large gain were expected and it seemed likely that the loop filter frequency response might be limited by the op-amp.

Given the above, the open loop frequency response of the PLL can be shown to be:

$$G(s) = \frac{K_dK_v(sR_1C_1+1)(sR_2C_2+1)e^{-sT}}{s^2R_1C_2(1+((s/\omega_c+1)/A_0)(1+(sR_1C_1+1)(sR_2C_2+1)/sR_1C_2))} \ast$$

$$\frac{1}{s^2R_3R_4C_\ell C_f+s(R_3C_\ell+R_3C_f+R_4C_f)+1}$$

Another program was written to calculate the response of the PLL to an unwanted signal injected onto the control voltage. The transfer function was calculated by rearranging the loop so that the point preceding R_4 was the input and the VCO output was the loop output. That expression is:

$$\frac{\phi_o(s)}{N(s)} = \frac{K_v}{s(sR_4C_f+1)(1+KG(s))}$$

This was a more useful function to calculate than the closed-loop frequency response of the PLL since suppression of VCO phase noise was an important concern. Also, to verify the model it was easier to measure the noise response than the closed-loop response because the former required a variable frequency oscillator while the latter would require an oscillator with provision for phase modulation.

If ω is small ($\omega RC \ll 1$), $\phi(s)/N(s)$ reduces to $j\omega R_1C_2/K_d$ with a slope of +20 dB/decade; if ω is large ($\omega RC \gg 1$) then $\phi(s)/N(s) \sim K_v/(j\omega)$ with a slope of -20 dB/decade. These simplified equations show that to minimize $\phi(s)/N(s)$ the gain of the loop filter should be maximized while the VCO gain is made as small as possible.

In practice the VCO gain was reduced by a factor of three by changing the tuning range of the VCO from 12 MHz to 4 MHz.

The first set of component values for the PLL was obtained without the benefit of a computer model. Design equations from Gardner were used. At first C_1 was not part of the circuit. The noise bandwidth was set at 10 kHz since this value would encompass the noise sidebands of the VCO and yet was not too wide for the op-amp. After some adjustment of component values, this prototype was made to work.

The computer software was later developed as an aid in component value optimization. In this process the noise response was minimized while the transient response was improved by changing the loop filter components and R_3 and R_4. The programs allowed many component combinations to be simulated easily and rapidly. The final component values after several iterations are shown in the PLL circuit diagram (Fig. 3.8). The calculated root locus is shown in Figure 3.19 along with loci for the PLL without delay. The root locus in Figure 3.19b is for the PLL with only one zero. The calculated noise response along with the measured noise response is plotted in Figure 3.20.

Figure 3.19 clearly shows the effects of various components upon the roots of the PLL. The transmission line delay bends the long branches towards the right where they cross the $j\omega$-axis. The delay has a relatively minor effect upon the locus extending from poles at the

6

origin to the zeros near -50×10^3. This region is essentially unchanged even if the poles near -135×10^3 and -445×10^3 are removed. The importance of the two zeros is demonstrated in the lower plot, where one of the zeros is eliminated. Here the branches from the two poles hug the $j\omega$-axis and then cross at a relatively low loop gain. This case would have an unsatisfactory transient response because the root locations are so close to the imaginary axis which results in a small damping ratio. Situations like this were found to be marginally stable: the loop could be locked and stable until a transient caused it to become unstable and oscillatory.

The theoretical noise response for two values of loop gain are shown together with the measured noise response in Fig. 3.20. Two different values of loop gain were used because of the uncertainty of the actual value of the phase detector gain. The two curves are based upon estimates of the incremental gain about the operating point. As the gain is increased, the curves are reduced in amplitude by the same factor, and the peak is shifted to a higher frequency. The slopes of the curves are correct: below the peak it is a function of frequency and above the peak it is a function of the reciprocal of frequency.

The noise response was measured in the following manner: a variable frequency oscillator was connected via a decoupling resistor to the coaxial line and the phase modulation was observed by comparing the two inputs to the phase detector with an oscilloscope. The step at

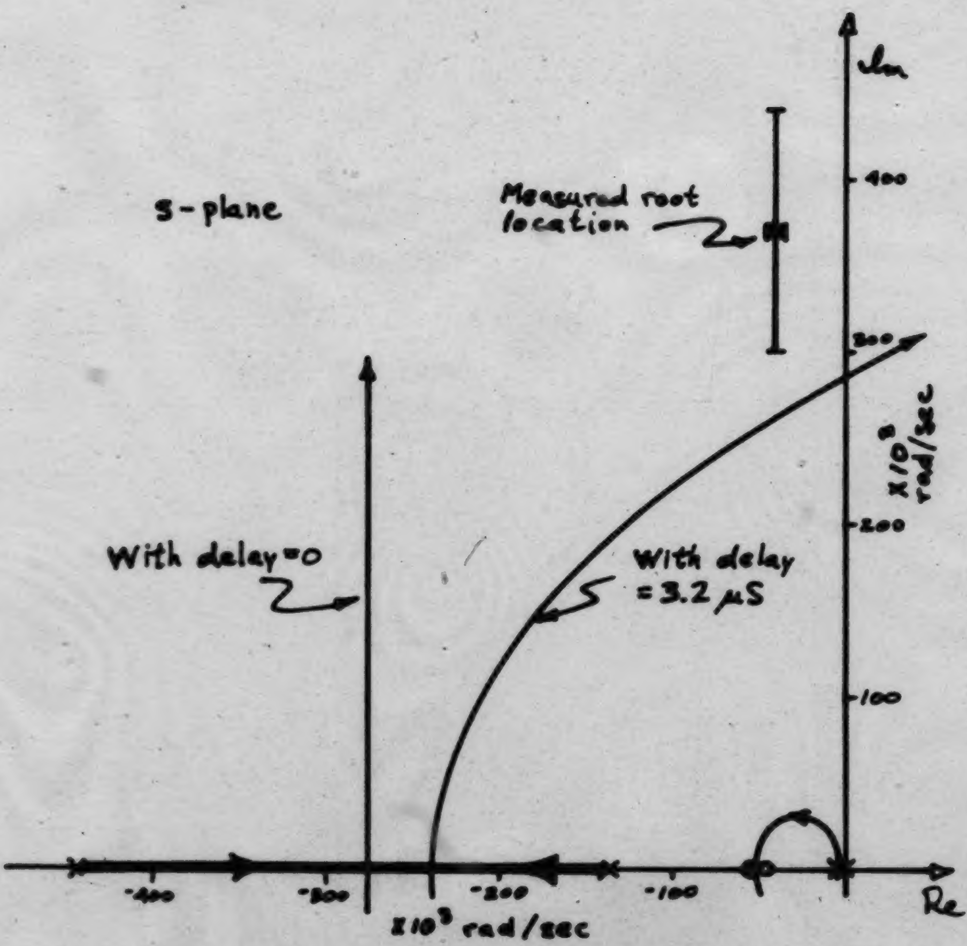

a) Effect of delay on root locus

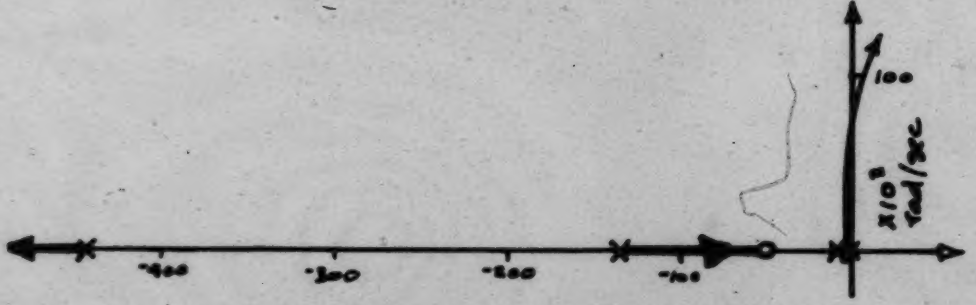

b) Effect of removal of one zero

Figure 3.19 Root Locus Plots

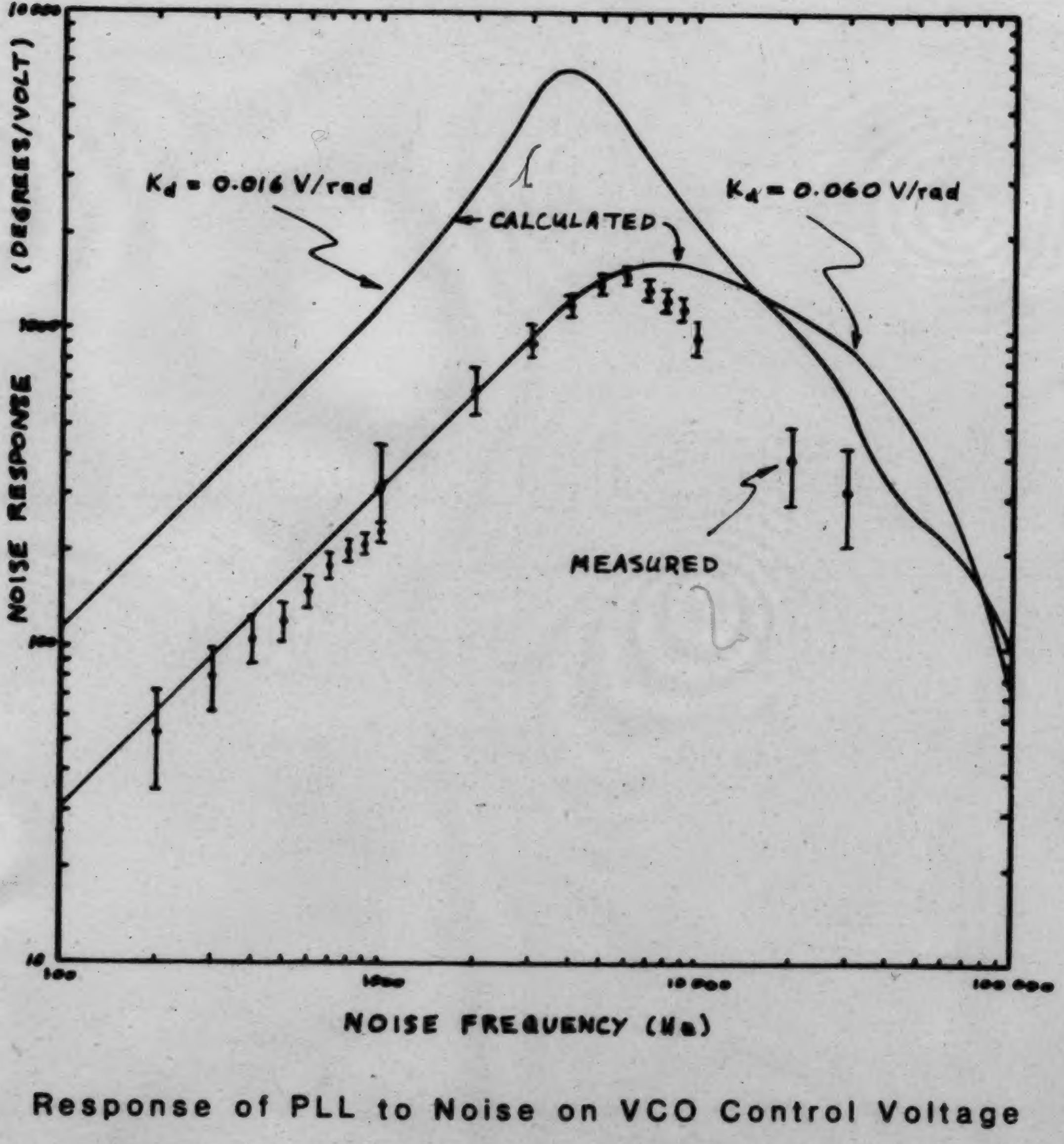

Response of PLL to Noise on VCO Control Voltage

Figure 3.20

1 kHz occurred because the level of oscillator had to be reduced to maintain linearity in the PLL and the phase measuring device.

Discrepancies between theory and practice can be explained several ways. Errors in the theoretical model, such as phase detector transfer function nonlinearities or errors in pole or zero locations, might be large enough to account for the differences. However, the striking similarities support the argument that the model is correct except for the small details.

The phase measuring technique will now be described briefly. Consider two sinusoids of equal amplitude and frequency (ω), but with a small phase difference $\phi(t)$. Subtracting these two waveforms results in a sinusoid of the same frequency with an amplitude envelope defined by $\phi(t)$. This is shown as follows:

$$\begin{aligned} &\sin(\omega t)-\sin(\omega t+\phi(t)) \\ &=-2\cos(\omega t+\tfrac{1}{2}\phi(t))\,\sin(\tfrac{1}{2}\phi(t)) \end{aligned}$$

For small phase errors, this envelope can be approximated with $\frac{1}{2}\phi(t)$ and the change in amplitude approaches $\frac{1}{2}\Delta\phi(t)$. Thus phase modulation of a signal can be measured using an oscilloscope. If the input gains are adjusted so that each input signal has an amplitude of 6 units, the screen will then read 10 degrees change in phase per unit of change in amplitude.

For completeness, the closed-loop frequency response has been plotted in Figure 3.21. This plot is not as useful as earlier plots mainly because it could not be measured with the equipment at hand, and since it is not an accurate portrayal of the expected function of the PLL. That is to say, the loop encounters phase steps rather than sinusoidal variations in phase, so the transient analysis (root locus) is more appropriate. There are several important results from this graph though: the output phase is shown to track the input phase at lower frequencies; and resonant peaks are not excessively large suggesting that the transient response will be well behaved.

From the PLL transient response, dominant root locations can be calculated. The impulse response of a complex conjugate pole pair is of the form

$$e^{\sigma t} \sin(\omega t+\phi)$$

where $\sigma+j\omega=s$ and ϕ is a constant. The transient response was measured by applying a phase step and observing the transient on the VCO control voltage. The waveform at this point is the derivative of the output phase so they differ only in magnitude and phase. Although the root locus consists of 4 roots, one pair was dominant and the transient waveform was an exponentially decaying sinusoid. The length of the transient and the length of one period was measured and one pole pair was calculated to be at

$$s=-40\times10^3(\pm3\times10^3)\pm j370\times10^3(\pm70\times10^3).$$

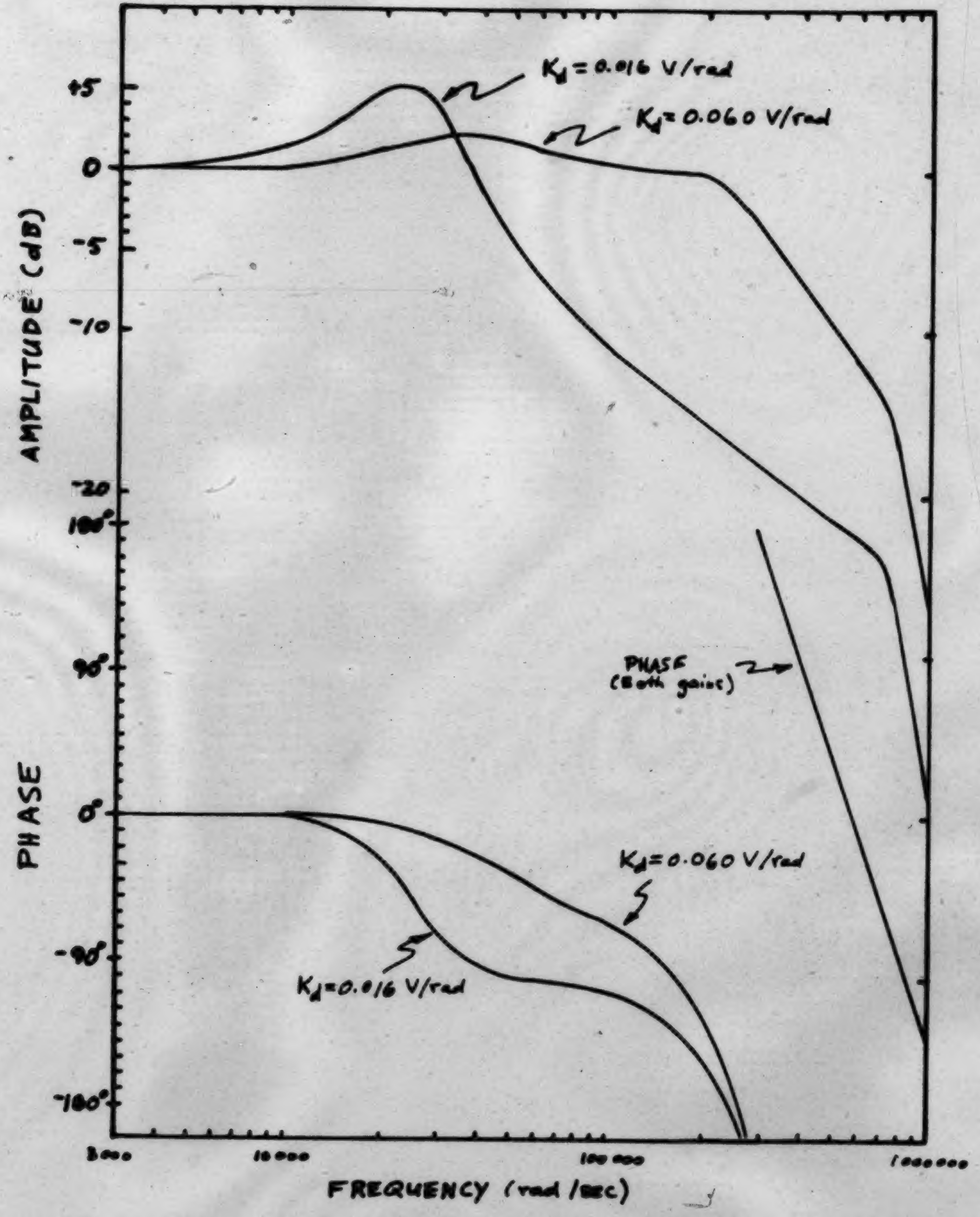

Calculated Closed Loop Response of PLL

Figure 3.21

The effect of the other pole was so small that accurate measurements could not be made. These points are in reasonable agreement with the theoretical predictions and help to support the validity of the model.

Filter Specification

Narrow-band lumped element filters are used to provide isolation in the various parts of the system that share a common signal path. Because of the relationship between the frequencies used, inadequate isolation can introduce phase errors. The isolation is a function both of the signal levels and of the filter skirts. Another important consideration is the pass band width, which must be wide enough to allow for changes of the LO frequency. The filters were specified using these considerations and were custom manufactured.

The front end filter is centred on 408 MHz and has a 10 MHz half power bandwidth. Although the observing bandwidth is only 4 MHz, this wider window was selected so the receiver could be retuned to avoid man-made interference.

The front end filter specifies the part of the spectrum that can be observed, which in turn specifies the LO tuning range and the LO filter widths. The receiver centre frequency can be varied 6 MHz and still keep the 4 MHz IF window within the 10 MHz front end filter band. Since deviation in the LO frequency is shared equally between the 174

MHz subsystem and the 204 MHz subsystem, each of these signals must be variable over 3 MHz. The bandwidths are actually enlarged so that an alternate LO frequency scheme could be used if the self-interference was found to be too large. If 20 MHz were used for the offset frequency instead of 15 MHz, then the interference would be at 40 MHz, outside the IF band. The increased phase uncertainty can be determined from Fig. 3.5 to be only 1/3 as bad as in receiver systems that do not correct the IF phase. Thus the filters had to accommodate 169±1.5 MHz and 209±1.5 MHz as well as 174±1.5 MHz and 204±1.5 MHz. In order to keep signal levels constant, it was decided to enclose these frequencies within the ½ dB bandwidth of the filters. Using the manufacturers tables, it was determined that this corresponds to 3 dB bandwidths of 12 MHz centred on 171.5 MHz and 206.5 MHz. Although the second frequency option has not been used, the wider bandwidths are desirable because the rate of change of phase with frequency is reduced and thus the filters should have smaller relative phase differences.

The place where any lack of isolation can produce a phase error is in the mixer that downconverts 174 MHz to 15 MHz for the phase detector. 204 MHz can also mix with 189 MHz to produce this same difference. The coupling path that is of most concern is via a reflection part way down the transmission line that sends a 204 MHz signal back to the local end, through the 174 MHz filter skirts, and into the mixer. The phase of this signal will be a function of line length. Coupling paths that do not include the transmission line introduce constant phase errors, and although they should be minimized, they are of secondary concern.

The total one-way line loss at 200 MHz is 20 dB. A reflection from the far end of the line will have the greatest length-dependent phase, but will be attenuated almost 40 dB since the signal traverses the length of the line twice. Nearby reflections have a greater amplitude, but the phase uncertainty is less. As well, unless there is a bad fault in the cable, only a small fraction of the signal is reflected back. A mediocre connector might have a voltage standing wave ratio (VSWR) of 1.2 which means the voltage reflection coefficient is 0.1 and the return loss is 20 dB. A good connector may have a VSWR of 1.02 or a reflection coefficient of 0.01 and a return loss of 40 dB.

The levels of the signals involved were estimated from the system plan (Fig. 3.6). The output power levels of the 174 MHz sources and the 204 MHz source will be similar because they both drive mixers at the other end of the transmission line.

With this information the filter skirts can be specified. Suppose reflections have a return loss of 20 dB, which is probably the worst case. If such a reflection occurs near the 204 MHz oscillator so that it is virtually unattenuated by the line loss, the reflection will be reduced 20 dB when it reaches the mixer input. The 174 MHz signal is produced with nearly the same strength and is attenuated 20 dB by the coaxial line loss and therefore is at a similar amplitude as the undesired 204 MHz signal at the local end. For a 0.2° error, the undesired signal should be attenuated by 50 dB. From the filter manufacturer's design charts a 4 section band-pass filter was selected that provides better than 50 dB isolation.

Another filter is required on the output of the LO. This filter prevents the second harmonics of 174 and 204 MHz from getting into the receiver mixer where they would mix with 378 MHz to produce 30 MHz. A 5 pole design with a 12 MHz 3 dB bandwidth was chosen. This design attenuates the unwanted signals by more than 70 dB.

A number of simple low-pass and high-pass filters were constructed. The 15 MHz output of the mixer preceding the phase detector is filtered with a 3 element Butterworth low-pass filter which has a 20 MHz corner frequency. The output of the loop filter is fed through a 1 MHz low-pass filter to remove any residual 15 MHz signals. At the remote unit, the 378 MHz amplifier has a 3 element high-pass filter on its input and on its output to reject the difference product (30 MHz) of the mixer before it.

Packaging of the System

A number of factors were taken into account when determining the physical structure and layout of the various subsystems. These were:

effective electromagnetic shielding; air cooling of heat generating components; ease of construction and servicing; interchangeability; and compactness to fit within the available space. The total system was broken up into a number of subsystems. Some, such as the 189 MHz and 15 MHz synthesizers, are common to all receivers. Other subsystems, such as the phase shifter, 204 MHz sources, and 189 MHz power splitter and amplifiers, were grouped according to function. The phase detector/loop filter, IF amplifier and signal combining networks, and the remote end of the LO each have a chassis for each receiver. The cable used between and within the subsystems was either double shielded RG-223 or solid shielded 0.141" diameter semi-rigid cable. BNC connectors were used for DC or IF signals, N connectors were used for high frequencies, and small SMA connectors were used where size was important.

The remote end LO chassis presented the greatest challenge. A large number of components had to be connected together within a space that would fit inside the focus box along with the 1420 MHz receiver and the components had to be arranged so that they could be installed or removed easily. The components were mounted within one and one half cast aluminum boxes with a total external dimension of 18.5x18.5x9.5 cm. Ventilation is provided through a sheet of perforated metal that is part of the lid. The extra layer of shielding provided by the chassis heavily attenuates spurious signals that might cause interference with either the 408 MHz receiver or the 1420 MHz receiver.

A local oscillator chassis is shown in Plates 3.1 and 3.2.

The other chassis were made with sheet aluminum boxes. All the chassis for the local end fit in one standard equipment rack.

6. System Tests

Before the receiver was used for astronomical observations, a number of tests were performed to determine the total system sensitivity and stability. These will be described here. Further measurements involving interferometric observations will be discussed in the next chapter.

The system temperature of each of the receivers on the dishes was measured. Here, system temperature refers to the noise added to the system due to spillover, losses, and noise generated within amplifiers and mixers. By this definition it does not include the galactic background. These measurements were made by connecting a total power detector to the receiver output and measuring the power from a region of the sky with a known brightness temperature. The difference between the source temperature and the measured temperature is the system temperature. The temperature scale was calibrated by observing two sources with known, but different brightness temperatures. The sky temperatures were obtained from Pauliny-Toth and Shakeshaft (1962). The zero level was established by turning off the IF amplifier. (It

Plates 3.1 and 3.2

The first plate shows an exterior view of a local oscillator chassis. This box contains all the remote end electronics except for the receiver mixer, low noise amplifier, and power supplies. The physical structure was constrained by the space available amongst the 1420 MHz electronics in the focus box, and by the requirement to have connectors easily accessible. The chassis is constructed with a 18.5x18.5x6.4cm cast aluminum box attached to a similar box 3.2cm high. A perforated metal sheet is attached to the lid to provide ventilation. The connectors are for the IF input (BNC), the LO output (SMA), the cable to Synthesis Telescope building (N), and power (Bendix).

The inside of the top part of the chassis is shown in the second plate. Since better ventilation is provided to this part of the chassis, all heat sources are located here. SMA connectors and semi-rigid coaxial cable is used throughout for compactness. The major challenge in the design of the layout of the chassis was to locate the components so that they could be easily connected or disconnected and removed from the chassis. The VCO, two power amplifiers (174 MHz and 378 MHz), and the 378 MHz filter are located in the top of the chassis, and the other filters, IF preamplifier, mixer, and directional coupler are in the bottom part.

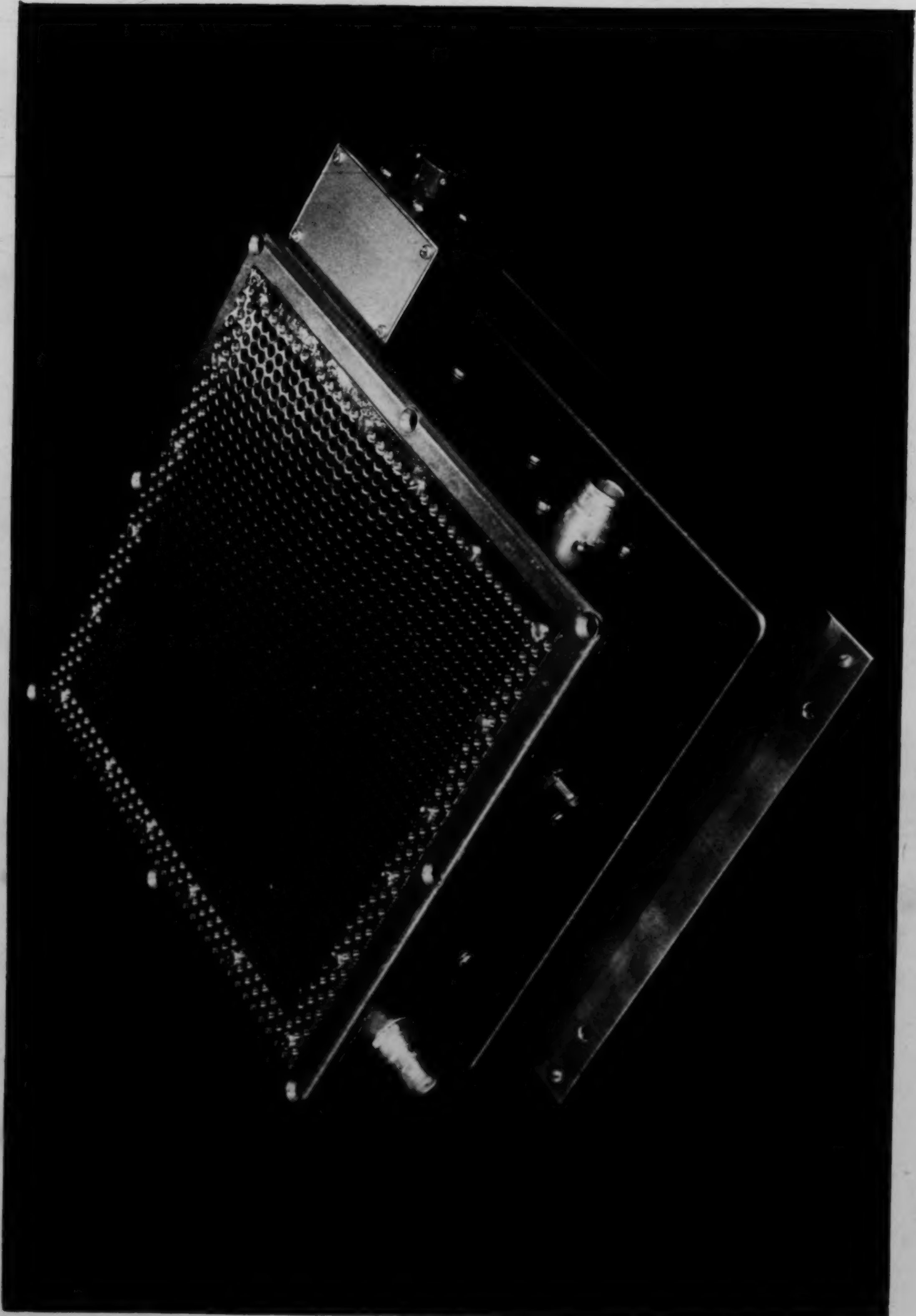

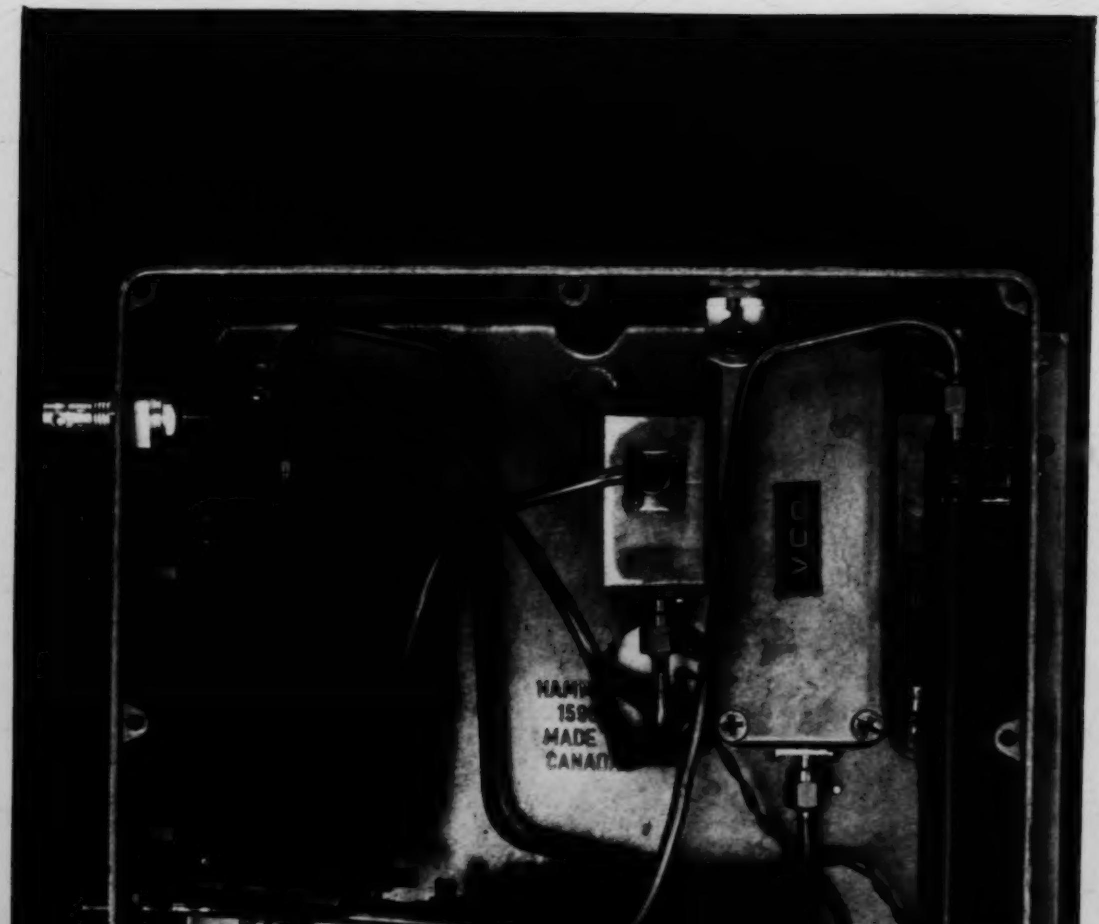
VCO
HAMM
159
MADE
CANADA

can be shown that this is equivalent to placing a load at zero Kelvin at the input of an ideal noiseless receiver.) This was done for each dish with the following results:

Far West	96±10K
West	105±10K
East	131±10K
Far East	85±10K
Average	104±20K

This agrees with other measurements. In Chapter 2 a spillover measurement was described where the zenith temperature less the galactic background was 64K. Using a GaAs FET LNA for the antenna combining network load has reduced this to about 55K. Typical front end noise figures were about 50±10K giving a total very similar to the measured values.

The amplitude stability of a receiver was measured using astronomical sources. The antenna was pointed at sources with two different brightness temperatures with the AGC on and with the AGC off. Although the source temperature had changed, from the AGC circuit's point of view, it was equally likely that the source temperature had remained constant, and the gain in a preceding stage had changed. The AGC circuit adjusted the IF amplifier gain to counter this change. This experiment tested the accuracy of this adjustment.

The two sources used gave antenna temperatures of 30K and 120K and the system temperature was 85K. Going from the cooler to the hotter produced the same effect as increasing the system gain by a factor of

$$\frac{85+120}{85+30} = 1.78.$$

With the AGC turned on, the change in antenna temperature was reduced to 0.7K. Thus the equivalent increase in gain was:

$$\frac{85+30+0.7}{85+30} = 1.006$$

Thus the AGC suppressed the change in gain by:

$$\frac{1.006-1}{1.78-1} = 0.008$$

This number should be viewed as an upper limit since the measured change was near the measurement accuracy of the equipment used. This is less than the 1% amplitude stability specified earlier.

An important system test was the measurement of spurious signals and noise on the LO signal generated. These were measured two ways: in the time domain and in the frequency domain. The former involved measuring the instantaneous phase error with the oscilloscope method described in the section on PLL design, and the latter used a spectrum analyzer to examine the noise sidebands.

Power cables induce small voltages composed of odd harmonics of 60 Hz onto the centre conductor of the coaxial transmission line. These signals modulate the VCO. The PLL tends to oppose these induced signals, but since the loop gain is finite, the cancellation is not exact.

This phase noise was measured and the maximum error was found to be 1±½° peak to peak. It is important to note that this peak phase error occurred for only a small portion of one 60 Hz period, and that the average phase noise was much less. This is completely adequate for a radio astronomy receiver since a 1° error results in the correlation being reduced 0.02%.

Another way to look at the phase modulation was to examine the sidebands with a spectrum analyzer. This was done, and the spectra are shown in Figure 3.22. The peak sidebands were -55 dB with respect to the carrier (dBc). The typical sideband levels were -63 dBc. Examination with narrow sweep widths showed that this noise floor was made up of the odd harmonics of 60 Hz. The close-in noise sidebands of the reference signal began at -70 dBc, so the noise performance obtained is approaching the best possible.

Phase fluctuations like these are unimportant because their period is much shorter than the integration period (90 seconds) and they are less than 1° peak so that loss in amplitude is small.

Phase fluctuations that are significant are those with periods longer than the integration period for they reduce the dynamic range of the map. Laboratory measurements of the long term stability will be given here, and astronomical measurements will be described in the next chapter.

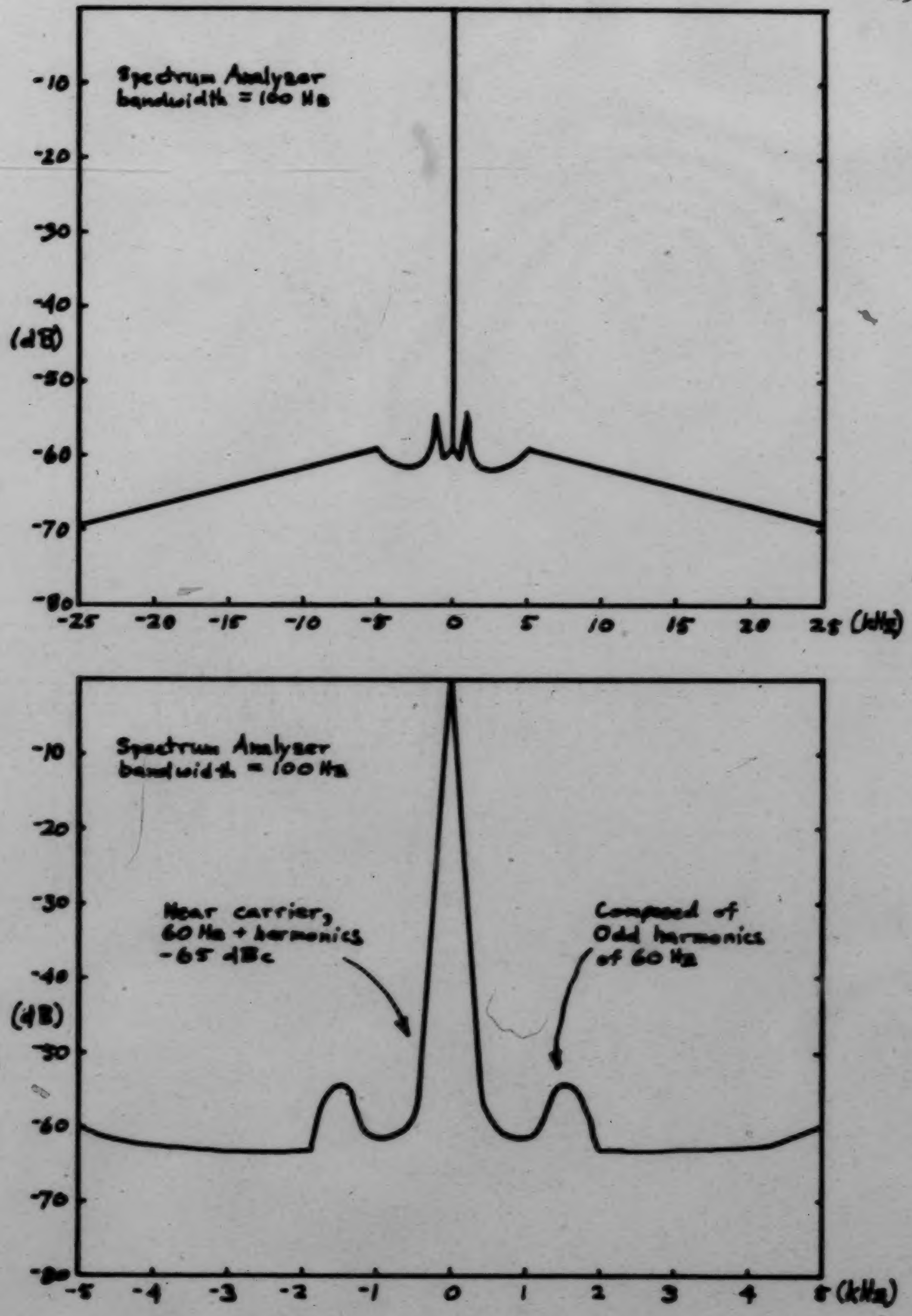

Figure 3.22 Local Oscillator Spectrum

The experimental apparatus consisted of a 408 MHz oscillator providing equal signals to two receivers on the bench, and a phase meter connected to the IF outputs of the receivers to measure the differential phase. One receiver had a short (~5m) cable joining the remote LO unit to the central unit. This provided the reference phase. The other receiver was connected to a roll of Heliax cable (~370m) outside the building. The Heliax was cut into two equal lengths and had a line stretcher joining the break. The line stretcher could be varied 0.5m (free space length) at a constant velocity by a motor. The change in phase due to line length variations was measured by comparing the receiver output phases. The long-term stability of the electronics was also measured by leaving the line length constant and recording the phase difference on a chart recorder overnight.

It was desirable to vary the line length by one wavelength at the lowest LO frequency. In this way errors due to reflections would stand out clearly since the interfering signal would rotate 4π with respect to the desired signal. But the line stretcher did not have a large enough range of variation, so to extend the range discrete lengths of cable were added.

The line length was varied 2 metres (free space) in 0.5 metre steps and the phase variations are shown in Figure 3.23. The length of each curve corresponds to a variation of 0.5 metre. The phase change ranged from 0.6° to 2° with the average being 1.2°. It is unlikely that the line length will change by this amount, so a more realistic measure of the phase stability would be the steepest slope on the curves, which would give the greatest change in phase per change in length. This was also calculated for a system that does not correct the IF phase but has a stable LO phase, and for a system that does not stabilize the LO phase. These values are:

measured:	5°/m
uncontrolled IF:	36°/m
uncontrolled LO: (neglecting IF phase)	454°/m

Thus it can be seen that the worst case phase stability of the 408 MHz system is 7 times better than a system that only stabilizes the LO phase, and 90 times better than a system that has no phase correction.

It was hoped that the phase versus length plots with the incremental lengths of line added could be connected together. This was only a partial success. After applying phase offsets, three of the curves could be joined together. It is very likely that these phase offsets are due to the insertion and removal of different pieces of cable. The reflection coefficients of the different connectors might have been different, changing the amplitude and phase of the undesired signal. But the most significant source of error is probably dual reflections or "zig-zag" paths. With a short piece of

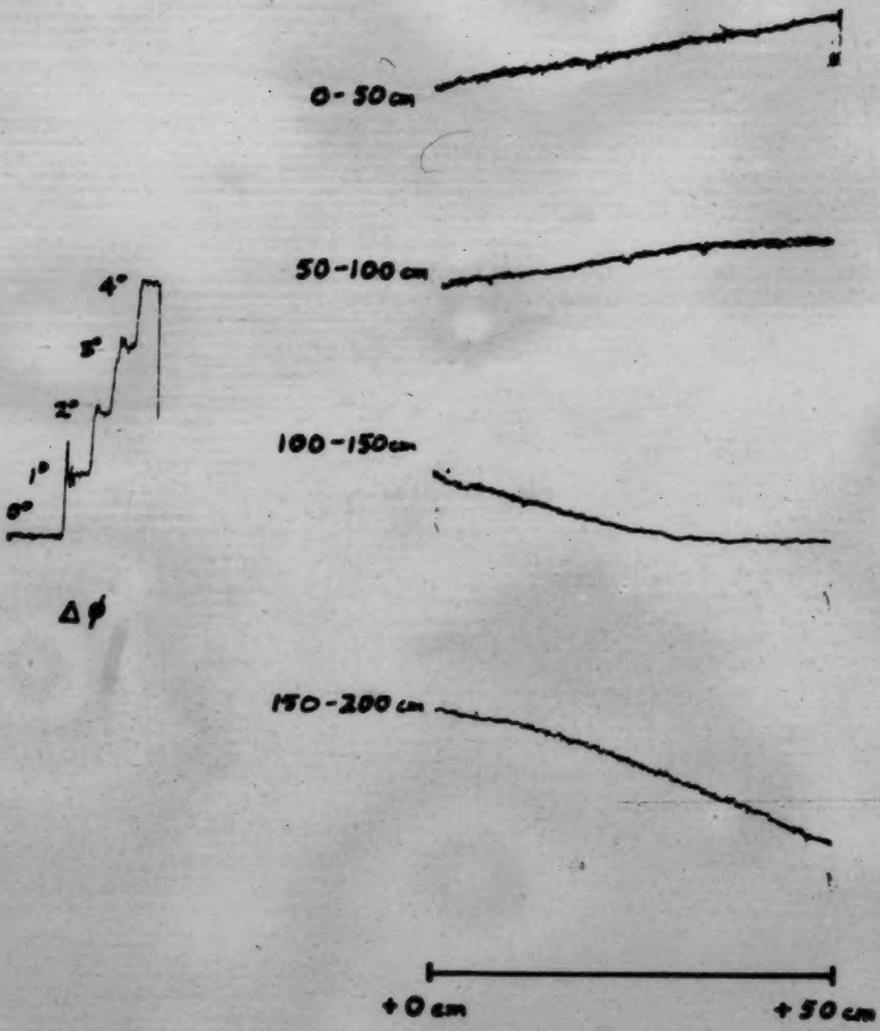

Figure 3.23 LO Phase Error vs. Line Length

cable inserted, the line attenuation between reflections is negligible so that the error component has a larger amplitude than it would if the reflections were separated by a greater length of cable (Thompson 1981). Thus, in a test like this, the system will be more prone to phase errors due to reflections.

The above can also be used in an argument that the phase errors measured in the test were larger than those which could occur in practice. There are two significant differences between the cable used in the telescope and the cables used in this experiment. First, the length changes are not as localized, they are distributed over a larger length of cable. Second, large lengths of cable are between connectors so that double reflections are attenuated. Thus the magnitude of the reflected signal was larger in the experiment and the phase errors can be expected to be lower in practice.

The long-term stability of the receiver system was also measured. The measurement setup was similar to that in the previous experiment, except that the line stretcher was removed, and the phase was measured with the Digital Signal Processor and plotted on a chart recorder. This experiment was left running overnight for a period of about 18 hours. The roll of Heliax cable was subject to a temperature variation of about 10°C.

The beginning, middle, and end of the chart record are shown in Figure 3.24. Short term cyclical variations which were ½° peak to peak are probably due to the cycling of the building's heater. The ambient temperature in the building can vary 3°C and this will affect the filters. No long term cycles or drifts were visible.

Another test was the resetting accuracy of the PLL. The phase of one receiver was changed with the phase shifter, and then it was reset. The PLL returned to its original phase. Any errors were beyond the measuring accuracy of the equipment used.

One problem that has had a significant impact upon the design of this system has been the spurious 30 MHz signal. Since all the signals used by the LO are coherent between receivers, the 30 MHz signals from each receiver are also coherent and hence will correlate. Also, because this signal is monochromatic, the delay compensation will not result in decorrelation. The steps taken to reduce this interference include: redesign of RF/DC combining network; redesign of RF combining network; inclusion of low pass filters on the inputs of the 378 MHz power amplifier; respecification of the 378 MHz filter to increase suppression of spurious signals at 348 MHz and 408 MHz; careful filtering of the output of the IF preamplifier and input of the IF amplifier to prevent mixing there; and very careful shielding of all subsystems.

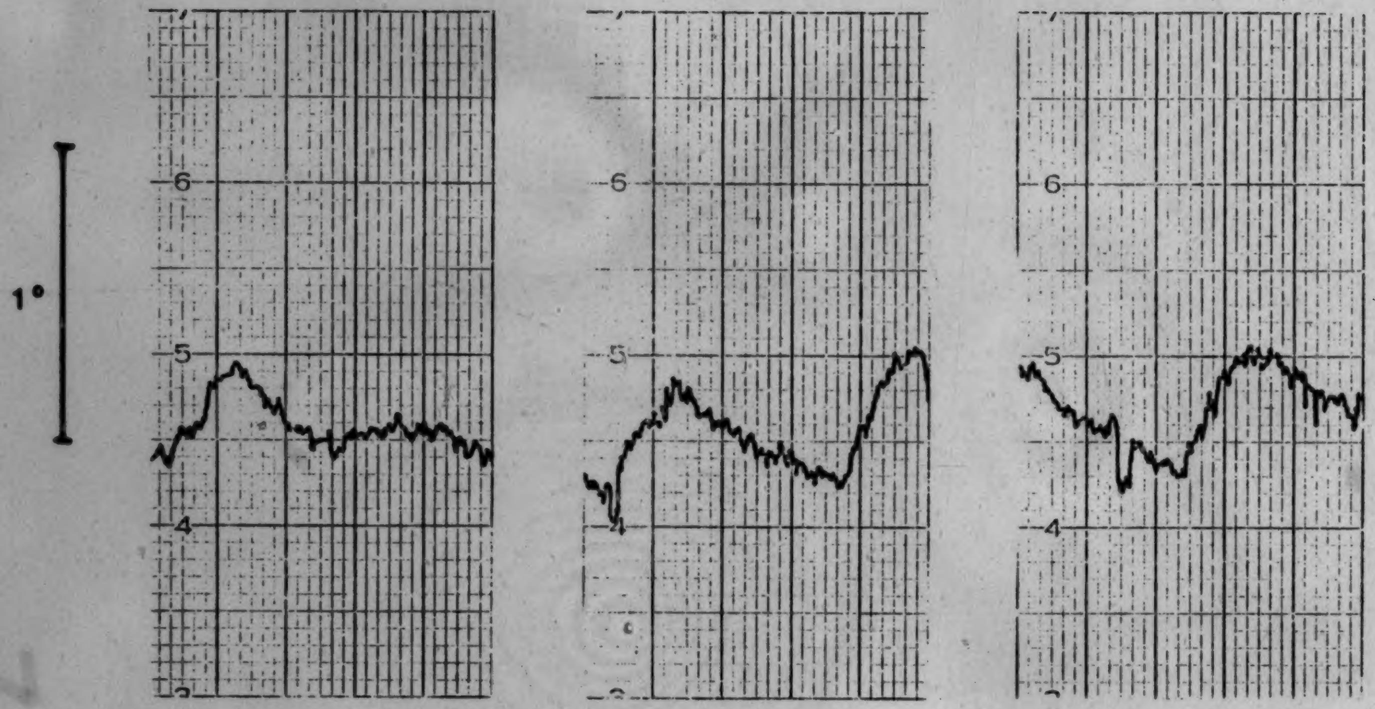

0-1hr 8-9hr 16-17hr

Figure 3.24 Long-term Phase Stability

Although the level of this signal has been reduced by at least 60 dB, it was still visible with a spectrum analyzer attached to the IF output. With the present component configuration the level is 10 dB above the noise with the spectrum analyzer bandwidth equal to 100 Hz. This is about 30 dB above the minimum level detectable by the Synthesis Telescope.

The minimum detectable interference level can be determined as follows: the sensitivity of the telescope is about 3 mJy/beam. The gain of an antenna is 1K/70 Jy, so a source of that intensity would increase the antenna temperature by $3\times10^{-3}/70$ or 43 μK. The system temperature is about 105K, so the power of this interfering signal is $43\times10^{-6}/110$ or $.4\times10^{-6}$ the total power received. The IF power can be obtained by multiplying the height of the spectrum analyzer display by the receiver IF bandwidth (4 MHz). The power in the interfering signal (which is monochromatic) can be determined by the product of the spectrum analyzer bandwidth (100 Hz) and the height of the signal. From this the ratio of the interference strength to the IF noise level can be determined and it is $(.4\times10^{-6})(4\times10^{6})/100=.016$ or -18 dB. It should be noted that this is for the special case where the phase of the interference is such that it appears at a single point in the map, otherwise it will be smeared across the map and the interference will have to be much stronger to be noticeable.

Attempts to further reduce the interference were not successful. Signals with such a small amplitude are very difficult to trace. The effects of this interference will be shown in the next chapter which describes aperture synthesis observations with the telescope. For strong sources, the instrument sensitivity is dynamic range limited, so the noise due to sidelobes of the synthesized beam is larger than the interference. For weak sources, the interference may be greater than the map noise level.

One other very significant system test was an evaluation of the system reliability. The receiving system developed has been in almost continuous operation for four months on four antennas with no failures. The VCO control voltage operating points have remained the same over this length of time. The system has survived power failures and the occasional disconnection of the coaxial transmission lines. It returns to normal operation immediately after power is supplied or the cable is reconnected.

CHAPTER 4: ASTRONOMICAL OBSERVATIONS

A. Introduction

The 408 MHz Synthesis Telescope was tested with observations of a number of astronomical sources. With these tests a number of effects were studied, such as receiver stability, interference from various sources, and ionospheric stability.

B. Repeatability

An essential quality of all scientific data is repeatability. A simple experiment was performed by repeating an observation and then comparing the visibilities recorded. In Fig. 4.1 the two sets of visibilities are superimposed and the agreement between the two is quite good. The eight strip charts show amplitude versus time for the real and imaginary outputs of each interferometer. Four interferometer correlations are obtained: Far East antenna and West antenna (FExW), Far East and East (FExE), Far West and East (FWxE) and Far West and West (FWxW). The observations were made a day apart. The rms difference between the two sets of visibilities is less than 6% of the amplitude of the visibilities. This result suggested that the instrumental stability and ionospheric stability are adequate for aperture synthesis mapping.

Since the source observed, 3C295, is effectively an isolated point source at the centre of the field of view (see Fig. 4.6), the

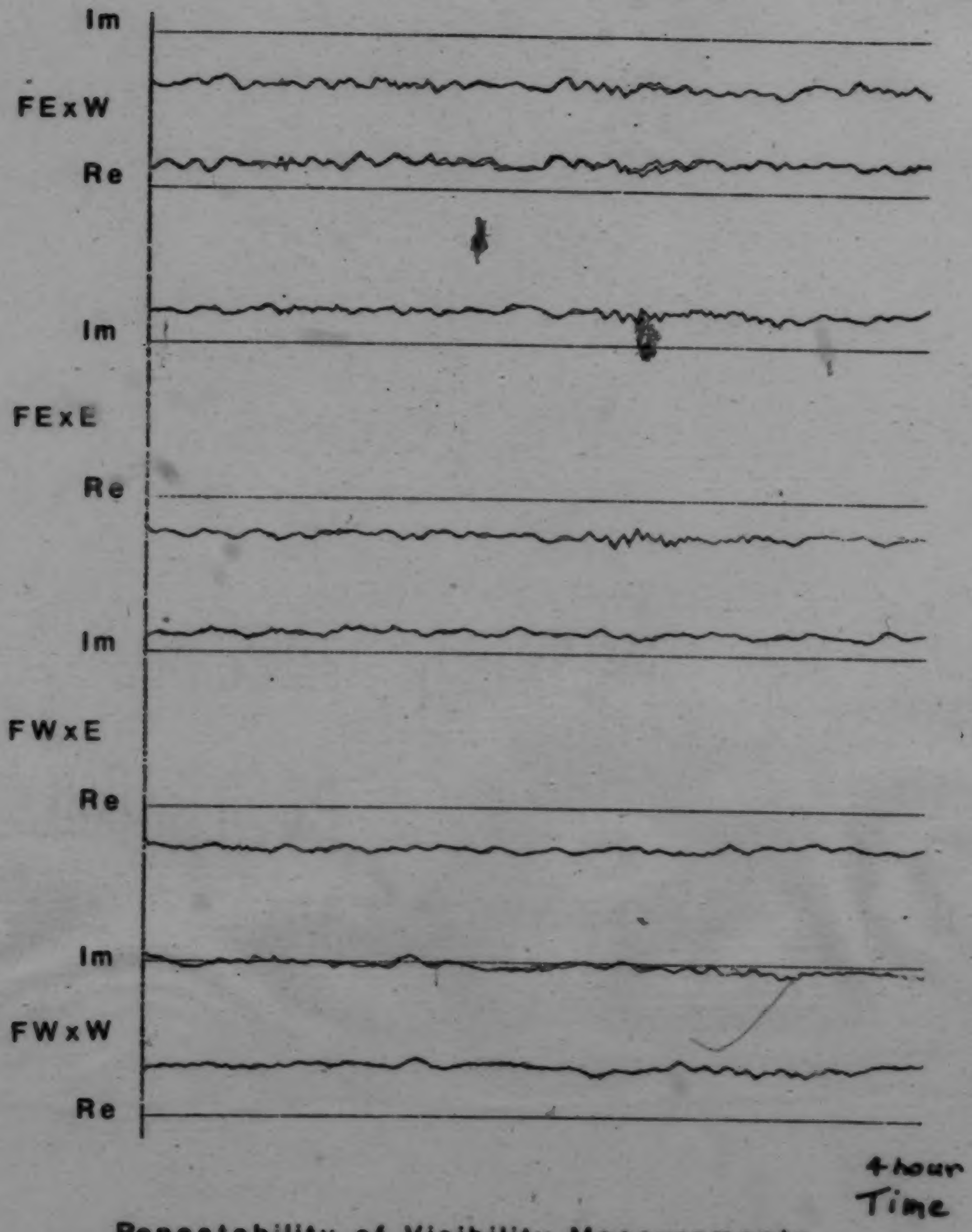

Repeatability of Visibility Measurements

Figure 4.1

visibilities are expected to be constant with time. This is because the earth's rotation sweeps the interferometer response pattern about field centre and therefore the interferometer output does not change with time. The measured visibilities were constant except for small ripples superimposed on the straight lines. These variations repeat and are probably due to the weak sources surrounding 3C295.

C. Long-term Phase Stability

A routine part of a synthesis telescope survey is short calibration observations to determine the interferometer gains and phases. The calibration observation involves observing an isolated point source and measuring the amplitude and phase of the visibilities. The 408 MHz calibration phases measured during one survey have been plotted in Figure 4.2. The calibration source was Cygnus A, which is a strong radio galaxy. The phase of each antenna and receiver with respect to the Far East antenna and receiver is plotted. The phase zero was arbitrarily chosen. The best-fit straight line through the data points is also shown.

Two things can be seen in each of these plots: a gradual phase drift, and a scatter around the best-fit line. The source of the phase drifts is unknown, but one possible source is aging of components. This slow drift is unimportant because the numbers from the calibration process are used to correct the visibilities.

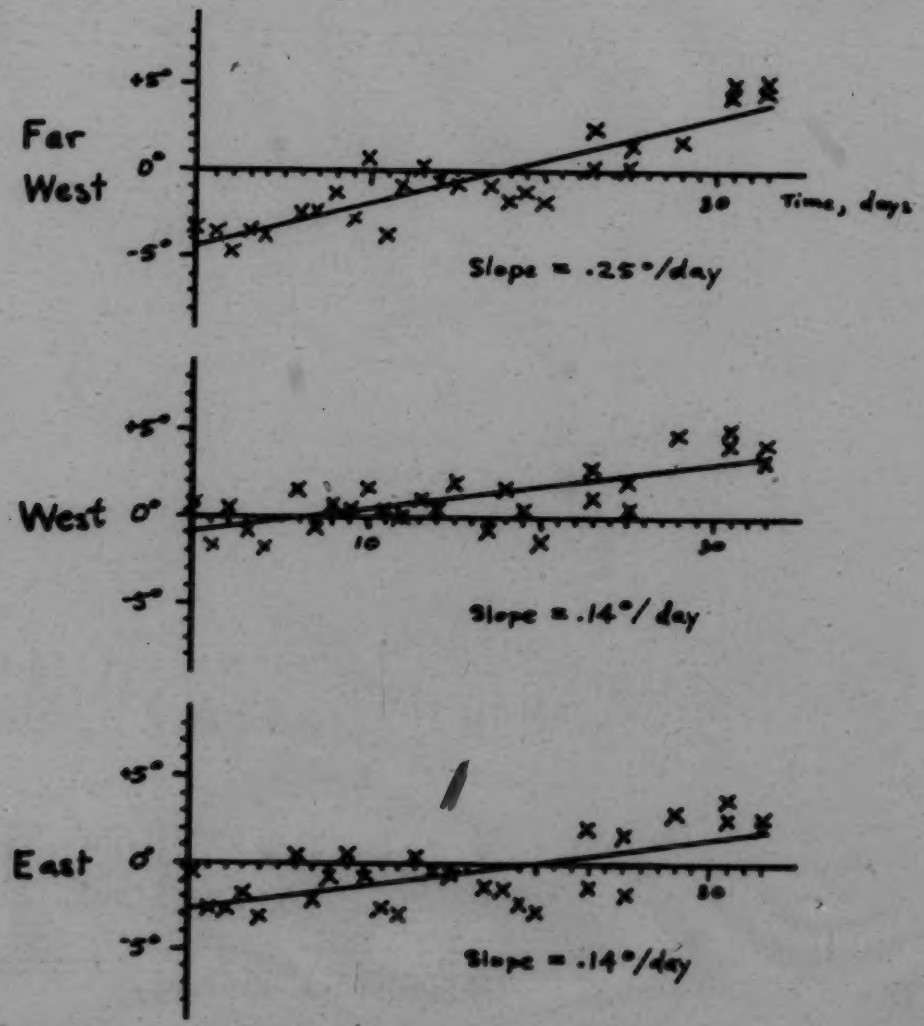

Calibration Phase vs. Time at 408 MHz

Figure 4.2

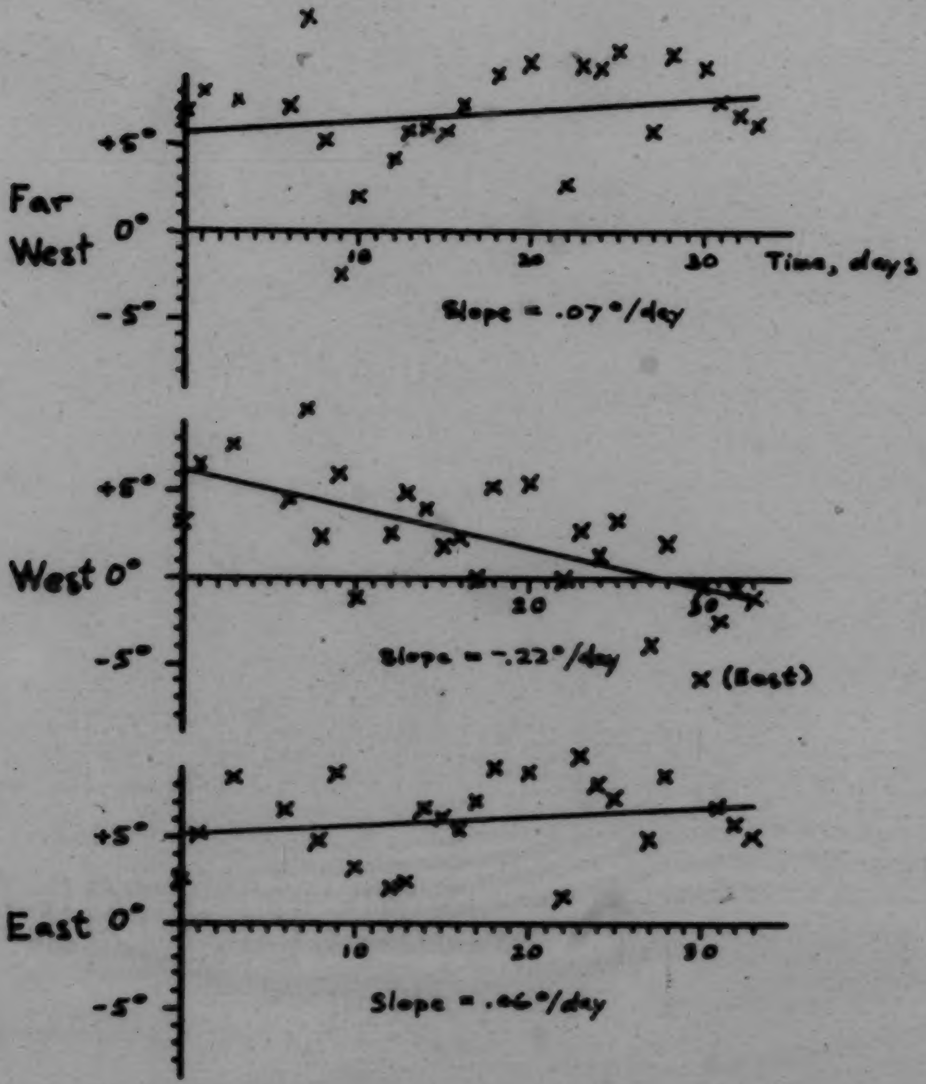

Calibration Phase vs. Time at 1420 MHz

Figure 4.3

The scatter of individual points is more worrisome since the phase has changed by as much as 5° from one day to the next. This variation may be due to effective path length variations in the ionosphere. These phase fluctuations can be compared with the phase at 1420 MHz plotted in Fig. 4.3. It can be seen that the variation is about a factor of 2 larger at 1420 MHz. This result agrees with the interferometer phase uncertainties experienced at Cambridge (Baldwin and Warner 1979). Low frequency work at other observatories (de Bruyn and van der Hulst 1983) suggested poorer phase performance at lower frequencies, but that information may not be entirely valid because it was obtained at a time when the sun was more active and the ionosphere was more disturbed than it is now. The source(s) of the phase variation at the two frequencies is not known, but the important conclusion that can be drawn is that since the phase stability at 408 MHz is superior to that at 1420 MHz, then it will be possible to produce maps at 408 MHz since good maps are routinely made at 1420 MHz.

D. Solar Interference

The sun is a strong, highly variable radio emitter at 408 MHz and can interfere with measurements made during the day. Figure 4.4 shows an example of solar interference on the FWxW visibilities. Although the antennas were not pointing at the sun, the sun was strong enough to be received through the sidelobes and produce significant effects. The interference fringes do not appear on the longer baselines because the

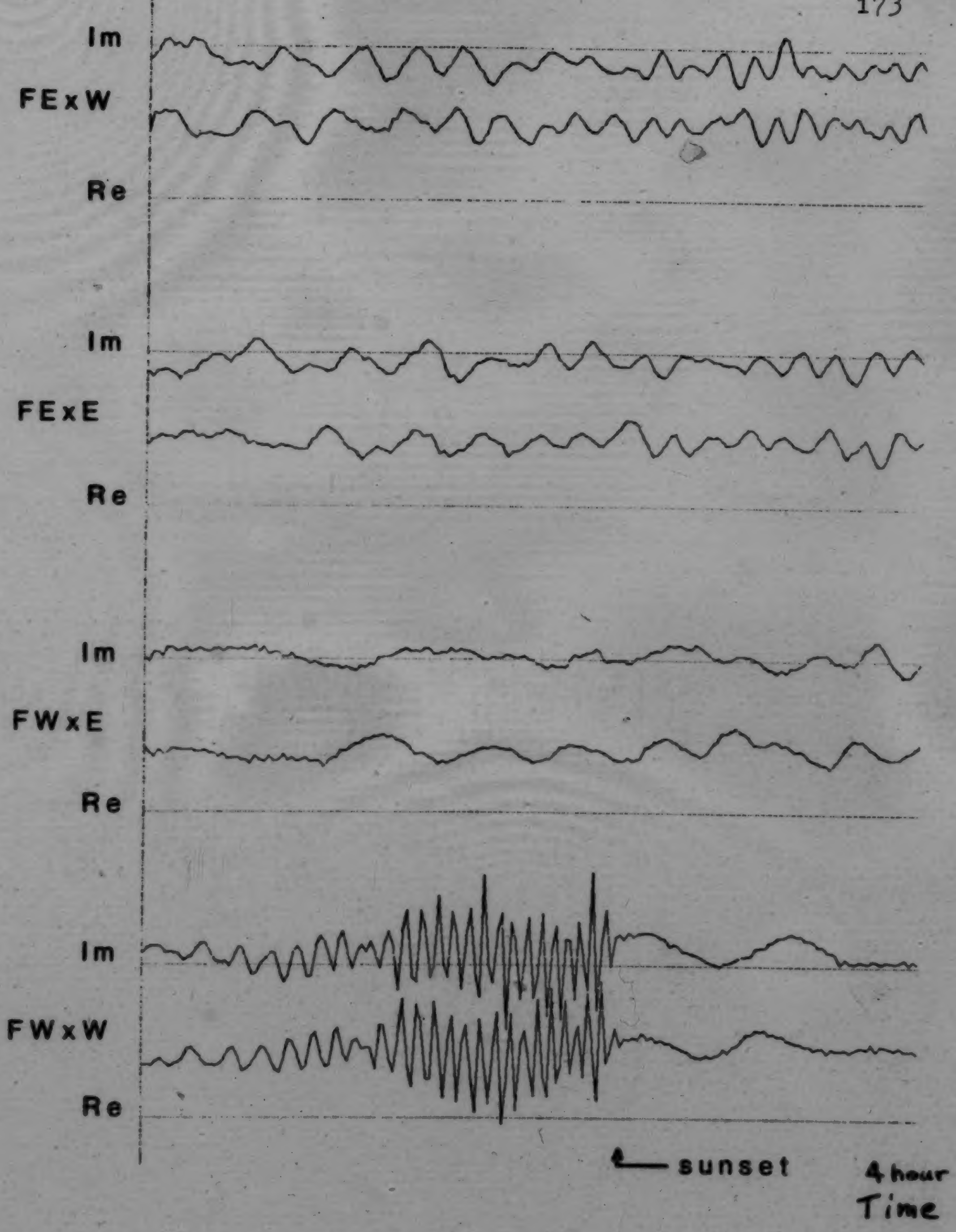

An Example of Solar Interference

Figure 4.4

geometric delay errors are larger and result in greater attenuation through decorrelation. Also the sources on the Sun are quite big and are resolved out at all but the shortest spacings.

This effect may limit the usefulness of the telescope for observations made during daylight hours. However, in the data reduction process, many of the short spacing visibilities are averaged together into a small number of u-v plane points, and this strongly attenuates the more rapid interference fringes.

Other synthesis telescopes, such as the Westerbork Synthesis Radio Telescope, also have this problem (de Bruyn and van der Hulst 1983).

E. Man-made Interference

Interference from man-made radio sources has also been observed. Like solar interference, the signals are received via antenna sidelobes, but unlike solar interference, manmade signals are narrowband (tens of kilohertz) and of short duration. Manual editing of the data has successfully dealt with interference at 1420 MHz and the same methods will have to be used with the 408 MHz data.

The narrow band nature of this type of interference is significant because this means that the decorrelation due to time delay errors in the signal paths to the correlator is less effective in attenuating the undesired signal. Thus the interference usually appears in all interferometer visibilities. The interference typically lasts for several minutes, so only a few visibility measurements are ruined. The interference is readily identifiable and deleted from the data. Effects on image quality are minimal.

This interference originates from satellites which transmit just outside the 406-410 MHz band and sometimes within the band. The incidence of interference was reduced greatly after sharp bandpass filters were installed following the IF output.

F. Cross Talk

Noise sources common to both receivers in an interferometer cause interference because the noise correlates. This interference is called cross talk and is observed at close spacings between the Far West and West antennas of the SST. The origin of the common noise is uncertain, but probable sources include thermal radiation from the ground between the antennas, and noise emanating out of one receiver which is picked up by the other receiver.

Test observations were made of 3C295 at a 17 metre spacing to measure the cross talk. The interference appeared as fringes. By comparing the fringe amplitude to the average visibility amplitude (ie. the flux of 3C295), the flux equivalent of the cross talk was found to be 20 Janskys. This interference is present over large hour angle ranges. However, it diminishes as the interferometer spacing is increased, and it is attenuated in the data reduction process because many short spacing visibilities are averaged together.

G. Telescope Dynamic Range: Observations of 3C295

The ultimate test of a synthesis telescope is to map a region of the sky. Two maps have been made of the region around the radio galaxy 3C295. One was made with the source at the centre of the field, and the other was made with the field centre moved 2.65° north so that the source was at a half-power point of the primary beam.

The two maps were each made with data collected over two nights. The eight interferometer spacings were selected so that the spacing interval from shortest to longest was fairly constant. However, many spacings were left out and this incomplete interferometer baseline coverage resulted in the generation of sidelobes that encircle the main lobe of the synthesized beam and are known as grating lobes. These can be seen in the map of 3C295 in Fig. 4.5. The map produced is the convolution of the sky brightness distribution with the synthesized beam. Using a computer algorithm called CLEAN (Högbom, 1974), it is possible to deconvolve the beam with grating lobes from the "dirty" map and then reconvolve with a beam that has no grating lobes (the

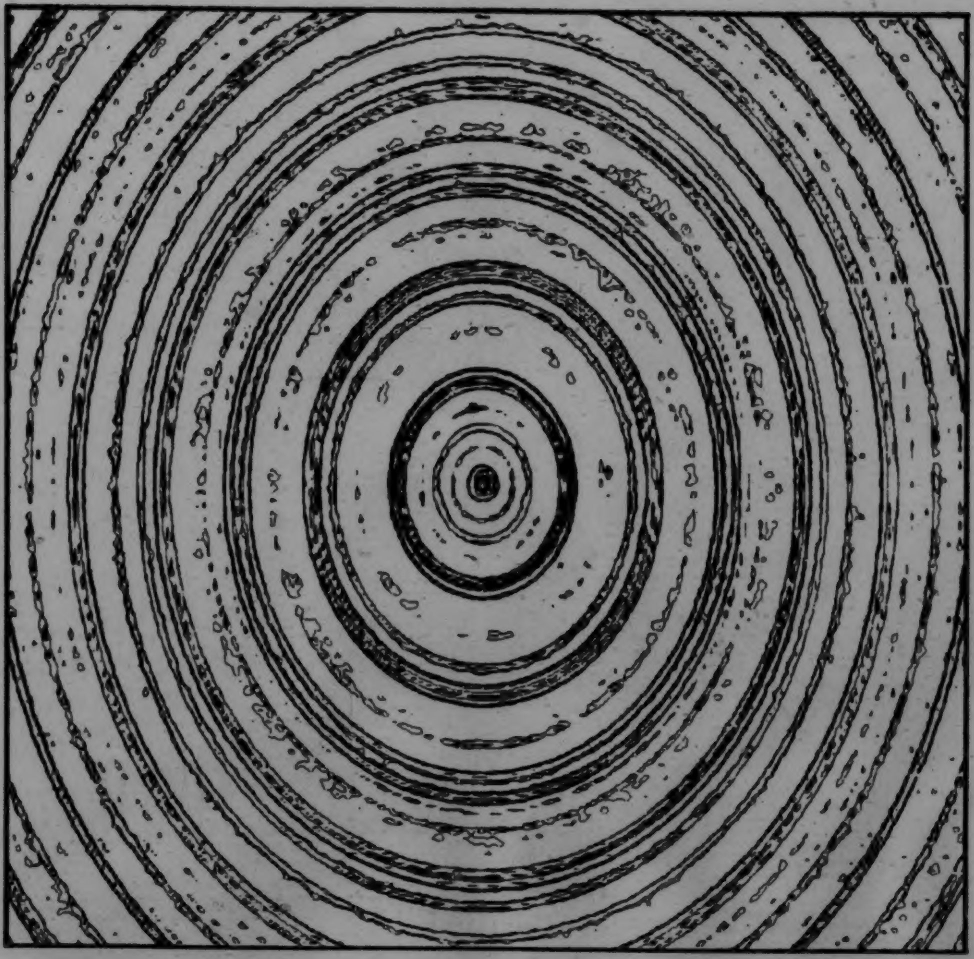

Contours 100.0 200.0 500.0 1000. 2000.

5000. 0.1000E+05 0.1500E+05 0.2000E+05

Map of 3C295 Region Before CLEANing

Figure 4.5

"clean" beam). The resulting "clean" map is the same as what would be obtained by a telescope that had no grating lobes. This routine was used on the map in Fig. 4.5 and the result is shown in Fig. 4.6.

Weaker sources that were previously obscured by grating lobes are now visible. This test confirms that the telescope has a high degree of stability since to properly remove the grating responses, the interferometer amplitudes and phases must be well known. Amplitude and phase errors would change the actual synthesized beam so that deconvolution with the calculated beam (that assumes no errors) will not remove the grating rings entirely.

The weak sources in the map have been identified from surveys of this part of the sky (Brundage et al. 1971, Stute et al. 1980). The dynamic range of this map is 200:1 and was obtained by comparing the amplitude of the strongest source with the weakest source. The peaks of the residual errors are also about 200 times weaker than the strongest source. A dynamic range of this order is very good for a telescope that does not use more sophisticated gain and phase calibration techniques.

The flux scale varies across the map because the map has not been corrected for the primary antenna response. The flux of 3C295 is 54 Janskys which corresponds to 22000 units at the centre of the map. The synthesized beam width is 4.4 arcminutes in the north-south direction

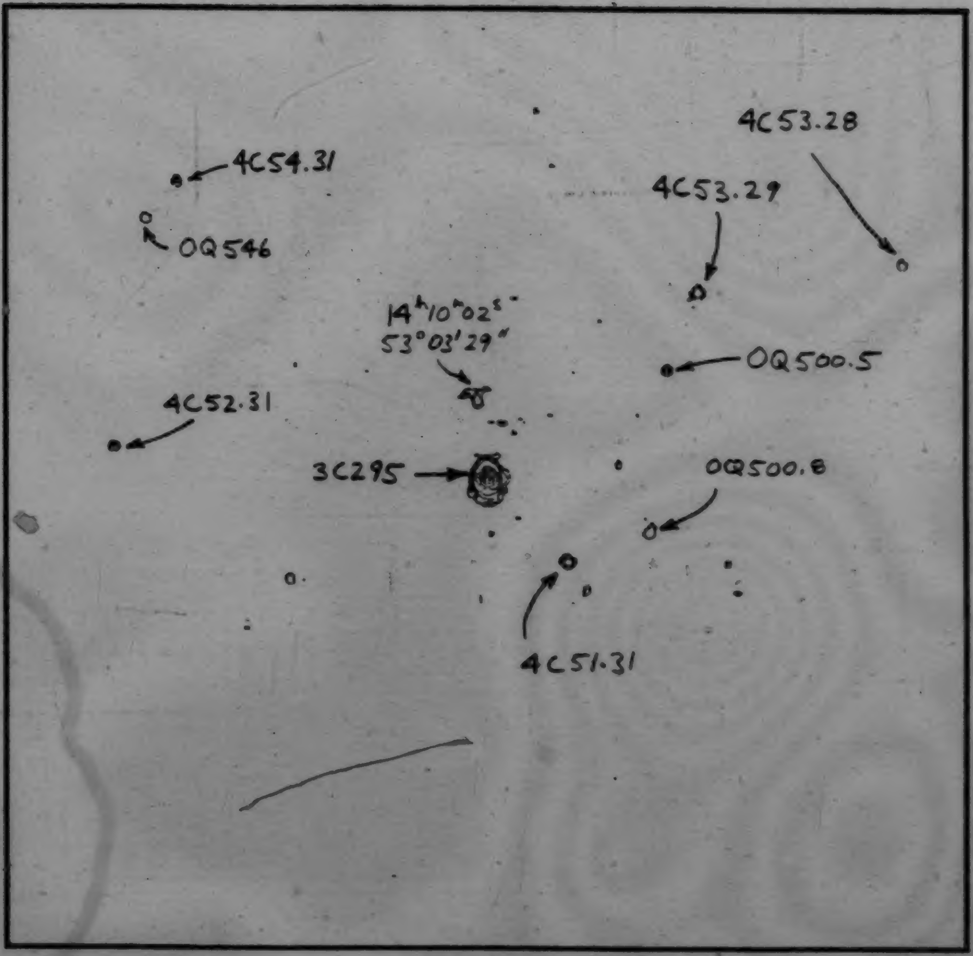

Contours 100.0 200.0 500.0 1000. 2000.

5000. 0.1000E+05 0.1500E+05 0.2000E+05

Map of 3C295 Region After CLEANing

Figure 4.6

and 3.7 arcminutes in the east-west direction. The map encloses 7.4°x7.4° of the sky.

A second map of the 3C295 region was made, but with the map centre moved north 2.65° so that 3C295 was at the half-power point of the primary antenna pattern. The CLEANed map is shown in Figure 4.7 with identified sources labelled. The flux scale is the same as the previous map.

The amplitude of 3C295 on this map is 8800 units, which is .4 of the field-centre intensity. However, one would expect it to be .5 times the field-centre intensity since it is at a half-power point of the primary beam. This discrepancy is due to a phenomenon known as radial smearing which is analogous to chromatic aberration in optical telescopes. Radial smearing occurs because the effective array size is a function of frequency which in turn means that the map radial scale is a function of frequency. Since broadband noise is received by the telescope, a point source in the sky will produce a point on the map only if it is at the centre of the map, otherwise the source on the map is broadened in a radial direction from the centre. Since the flux is spread over a greater area on the map, the peak intensity is less. If the beam is assumed to be Gaussian, then from a graph plotted by Thompson (1982) it can be estimated that the peak flux will drop to 95% of its centre value. A value of 80% was obtained in this experiment. The difference between the two numbers may be due to the actual beam

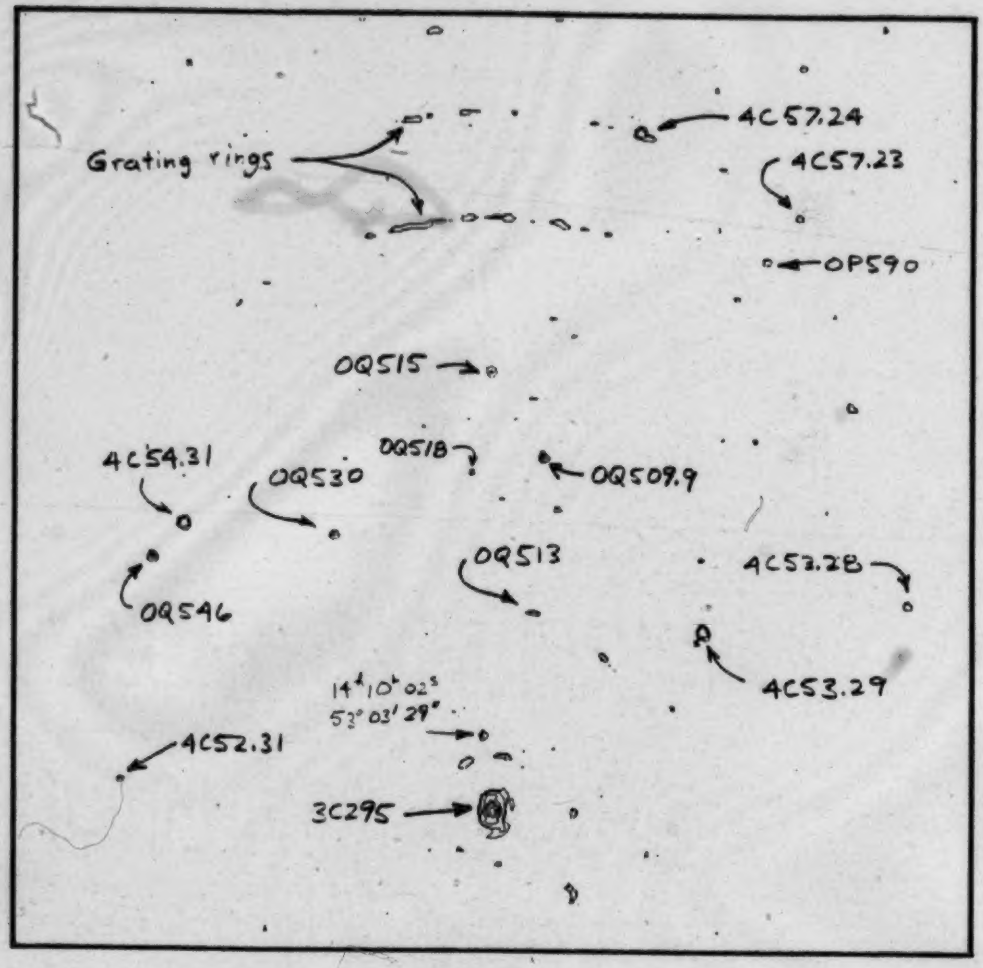

Contours 100.0 200.0 500.0 1000. 2000.

5000. 0.1000E+05 0.1500E+05 0.2000E+05

Map of Region 2.65° North of 3C295

Figure 4.7

shape, the actual bandpass shape, and errors in the measurement of the half-power beamwidth.

H. Telescope Sensitivity: Maps of the 5C2 Region

The previous maps have included strong sources and the map sensitivities were limited by the dynamic range of the map rather than the noise temperature of the receiver. Thus it was desirable to observe part of the sky where there are no bright sources in order to push the instrument to its sensitivity limit.

The region mapped is called the 5C2 region and was originally mapped at 408 MHz with the Cambridge One-Mile Telescope (Pooley and Kenderdine 1968). Two nights were used to map the region in this test and the CLEANed map is shown in Fig. 4.8. The source positions and fluxes were compared with the original Cambridge survey and with later surveys (Gillespie 1979, Pauliny-Toth et al. 1972, Brundage et al. 1971, Maslowski 1971, Katgert 1975). The numbers by the sources are the 5C2 survey number, OM and OL prefixes designate Ohio Survey identifications, and other numbers refer to other surveys. 48 sources have been identified in this map.

There are a number of flaws in this map. The first indication of this is that the noise level in the map is at least a factor of three too high. Thus the number of sources identified is too low. When the

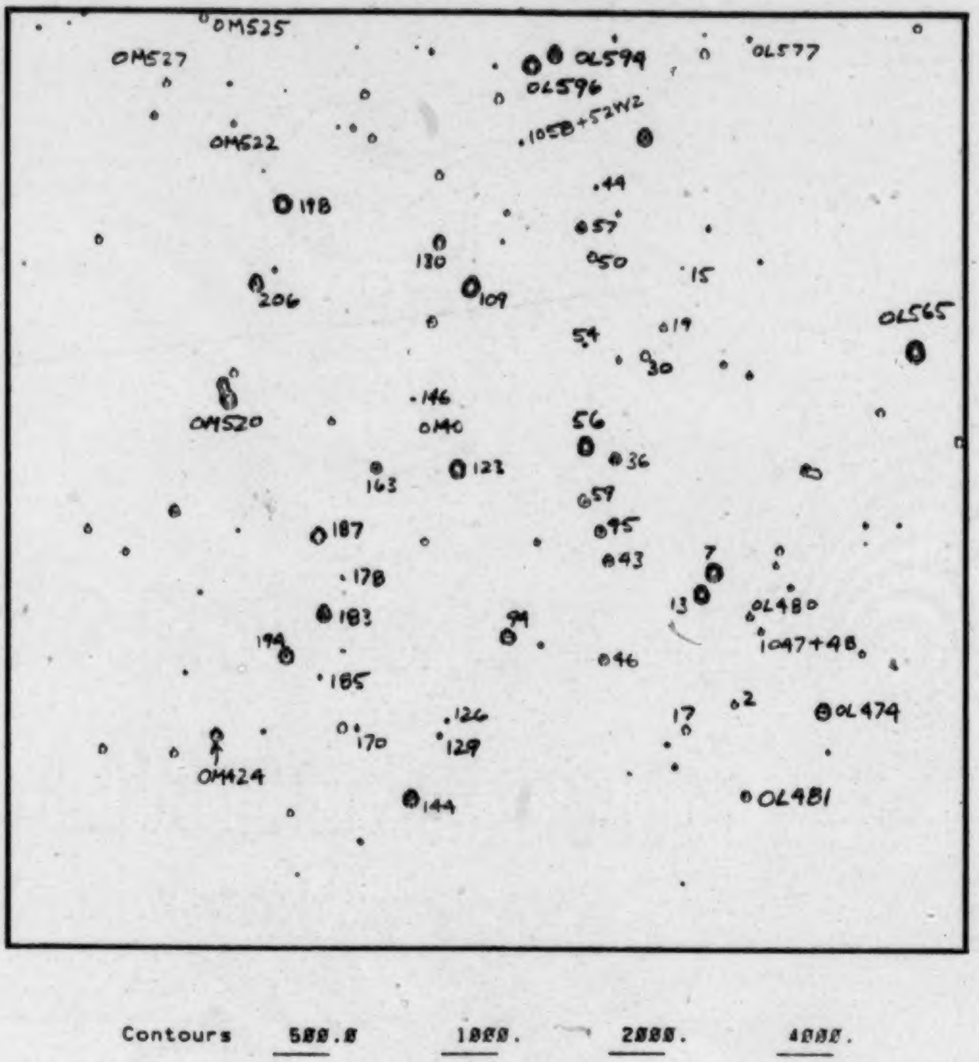

Identified Sources in 5C2 Region

Figure 4.8

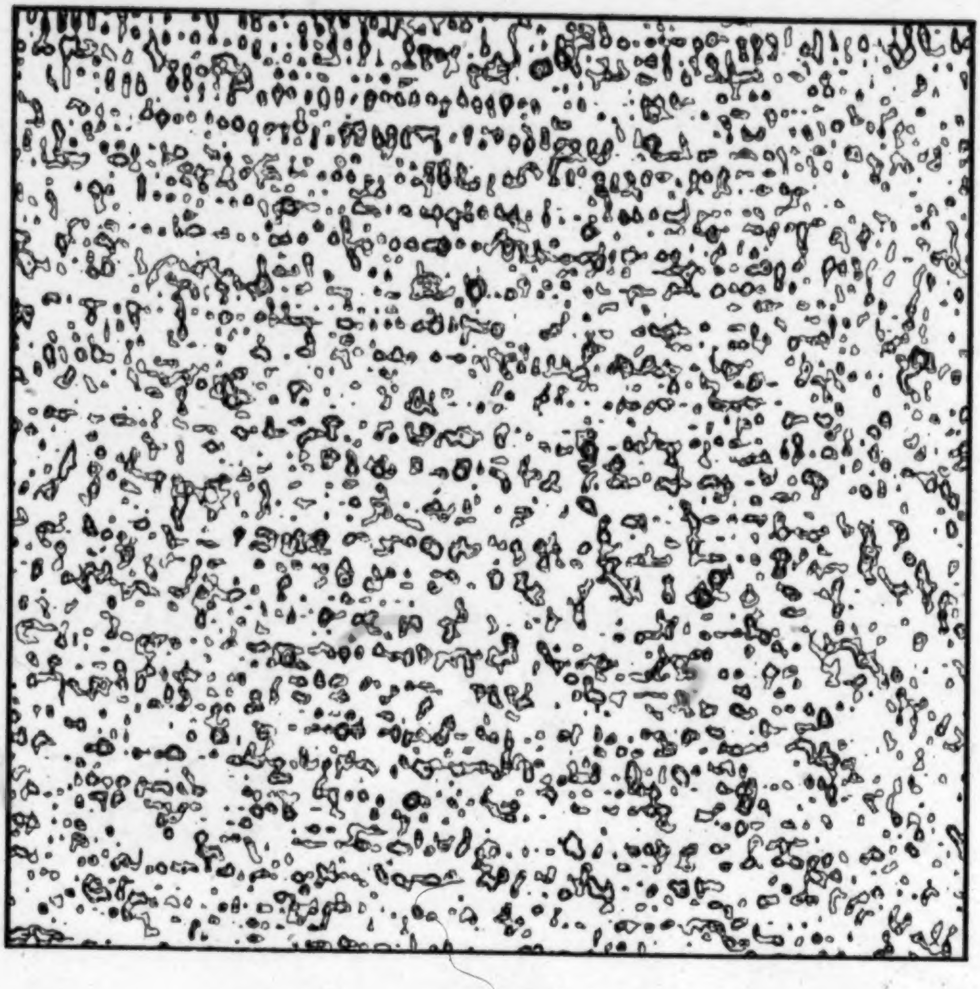

CLEANed 5C2 Map with Residuals Added

Figure 4.9

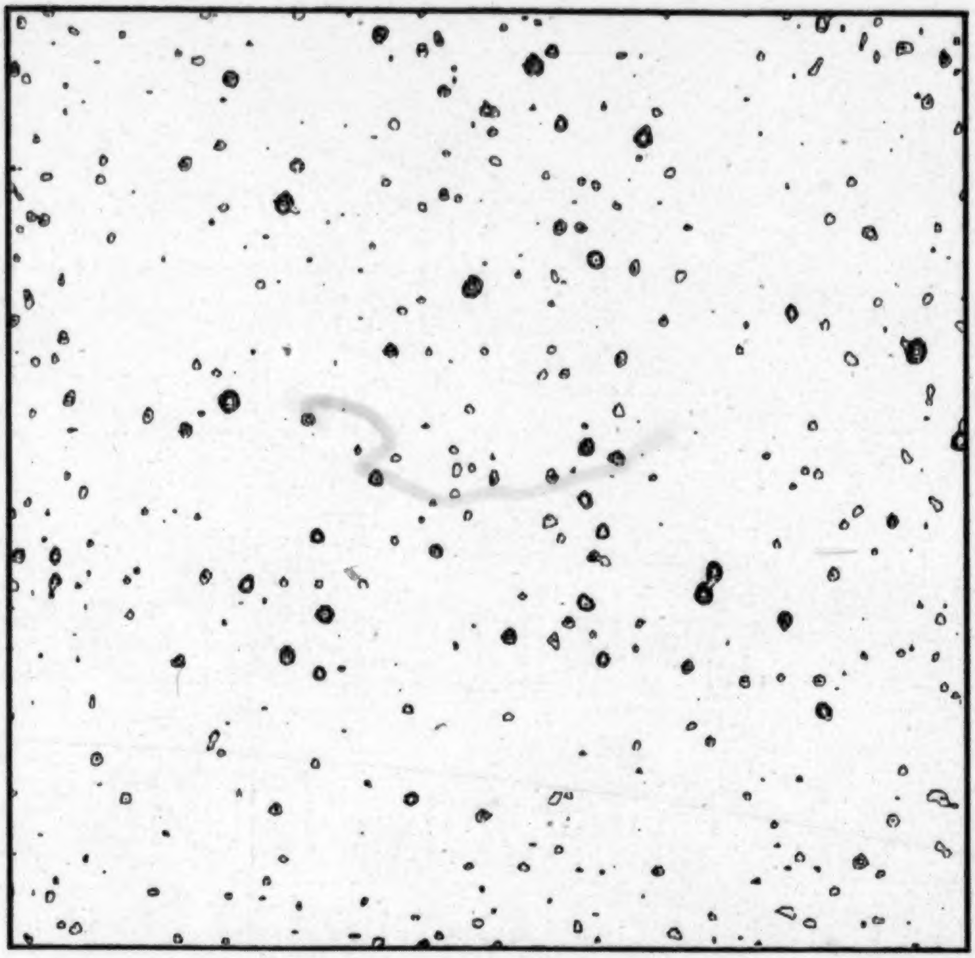

Contours 250.0 500.0 1000. 2000. 4000.

Second 5C2 Map with Residuals

Figure 4.10

residuals from the CLEAN process are added back to the map (as was done with Figs. 4.6 and 4.7), Fig. 4.9 is obtained. The residuals are very large, peaking between 500 and 1000 units, and have a "striped" appearance. As shown by Thompson (1982), artifacts of this type are due to interference. With this telescope, the most probable interference signal is the spurious signal at the centre of the IF band.

A set of simple L-C notch filters were constructed and placed in the signal lines preceding the correlator. The filters have notch depths between 11 dB and 16 dB with half-power bandwidths of 120 kHz. The reduction in sensitivity due to the filters is about 1%. The 5C2 region was observed again, but for only one night, and the CLEANed map with residuals added is shown in Fig. 4.10. Stripes are not present in these residuals. This map is plotted at the same scale as the previous map. The residual peaks and standard deviation are a factor of 3.4 larger in the old map than the new map.

Before the measured map noise levels can be compared with the theoretical noise levels, the map flux scale must be calibrated. In the map making process, the calibration coefficients were selected to give a map scale of 10 units/milliJansky (mJy). However, comparison of source intensities in the first map (Fig. 4.9) with well-known fluxes in previous surveys has given a ratio of 6.8 units/mJy. The source of this error is not known for certain, but it may be due to errors introduced by the large residuals.

For a two-night map, the theoretical rms noise level is 11 mJy, and for one night it is 16 mJy. Using a conversion factor of 10 map units/mJy (6.8 units/mJy) the rms noise in the first 5C2 map is 37 mJy (54 mJy) and 11 mJy (16 mJy) in the second map. Thus it can be concluded that the notch filter has reduced the noise level in the map to approximately its theoretical level.

One further comment should be made about these maps: they were made for engineering purposes and have little astronomical value. This is because the total observing time was short and hence the amount of independent data available to make the map is small. This is especially true with the one-night 5C2 observation where a small number of data points must define a large number of sources. Thus it is not surprising to find that some real sources in the first 5C2 map are not present in the second map. However, this was a very useful engineering test to determine the suppression of the self-interference.

I. A Complete Survey: HB3 Supernova Remnant

The first complete survey made at 408 MHz was of the supernova remnant HB3 and environs. HB3 subtends 70 arcminutes and the 408 MHz field also includes the HII regions W3 and W4 as well as another supernova remnant called 3C58. Maps at 38 MHz (45 arcminute beam) and

178 MHz (21 arcminute beam) were described by Caswell (1967). It has also been mapped at 2700 MHz with a 5 arcminute beam by Velusamy and Kundu (1974) and with a 12 arcminute beam by Wendker and Altenhoff (1977) and at 1420 MHz with a 9 arcminute beam (Kallas and Reich 1980). The complete shell has been observed optically by Fesen and Gull (1983) and X-ray emissions have been detected by Galas, Tuohy and Garmine (1980) using the HEAO 1 satellite. From these observations it is clear that the object is a supernova remnant because of its shell-like appearance with a central depression and its non-thermal spectral index with α=-0.52.

These earlier observations have prompted a number of questions. HB3 lies to the north west of a "chain" of HII regions composed of W3, W4, and W5. It is not yet certain if HB3 is at the same distance as the HII regions. If it is, the expanding shock front from the supernova may be interacting with W3. In any case, the true extent of the supernova remnant has not been established because the edge of the shell is along the same line of sight as the edge of W3. Read (1981) has made HI emission maps of the region around W3 and has evidence that the neutral hydrogen is being swept up by the expanding shell.

The observations at 408 MHz are part of an attempt to answer some of these questions. The set of maps at the two frequencies can help to separate the non-thermal emission of HB3 from the thermal emission of the HII region beside it. Only preliminary results will be shown here.

Detailed analysis and interpretation are beyond the scope of this thesis. Figures 4.11 and 4.12 present the results of the HB3 survey. These maps are superior to the previous surveys in a number of ways. Most of the earlier maps suffered from poor dynamic range, which can be inferred from the fact that they displayed only 3 or 4 contour levels. The other main deficiency in the earlier maps is poor resolution; the resolution in these new maps is a factor of three better than previous maps.

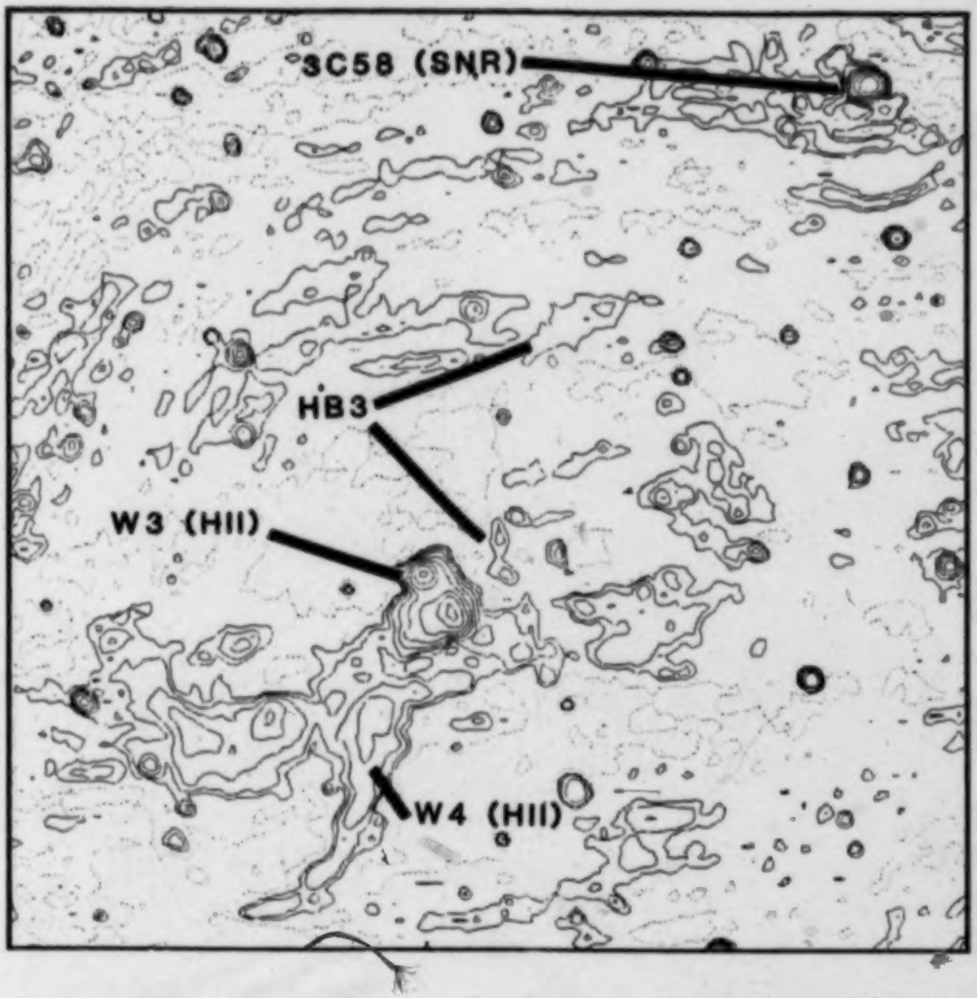

Contours -2.001 2.001 4.001 8.001 16.00
32.00 64.00 128.0 256.0 x 10 [illegible]

408 MHz Map of HB3 and Environs

(5X5 degrees)

Figure 4.11

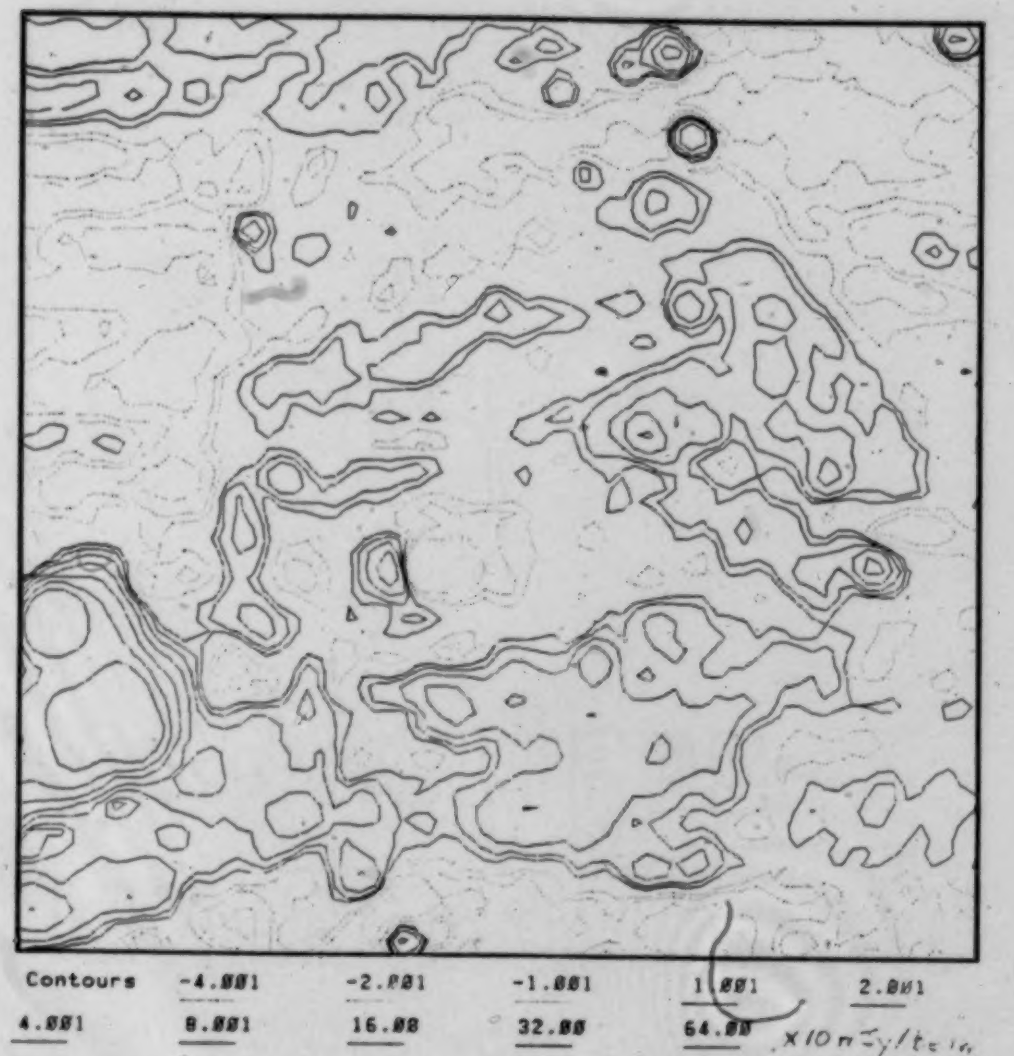

408 MHz Map of HB3 SNR (2X2 degrees)

Figure 4.12

References

Anastassiou, A., Strutt, M.J.O., 1974, "Effect of Source Lead Inductance on the Noise Figure of a GaAs FET", Proc. IEEE 62 p406

Archer, J.W., 1977, "A Precision Phase-Controlled Local Oscillator System for a Millimetre-Wave Interferometer", IREE 16th International Radio & Electronics Engineering Convention Digest, Melbourne Aug. 8-12 pp100-102

ARRL, 1974, The ARRL Antenna Book, American Radio Relay League, Newington, Conn.

Baars, J.W.M., Genzel, R., Pauliny-Toth, I.I.K., Witzel, A., 1977, "The Absolute Spectrum of Cas A; An Accurate Flux Density Scale and a Set of Secondary Calibrators," Astronomy & Astrophysics 61, p99

Baldwin, J.E., Warner, P.J., 1979, "Fundamental Aspects of Aperture Synthesis with Limited or no Phase Information," Image Formation from Coherence Functions in Astronomy, C. van Schooneveld (ed.), Reidel, Dordrecht, p67

Blythe, J.H., 1957, "A New Type of Pencil Beam Aerial for Radio Astronomy", Mon. Not. R. Astr. Soc., 117 p644

Bracewell, R., 1965, The Fourier Transform and Its Applications, McGraw-Hill, Toronto

Brundage, R.K., Dixon, R.S., Ehman, J.R., Kraus, J.D., 1971, "The Ohio Survey Between Declinations of 40° and 63° North", Astronomical Journal 76 p777

Carpenter, D.D., 1973, "The Effects of Time Delays on the Stability of Practical Phase Locked Receivers with Multiple Conversion by Utilizing Root Locus with Positive Feedback", 1973 IEEE Int. Conf. on Commun., 11 pp33-14 - 33-19

Casse, J.L., Muller, C.A., 1974, "The Synthesis Radio Telescope at Westerbork. The 21cm Continuum Receiver System", Astronomy & Astrophysics 31 p333

Caswell, J.L., 1967, "Radio Observations of Two Supernova Remnants", Mon. Not. R. Astr. Soc. 136 p11

Cooke, H.F., 1982, Introduction to Microwave FETs, Varian Associates Santa Clara, CA deBruyn, A.G., van der Hulst, J.M., 1983, "327 MHz: Status Report and Future Outlook", Netherlands Foundation for Radio Astronomy Note 398, June 1

Dewdney, P.E., Roger, R.S., 1982, "The HI Cloud Surrounding the Emission-Like Star LkHα 101 in the Region of NGC 1579", Astrophysical Journal 255 p564

Dragone, C., Hogg, D.C., 1963, "Wide-Angle Radiation due to Rough Phase Fronts", Bell System Technical Journal 42 p2285

Fesen, R.A., Gull, T.R., 1983, "The Optical Emission from the Supernova Remnant HB3", Pub. Astr. Soc. Pacific 95 p196

Fomalont, E.B., 1973, "Earth-Rotation Aperture Synthesis", Proc. IEEE 61 p1211

Fomalont, E.B., Wright, M.C.H., 1974, "Interferometry and Aperture Synthesis", Galactic and Extra-Galactic Radio Astronomy, Verschuur, G.L., Kellermann, K.I. (eds.), Springer-Verlag, New York, p256

Forward, R.L., Cisco, T.C., 1983, "Electronically Cold Microwave Artificial Resistors", IEEE Trans. Microwave Theory Techniques MTT-31 p45

Frater, R.H., Williams, D.R., 1981, "An Active 'Cold' Noise Source", IEEE Trans. Microwave Theory Techniques MTT-29 p344

Galas, C.M.F., Tuohy, I.R., Garmire, G.P., 1980, "Soft X-Ray Observations of the Supernova Remnants HB3 and 3C58", Astrophysical Journal 236 pL13

Gardner, F.M., 1979, Phaselock Techniques, Wiley, Toronto

Gillespie, A.R., 1979, "Observations of the 5C1-5 Survey Areas at 1421 MHz", Mon. Not. R. Astr. Soc. 188 p481

Goodman, J.W., 1968, Introduction to Fourier Optics, McGraw-Hill, Toronto

Hacker, P.S., Schrank, H.E., 1982, "Range Distance Requirements for Measuring Low and Ultralow Sidelobe Antenna Patterns", IEEE Trans. Antennas Propagation AP-30 p956

Haslam, C.G.T., Klein, U., Salter, C.J., Stoffel, H., Wilson, W.E., Cleary, M.N., Cooke, D.J., Thomasson, P., 1981, "A 408 MHz All-sky Continuum Survey I. Observations at Southern Declinations and for the North Polar Region", Astronomy & Astrophysics 100 p209

Haslam, C.G.T., Salter, C.J., Stoffel, H., Wilson, W.E., 1982, "A 408 MHz All-sky Continuum Survey. II. The Atlas of Contour Maps", Astronomy & Astrophysics Sup. 47 pp1-143

Henyey, L.G., Keenan, P.C., 1940, "Interstellar Radiation from Free Electrons and Hydrogen Atoms", Astrophysical Journal 91 p625

Hertz, D., Jury, E.I., Zeheb, E., 1984, "Simplified Analytical Stability Test for Systems with Commensurate Time Delays", IEE Proc. 131 Part D p52

Högbom, J.A., 1974, "Aperture Synthesis with Non-Regular Distribution of Interferometer Baselines", Astronomy & Astrophysics Sup. 15 p417

ITU, 1982, Radio Regulations, International Telecommunications Union, Geneva

Jansky, K.G., 1933, "Electrical Disturbances Apparently of Extraterrestrial Origin", Proc. IRE 21 p1387

Kallas, E., Reich, W., 1980, "A 21cm Radio Continuum Survey of the Galactic Plane Between ℓ=93° and ℓ=162°", Astronomy & AStrophysics Sup. 42 p227

Katgert, P., 1975, "A Third 1415 MHz Survey with the Westerbork Synthesis Radio Telescope: the 5C2 Region (Part I)", Astronomy & Astrophysics 38 p87

Kiepenheuer, K.O., 1950, "Cosmic Rays as the Source of General Galactic Radio Emission", Physical Review 79 p738

Koch, G.F., 1973, "Coaxial Feeds for High Aperture Efficiency and Low Spillover of Paraboloidal Reflector Antennas", IEEE Trans. Antennas Propagation AP-21 p164

LaGrone, A.H., Roberts, G.F., 1966, "Minor Lob Suppression in a Rectangular Horn Antennas Through the Utilization of a High Impedance Choke Flange", IEEE Trans. Antennas Propagation AP-14 p102

Landecker, T.L., 1980, A Proposal for a Low Frequency Continuum Channel for the Synthesis Telescope, Dominion Radio Astrophysical Observatory, Penticton, B.C.

Landecker, T.L., Pineault, S., Routledge, D., Vaneldik, J.F., 1982, "VRO 42.05.01 - One Supernova Remnant or Two?", Astrophysical Journal 261 pL41

Landecker, T.L., Vaneldik, J.F., 1982, "A Phase-stabilized Local-oscillator System for a Synthesis Radio Telescope", IEEE Trans. Instrumentation Measurement IM-31 p185

Little, A.G., 1969, "A Phase-measuring Scheme for a Large Radiotelescope", IEEE Trans. Antennas Propagation AP-17 p547

Little, A.G., Hunstead, R.W., Calhoun, G.G., 1966, "A Constant Phase Local Oscillator System for a Cross Type Radio Telescope", IEEE Trans. Antennas Propagation AP-14 p645

Lo, W.F., 1982, A Digital Signal Processor for a 408 MHz Supersynthesis Telescope, M.Sc. Thesis, University of Alberta, Edmonton

Maslowski, J., 1972, "A Green Bank Sky Survey in Search of Radio Sources at 1400 MHz. II. Spectral Properties of the 5C1 and 5C2 Sources", Astronomy & AStrophysics 16 p197

Millman, J., Halkias, C.C., 1972, Integrated Electronics: Analog and Digital Circuits and Systems, McGraw-Hill, Toronto

Minnett, H.C., Thomas, B.M., 1968, "Fields in the Image Space of Symmetrical Focusing Reflectors", Proc. IEE 115 p1419

Napier, P., 1982, "VLA 327 MHz Prototype Feed System", VLA Electronics Memorandum #206, NRAO, Socorro, N.M.

Napier, P.J., Crane, P.C., 1982, "Signal-to-Noise Ratios", Lecture #3, Synthesis Mapping, Proc. NRAO-VLA Workshop, Socorro, NM, June 21-25, Thompson, A.R., D'Addario, L.R. (eds.) National Radio Astronomy Observatory, Green Bank, W.V.

Napier, P.J., Thompson, A.R., Exers, R.D., 1983, "The Very large Array: Design and Performance of a Modern Synthesis Radio Telescope", Proc. IEEE 71 p1295

NRAO, 1967, A Proposal for a Very Large Array Radio Telescope, National Radio Astronomy Observatory, Green Bank, W.V.

Ogata, K., 1970, Modern Control Engineering, Prentice-Hall, Englewood Cliffs, N.J.

Oort, J.H., Kerr, F.T., Westerhout, G., 1958, "The Galactic System as a Spiral Nebula", Mon. Not. R. Astr. Soc. 118, p379

Pauliny-Toth, I.I.K., Shakeshaft, J.R., 1962, "A Survey of the Background Radiation at a Frequency of 404 Mc/s", Mon. Not. R. Astr. Soc. 124 p61

Pauliny-Toth, I.I.K., Kellerman, K.I., Davis, M.M., Fomalont, E.B., Shaffer, D.B., 1972, "The NRAo 5-GHz Radio Source Survey. II. The 1420-Ft. 'Strong','Intermediate', and 'Deep' Source Surveys", Astronomical Journal, 77 p265

Percival, W.S., 1939, "An Electrically 'Cold' Resistance", Wireless Engineer, May 1939, p237

Pooley, G.G., Kenderdine, S., 1968, "The 5C2 Survey of Radio Sources", Mon. Not. R. Astr. Soc. 139 p529

Purton, C.R., 1983, Proposal for Observations with the Synthesis Telescope, Dominion Radio Astrophysical Observatory, Penticton, B.C.

Rahmat-Samii, Y., 1983, "An Efficient Computational Method for Characterizing the Effects of Random Surface Errors on the Average Power Pattern of Reflectors", IEEE Trans. Antennas Propagation AP-31 p92

Read, P.L., "HI Aperture Synthesis Observations Towards Galactic HII Regions - II. W3", Mon. Not. R. Astr. Soc. 194 p863

Reber, G., 1940, "Cosmic Static", Proc. IEEE 28 p68

Reber, G., 1944, "Cosmic Static", Astrophysical Journal, 100 p279

Roger, R.S., Costain, C.H., Lacey, J.D., Landecker, T.L., Bowers, F.K., 1973, "A Supersynthesis Radio Telescope for Neutral Hydrogen Spectroscopy at the Dominion Radio Astrophysical Observatory", Proc. IEEE 61 p1270

Ryle, M., 1962, "The New Cambridge Radio Telescope", Nature 194 p517

Saleh, A.A.H., 1981, "Planar Multiport Quadrature-like Power Dividers/Combiners", IEEE Trans. Microwave Theory Techniques MTT-29 p332

Scheffer, H., 1975, "Improvements in the Development of Coaxial Feeds for Paraboloidal Reflector Antennas", Paper B1/2, 5th European Microwave Conference, Hamburg

Shimozawa, D.T., 1968, Coherent Local Oscillators for a 21 cm Supersynthesis Experiment, MASc Thesis, University of British Columbia, Vancouver

Silver, S., 1949, Microwave Antenna Theory and Design, McGraw-Hill, Toronto

Steer, D.G., 1984, "A Study of Image Recovery Techniques for Radio Long Baseline Interferometry", Ph.D. Thesis, University of British Columbia, Vancouver

Stute, U., Reich, W., Kalberla, P.M.W., 1980, "High Dynamic Range Observations in the Fields of Strong Extragalactic Radio Sources", Astronomy & Astrophysics Sup. 42 p299

Swarup, G., Yang, K.S., 1961, "Phase Adjustment of Large Antennas", IRE Trans. Antennas Propagation AP-9 p75

Thompson, A.R., 1981, "Directional Frequency Offsets in Round-trip Phase-measuring Schemes, With Application to the IRAM Array and the VLA", VLA Electronics Memo #202, National Radio Astronomy Observatory, Socorro, N.M.

Thompson, A.R., D'Addario, L.A., 1982, "Frequency Response of a Synthesis Array: Performance Limitations and Design Tolerances", Radio Science 17 p357

Thompson,A.R., 1982, "The Effects of Bandwidth and Similar Parameters", Lecture #5, Synthesis Mapping, Proc. NRAO-VLA Workshop, Socorro, N.M., June 21-25, Thompson, A.R., D'Addario, L.R., (eds.), National Radio Astronomy Observatory, Green Bank, W.V.

Thompson, A.R., 1982, "The Response of a Radio-Astronomy Synthesis Array to Interfering Signals", IEEE Trans. Antennas Propagation AP-30 p450

van der Hulst, H.C., 1945, "Herkomst der radiogolven uit het wereldruim", Nederlandsch Tijdschrift voor Natuurkunde 11 p210; or in English, Classics in Radio Astronomy, SUllivan, W.T. (ed.) Reidel, Dordrecht, p302

Velusamy, T., Kundu, M.R., 1974, "Observations of Intensity and Linear Polarization in Supernova Remnants at 11cm Wavelength", Astronomy & Astrophysics, 32 p375

Weinreb, S., Fenstermacher, D.L., Harris, R.W., 1982, "Ultra-low-noise 1.2-to 1.7-GHz Cooled GaAsFET Amplifiers", IEEE Trans. Microwave Theory Techniques MTT-30 p849

Wendker, H.J., Altenhoff, W.J., 1977, "A 2695 MHz Map of the IC1795 1805/1848 Region", Astronomy & Astrophysics 54 p301